Enclosure 2

MFN 10-093

GEH Licensing Topical Report NEDO-33440, "ESBWR Safety Analysis - Additional Information," Revision 2, March 2010

Public Version

IMPORTANT NOTICE REGARDING CONTENTS OF THIS REPORT

Please Read Carefully

The design, engineering, and other information contained in this document is furnished for the purpose of obtaining NRC approval of the ESBWR certification and implementation. The only undertakings of GEH with respect to information in this document are contained in the contracts between GEH and its customers or participating utilities, and nothing contained in this document shall be construed as changing those contracts. The use of this information by anyone for any purpose other than that for which it is intended is not authorized; and with respect to any unauthorized use, GEH makes no representation or warranty, and assumes no liability as to the completeness, accuracy, or usefulness of the information contained in this document.

No use of or right to copy any of this information contained in this document, other than by the NRC and its contractors in support of GEH's application, is authorized except by contract with GEH, as noted above. The information provided in this document is part of and dependent upon a larger set of knowledge, technology, and intellectual property rights pertaining to ESBWR certification and implementation. Without access and a GEH grant of rights to that larger set of knowledge, technology, and intellectual property rights, this document is not practically or rightfully usable by others, except by the NRC or through contractual agreements with Combined License Applicants and Licensees or customers or participating utilities, as set forth in the previous paragraph.

HITACHI

GE Hitachi Nuclear Energy

NEDO-33440
Revision 2
Class I
DRF 0000-0089-0134, Revision 3
March 2010

Licensing Topical Report

ESBWR Safety Analysis - Additional Information

Copyright 2009, 2010 GE-Hitachi Nuclear Energy Americas LLC

All Rights Reserved

NON-PROPRIETARY INFORMATION NOTICE

This is a non-proprietary version of NEDE-33440P Revision 2, which has the proprietary information removed. Portions of the document that have been removed are indicated by an open and closed bracket as shown here [[ ]].

IMPORTANT NOTICE REGARDING CONTENTS OF THIS REPORT

Please Read Carefully

The design, engineering, and other information contained in this document is furnished for the purpose of obtaining NRC approval of the ESBWR certification and implementation. The only undertakings of GEH with respect to information in this document are contained in the contracts between GEH and its customers or participating utilities, and nothing contained in this document shall be construed as changing those contracts. The use of this information by anyone for any purpose other than that for which it is intended is not authorized; and with respect to any unauthorized use, GEH makes no representation or warranty, and assumes no liability as to the completeness, accuracy, or usefulness of the information contained in this document.

No use of or right to copy any of this information contained in this document, other than by the NRC and its contractors in support of GEH's application, is authorized except by contract with GEH, as noted above. The information provided in this document is part of and dependent upon a larger set of knowledge, technology, and intellectual property rights pertaining to ESBWR certification and implementation. Without access and a GEH grant of rights to that larger set of knowledge, technology, and intellectual property rights, this document is not practically or rightfully usable by others, except by the NRC or through contractual agreements with Combined License Applicants and Licensees or customers or participating utilities, as set forth in the previous paragraph.

Copyright 2009, 2010, GE-Hitachi Nuclear Energy Americas LLC, All Rights Reserved

Table of Contents

List of Tables

List of Figures

NEDO-33440 Summary of Changes

NEDO-33440 Changes from Revision 0 to Revision 1 are listed below.

Item	Location	Description of Change
1	Table 1.1	Added 5 rows for the changes from Revision 0 to Revision 1
2	Section 12	Added Section 12 in its entirety in response to RAI 21.6-98 S01
3	Section 13	Added Section 13 in its entirety in response to RAI 21.6-96 S02
4	Section 14	Added Section 14 in its entirety in response to RAI 6.2-98 S02
5	Section 15	Added Section 15 in its entirety in response to RAI 6.2-98 S02
6	Section 12, RAI 21.6-98 Table 1	Added items 29 and 30 in Table 1 of Section 12 in response to RAI 6.2-185 S02

NEDO-33440 Changes from Revision 1 to Revision 2 are listed below.

Item	Location	Description of Change
1	Section 16 and Appendix A	Added Section 16 and Appendix A in their entirety in response to RAI 3.6-11 S03.
2	Section 17 and Appendix B	Added Section 17 and Appendix B in their entirety in response to RAI 3.6-6 S04.

1.0 INTRODUCTION

The purpose of this document is to compile the information requested and commitments made in miscellaneous RAIs resulted from the NRC review on the ESBWR design certification. Those RAIs and associated MFN letters are listed in Table 1.1 and details are presented in the following sections. Only the material included in the RAI submittal is presented in this document. There is no computer analysis or technical evaluation required to support this report. Therefore, there is no conclusions or recommendations included in this report.

Table 1.1

Miscellaneous RAIs

RAI	MFN	Info requested/commitment
6.2-19	06-159	Sensitivity studies to justify time steps and nodalization.
6.2-20 Supplement 1	08-362	Justification on initial conditions assumed in the analysis.
6.2-22	06-159	Description of the piping system within a subcompartment that is assumed.
6.2-23	06-159	Provide the subcompartment nodalization information.
6.2-23 Supplement 1	06-159 Supplement 1	TRACG analysis related information
6.2-23 Supplement 2	08-270	Correct the velocity input errors and resubmit the corrected shield wall pressurization analyses.
6.2-23 Supplement 3	08-681	Provide the basis for selecting of inventory multiplier, updated results in graphical form and include responses to RAI 6.2-23 and associated supplements in a licensing document.
6.2-24	06-159	Provide graphs/results of the pressure responses.
6.2-25	06-159	Provide the mass and energy release data.
21.6-107	08-351	Provide the updated figures and associated description. This request is issued in RAI 21.6-107 S01.
21.6-98	08-545	Provide the response to Confirmatory Items 13 and 20. This request is issued in RAI 21.6-98 S01.
21.6-96 S02	09-216	Provide the response to RAI 21.6-96 S02.

Table 1.1

Miscellaneous RAIs

RAI	MFN	Info requested/commitment
6.2-98 S01	08-011	(A –D) Response to RAI. Understand TRACG calcs for bounding scenario. This request is issued in RAI 6.2-98 S02.
6.2-98 S01 Rev 1	08-454	(E) Response to RAI. Understand TRACG calcs for bounding scenario. This request is issued in RAI 6.2-98 S02.
6.2-185 S01	09-023	Add Table 6.2-185 S01-1 to Section 12 RAI 21.6-98 Table 1. This request is issued in RAI 6.2-185 S02.
3.6-11 S03	09-635	GEH Technical Report 0000-0102-6265-R0 on blast wave calculations.
3.6-6 S04 Part B	09-787 Supplement 3	GEH Technical Report 0000-0105-2955-R6 on jet impingement calculations.

2.0 NRC RAI 6.2-19

Provide a description of the computer program used to calculate the pressures, differential pressures and flow rates between subcompartment. Discuss the conservatism of the model with respect to the pressure response of the subcompartment. Include a discussion of sensitivity studies to justify time steps, nodalization, and any other criteria used by GE to justify the final model used for licensing evaluations. If the computer code being used has not been previously reviewed by the staff, provide a comparison of the results to those predicted by an accepted code as justification for its use. Provide this information in DCD Tier 2, Section 6.2.1.2.3, "Design Evaluation." This information is necessary to evaluate ESBWR subcomparment loads per SRP 6.2.1.2 and RG 1.70, Section 6.2.1.2.

2.1 GE RESPONSE

TRACG was used to calculate the pressures, differential pressures and flow rates between

subcompartment. TRACG was qualified for analysis SBWR and ESBWR reactor system and containment in references listed below, respectively. Four additional TRACG runs have been submitted to determine the effect of time step on the calculated pressure differentials, using timesteps of [[ ]]. All sampled peak maximum pressures are within [[ ]] of the value documented in the analysis of record.

As shown in the response to RAI 6.2-23, the smallest nodes are located around the postulated break. These small nodes have a height of [[ ]] and a width of [[ ]] These dimensions are comparable to the diameter of pipes that are postulated to break. Sensitivity studies have been performed to assess the effects of Annulus Volume, RSW Vent Flow Area and Annulus Hydraulic Diameters. The effects are found to be minor.

2.2 REFERENCES

2-1 "TRACG Qualification for SBWR." GE Nuclear Energy Report NEDC-32725P, September 1997.

2-2 "TRACG Application for ESBWR." GE Nuclear Energy Report NEDC-33083P, November 2002.

3.0 NRC RAI 6.2-20 SUPPLEMENT 1

The GENE response to RAI 6.2-20 provided in GENE letter MFN 06-159, dated June 5, 2006, states that "the reactor is operating at full power and the containment is filled with dry air at atmospheric pressure and 100°C when the postulated pipe break occurs". Confirm whether 2% measurement uncertainty for the reactor power was used and explain why the containment atmosphere was assumed to fill with air instead of nitrogen.

3.1 GEH RESPONSE

The energy of the break flow entering the annulus is the source for the annulus pressurization analysis. Break flow was determined with HEM model based on the pressure and temperature (enthalpy) at the break locations. The current analyses show that the limiting case is the reactor water cleanup (RWCU) line break. The break location is at the RWCU elevation in the downcomer.

The initial pressure and liquid temperature for the 100% power and 102% power cases are compared at the downcomer location. The result shows that the pressure is about the same, and the liquid temperature for the 100% power case is about 1°K higher than that for the 102% case. For bounding break flow and energy entering into the annulus, the current analyses used the downcomer conditions at 100% power for the RWCU break.

The annulus pressurization is a very short term transient. The time duration of interest is completed within a few seconds after the break. The current analyses assumed that the annulus is initially filled with air, instead of nitrogen. This assumption is expected to have little or no impact on the calculated peak subcompartment pressure responses. This assumption is judged to be acceptable because a multiplier of 1.2 was applied to the peak pressures calculated for annulus pressurization before being applied to the structural analyses. This 1.2 multiplier ensures at least 15% margin above the analytical determined pressures (See response to RAI 6.2-18 S01, MFN 06-159 Supplement 1, dated September 12, 2007).

4.0 NRC RAI 6.2-22

Provide a description of the piping system within a subcompartment that is assumed to rupture, the location of the break within the subcompartment, and the break size. Give the inside diameter of the rupture of line and the location and size of any flow restrictions within the line postulated to fail. Provide this information in DCD Tier 2, Section 6.2.1.2.3, "Design Evaluation." This information is necessary to evaluate ESBWR subcompartment loads per SRP 6.2.1.2 and RG 1.70, Section 6.2.1.2.

4.1 GE RESPONSE

Feedwater and RWCU lines are postulated to break separately inside the Reactor Shield Annulus. An instantaneous guillotine break is assumed for each break type. The mass and energy releases from two ends of the break are lumped. [[

]] The feedwater break flow from RPV is restricted by the spargers inside the RPV.

The MSL and DPV pipe breaks are not analyzed in this analysis. The safe end of these pipes extends beyond the annulus region, such that a break would occur outside the RSW and thus not directly pressurize the annulus region. In addition, the IC return and GDCS line pipe breaks are not calculated because the these pipes are smaller than the RWCU and FW lines and will be bounded by breaks in the larger pipes.

5.0 NRC RAI 6.2-23

Provide the subcompartment nodalization information in accordance with the formats of Regulatory Guide 1.70, "Standard Format and Content of Safety Analysis Reports for Nuclear Power Plants (LWR Edition) Rev. 3 (ADAMS ML011340072, ML011340108, and ML011340116), Section 6.2.1.2. Demonstrate that the selected nodalization maximizes the differential pressures as a basis for establishing the design pressures for the structures and component supports. Provide this information in DCD Tier 2, Section 6.2.1.2.3, "Design Evaluation." This information is necessary to evaluate ESBWR subcompartment loads per SRP 6.2.1.2 and RG 1.70, Section 6.2.1.2.

5.1 GE RESPONSE

[[

]]

Sensitivity study of geometric input has been performed as described in the response to RAI 6.2-19.

[[

]]

RAI 6.2-23, Figure 1 – Nodalization Scheme

RAI 6.2-23 Table 1 – Axial (z) Nodalization

[[

]]

RAI 6.2-23 Table 2 – Azimuth (θ) Nodalization

[[

]]

6.0 NRC RAI 6.2-23 SUPPLEMENT 1

In RAI 6.2-23 the staff requested for subcompartment nodalization information in accordance with the formats of Regulatory Guide 1.70, "Standard Format and Content of Safety Analysis Reports for Nuclear Power Plants (LWR Edition) Rev. 3, Section 6.2.1.2. In GE's response, MFN 06-159, GE provided nodal data but stated without specifics that it calculated large pipe and vessel support structure volumes and hydraulic diameters and accounted for the additional obstructions by applying a 10% reduction factor in the annulus volume for cells where a specific obstruction is not modeled.

Please provide the following information needed to perform a confirmatory subcompartment analysis of the vessel/shield wall annular volume:

A. The TRACG input for the reactor shield wall subcompartment analysis.

B. The results of a sensitivity analysis on the number and size of the control volumes used in the shield wall subcompartment analysis. This information is needed to verify the appropriateness of the control volume nodalization used in the final reported analysis.

C. A copy of the calculation used to obtain the break mass and energy releases. This information is needed to confirm the appropriateness of the assumptions used in this calculation.

D. Detailed information and/or drawings describing the space between the reactor vessel and shield wall to include the following:

   1. The outer diameter of the reactor vessel.
   2. A description of the upper and lower heads of the reactor vessel.
   3. A description of the shield wall including inner diameter and the volumes surrounding the upper and lower vessel heads.
   4. The type and thickness of the reactor vessel insulation, and information on how the insulation is treated in the subcompartment analysis (i.e., whether the insulation is assumed to stay in place or blown away and its affect on the calculated volume and nodalization of the annular volume).
   5. A description of the flow obstructions in the reactor vessel/shield wall annular volume: flow area, flow resistance, and flow obstructions providing boundaries for the control volume nodalization.
   6. A description of the flow connections (i.e., flow area and flow resistance) between the reactor vessel/shield wall annulus and the upper part of the drywell.

6.1 GEH RESPONSE

A. Two TRACG input decks are included as Attachments 1 and 2.

FW_r2.bdk for FWL break.

RWCU_r2.bdk for RWCU Line break.

B. The GE experience with annulus pressurization of previous BWRs has indicated that smaller node sizes around the break location resulted in higher pressures. Based on this, smaller node sizes are applied near the break location. The nodalization of ESBWR annulus pressurization was supplied with the response to RAI 6.2-23. The nodes around the postulated breaks, (i.e., Levels 7 through 14) have a dimension of 0.34 m, the smallest size without encroaching the inside diameter of Feedwater or RWCU line.

A sensitivity study was performed to show the impact of the annulus volume. Annulus volumes where no specific obstructions are present were increased by 10%, and the cell volume where the peak pressure occurs was not changed due to presence of obstruction. For a RWCU line break, the peak pressure of the sensitivity cases is reduced to 1.228 MPa, compared to 1.267 Mpa of the base case.

C. Pages showing calculations of mass and energy releases are included as Attachment 3.

D. Following are item-by-item responses.

1. The outer diameter of reactor vessel is 7.476 meters.
2. Descriptions of reactor vessel, including upper and lower RPV heads, are provided in DCD Tier 2, subsection 5.3.3.2.1.
3. The geometry of Reactor Shield Wall (RSW) is shown in the attached figure (Figure 2 Upper Drywell). The inner diameter of RSW is 9.292 meters. The thickness is 0.016 meter.
4. A description of RPV insulation is provided in DCD, Tier 2, subsection 5.3.3.2.2, under the heading "Reactor Vessel Insulation." The insulation is designed to remain in place and resist damage during a safe shutdown earthquake. The reactor insulation is not modeled in the annulus pressurization analysis.

   The effect of blown-away insulation is addressed in a sensitivity study of reduced vent area between the annulus and drywell. A decrease in the RSW to drywell vent flow area (50% reduction) results in practically no change in the peak annulus pressure. Decreasing drywell venting does show a moderate increase in the annulus pressures as the transient progresses, however, since the peak pressure occurs so soon (3 ms) into the transient, the drywell venting does not affect the peak annulus pressures.
5. The annulus contains various piping and support structures that presents a reduction in volume from the ideal cylinder. Large Piping and vessel support structure volumes and hydraulic diameters are calculated to model the obstruction in the annulus nodal volumes. Volumes are minimized for conservatism and simplicity where necessary. For this analysis, the main steam line, feedwater, DPV, and RWCU piping is specifically incorporated. Also, the RPV stabilizer and vessel support structure are incorporated. All other smaller geometries are assumed to be distributed about the annulus. These

additional obstructions are accounted for by applying a 10% reduction in the annulus volume for cells where a specific obstruction is not modeled.

6. The geometry of upper drywell head is shown in DCD Tier 2, Figure 3G.1-51. The flow paths between the drywell head and RSW are shown in the attached figure. The upper drywell head volume is not credited in the annulus pressurization calculation to maximize the annulus pressure.

RAI 6.2-23 Supplement 1, Attachment 1 - FW_r2.bdk for FWL break

[[

]]

RAI 6.2-23 Supplement 1, Attachment 2 - RWCU_r2.bdk for RWCU Line break

[[

]]

RAI 6.2-23 Supplement 1, Attachment 3

[[

]]

[[

]]

RAI 6.2-23 Supplement 1, Figure 2 Upper Drywell.

7.0 NRC RAI 6.2-23 SUPPLEMENT 2

In GEH's response to RAI 6.2-23, Supplement No. 1, Attachment 3, provided detailed calculations of the break boundary conditions for the feedwater line and RWCU/SDC line breaks. For the feedwater line break, page 2 of this attachment indicates that the calculated break velocity is 55.207 m/s for the feedwater line break. Similarly, page 3 of this attachment indicates that the calculated break velocity for the RWCU/SDC line break is 31.764 m/s. The velocity calculations used half the break flow to accommodate the 180° model of the shield wall annulus; however, the full break area, instead of half the break area, was used in the velocity calculations. Consequently, the calculated break velocities were in error by a factor of 2. The correct feedwater break velocity is 110.414 m/s and the correct RWCU/SDC break velocity is 63.528 m/s. These break velocities were directly used in the inputs for the shield wall pressurization analyses provided in Attachments 1 and 2. Please correct the velocity input errors and resubmit the corrected shield wall pressurization analyses for the feedwater and RWCU line breaks.

7.1 GEH RESPONSE:

In the revised annulus pressurization analysis using TRACG computer program, a control block to model the break flow was added to replace the velocity input in the FILL component. In addition, the PIPE component between the VSSL and FILL was removed since this artificially added component was not necessary in the current TRACG version. Only the final cases were rerun and updated since the conclusions from the sensitivity study were not affected.

The reactor water cleanup (RWCU) and feedwater (FW) line pipe break critical mass flow rates are calculated in the updated Attachment 3 below. The total blowdown break flow into the annulus consists of two components, one from the reactor pressure vessel (RPV) side of the break and the other from the pipe side of the break. A critical flow inventory multiplier of 0.5 (Reference 7-1) was applied in the blowdown break flow on the pipe side of the break. There is no change on the RPV side. The break is modeled in TRACG as a FILL component with a control block providing constant break flow rate. Modifications to the input files for the final RWCU and FW cases are presented in Attachments 1 and 2 below.

Results show the RWCU line break to be limiting, with a peak annulus pressure of 1.2124 MPa reached at 1.5 msec after the break, compared to 1.521 MPa at 3 msec from the previous analysis. For FW line break, the peak pressure is 0.8852 MPa and occurs at 13 msec into the transient, compared to 0.877 MPa at 3 msec from the previous analysis.

7.2 REFERENCES

7-1 NEDO-20533-1, "The General Electric Mark III Pressure Suppression Containment System Analytical Model Supplement 1," Appendix B, September 1975.

RAI 6.2-23 Supplement 2, Attachment 1

[[

]]

RAI 6.2-23 Supplement 2, Attachment 2

[[

]]

RAI 6.2-23 Supplement 2, Attachment 3

[[

]]

8.0 NRC RAI 6.2-23 SUPPLEMENT 3

(A) In response to RAI 6.2-23 Supplement 2, GEH changed the critical flow inventory multiplier in the blowdown break flow on the pipe side of the break from the previously used value of 1.0 to 0.5. Please provide the basis for selecting this value.

(B) In response to RAI 6.2-23 Supplement 2, GEH states the following:

"Results show the RWCU line break to be limiting, with a peak annulus pressure of 1.2124 MPa reached at 1.5 msec after the break, compared to 1.521 MPa at 3 msec from the previous analysis. For FW line break, the peak pressure is 0.8852 MPa and occurs at 13 msec into the transient, compared to 0.877 MPa at 3 msec from the previous analysis."

GEH provided previous results in graphical form in letter MFN 06-159, dated June 5, 2006. Please provide the updated results in graphical form.

(C) GEH should include responses to RAI 6.2-23 and associated supplements in a licensing document (such as the proprietary licensing topical report as described in GEH's response to RAI 6.2.-23 in MFN-06-159 dated June 5, 2006).

8.1 GEH RESPONSE

(A) The selection of the multiplier in the blowdown break flow on the pipe side of the break is based on the modeling assumption provided on Page B-12 of the following reference:

NEDO-20533-1, "The General Electric Mark III Pressure Suppression Containment System Analytical Model Supplement 1," Appendix B, September 1975.

The pipe inventory blowdown study documented in NEDO-20533-1 is for the Mark III containment and also applicable to the ESBWR design since the phenomena of the inventory effect is independent of the containment type. The modeling change on the inventory multiplier assumption in the annulus pressurization reanalysis is consistent with the recommendation provided in NEDO-20533-1 and relaxed the overly conservative assumption adopted in the previous analysis.

(B) The updated results in graphical form are presented in the following attachments:

Enclosure 2: RWCU Line Break Result

Enclosure 3: FW Line Break Result

(C) The responses to RAI 6.2-23 and associated supplements will be provided in a new Licensing Topical Report (LTR) entitled: "NEDE-33440P, "ESBWR Safety Analysis – Additional Information," October 2008.

RAI 6.2-23 Supplement 3, Enclosure 2 - RWCU Line Break Result

]]

]]

]]

]]

]]

RAI 6.2-23 Supplement 3, Enclosure 3 - FW Line Break Result

]]

]]

]]

]]

]]

]]

9.0 NRC RAI 6.2-24

Provide graphs of the pressure responses of all subnodes within a subcompartment as functions of time to permit evaluations of the effect on structures and component supports. Provide this information in DCD Tier 2, Section 6.2.1.2.3, "Design Evaluation." This information is necessary to evaluate ESBWR subcompartment loads per SRP 6.2.1.2 and RG 1.70, Section 6.2.1.2.

9.1 GE RESPONSE

The pressure responses of all subnodes (see response to 6.2-23) within the reactor shield annulus as consequence of RWCU and FWL pipe breaks are presented in the attached files. The data cover 0.2 second following the pipe break. Since peak pressures occur at around [[ ]] second, nodal pressures are steady at 0.2 second.

- Final RWCU Line Break
- Final FW Line Break

Each attachment contains nodal pressure charts for different elevations, with curves for different azimuths in each chart. There is also a tabular presentation of the pressures. The plot and column labels follow the TRAC/GRIT labeling convention (Ref TRACG04 User Manual, Table 4.1-1). See also the nodalization diagram provided in RAI 6.2-23.

RAI 6.2-24, Attachment 1 – Final RWCU Line Break

]]

]]

]]

]]

]]

]]

]]

]]

RAI 6.2-24, Attachment 2 – Final FW Line Break

]]

]]

10.0 NRC RAI 6.2-25

Provide the mass and energy release data for the postulated pipe breaks in tabular form, with time in seconds, mass release rate in kg/sec, enthalpy of mass released in kJ/kg, and energy release rate in W/sec. A minimum of 20 data points should be used from time zero to the time of peak pressure. The mass and energy release data should be given for at least the first three seconds. Provide this information in DCD Tier 2, Section 6.2.1.2.3, "Design Evaluation." This information is necessary to evaluate ESBWR subcompartment loads per SRP 6.2.1.2 and RG 1.70, Section 6.2.1.2.

10.1 GE RESPONSE

Steady mass and energy releases, based on the initial operating condition, are assumed for each analysis. The mass release rate is determined with the Moody critical mass flux model.

Feedwater and RWCU lines are postulated to break separately inside the Reactor Shield Annulus. The RWCU line break, from both ends of a guillotine break, is represented by a break area of [[ ]] at an elevation of [[ ]] above the vessel zero. Since only a half annulus is analyzed, the break area for TRACG analysis is [[ ]] The RWCU line assumed upstream coolant temperature and pressure are [[ ]] respectively, representative of the downcomer hydraulic conditions. The discharge velocity is]]

The FW line break is represented by a break area of [[ ]] at an elevation of [[ ]] above the vessel zero. Since only a half annulus is analyzed, the break area for TRACG analysis is [[ ]] The assumed FW line upstream coolant temperature and pressure are [[ ]] respectively, representative of the FW line hydraulic conditions. The discharge velocity is [[ ]]

11.0 NRC RAI 21.6-107

Justify the removal of the figures, or include the updated figures and associated description back into the report.

This RAI is concerning Confirmatory Item No. 4 in NEDC-33083P-A, "TRACG Application for ESBWR," March 2005:

GEH had taken the entire Section 7.1 1 (Containment Components) out of the "Component Model" section in Licensing Topical Report, TRACG Model Description (NEDE-32176P), Rev. 1. As a result, the information on Drywell, Wetwell Air Space, Suppression Pool, and Main Vents, such as included in Table 6.5-3 in Rev. 1, was not present in Rev. 2. Though, GEH has put back Section 7.1 1 in Rev. 3, the Rev. 1 subsection "Model Assessment" has been significantly shortened to "7.1 1.7.7 Model Applicability" in Rev. 3, by removing three figures (Figure 7.1 1-5 Pressure Suppression Test Facility; Figure 7.1 1-6 Drywell Pressure Response; and Figure 7.1 1-7 Vent Flow Transient), and the related description. The staff considers these figures to be important as they showed the facility schematics and dimensions; and compared the TRACG predictions with the measured drywell pressure and vent flow rate data.

Please justify the removal of these figures, or include the updated figures and associated description back into the report.

11.1 GEH RESPONSE

The Figures 7.11-5, 7.11-6, and 7.11-7 [[

]] This rationale provides justification for not including these Figures in the TRACG model description report.

Items a) and b) below provide suitable alternative locations for these Figures.

a) Figure 7.11-5 of Reference [11-1] is [[
]]

b) The TRACG vs. PSTF data comparisons previously reported in Figures 7.11-6 (Drywell pressure) and 7.11-7 (Vent flow rate) of Reference [11-1] have been [[

]]

11.2 REFERENCES

11-1 TRACG Model Description, NEDE-32176P, Revision 1, Class 3, February 1996.

11-2 TRACG Qualification for SBWR, NEDC-32725P, Class 3, September 1997.

11-3 MFN 02-053, Enclosure 1, TRACG Qualification for SBWR , NEDC-32725P, Revision 1, August 2002

[[ ]]

RAI 21.6-107, Figure 21.6-107-1 Drywell Pressure Response (PSTF Test 5703-1)

[[ ]]

RAI 21.6-107, Figure 21.6-107-2 Vent Flow Transient (PSTF Test 5703-1)

12.0 NRC RAI 21.6-98

The staff noted in its acceptance review of ESBWR (Reference 1) that GE did not address all of the confirmatory items that were to be performed at the Design Certification stage as stated in the Staff's SER on TRACG for ESBWR loss of coolant accident (LOCA) analyses (Reference 2). In response to the staff's acceptance review of ESBWR, GE submitted some information (Reference 3) to address the confirmatory items in Reference 2, but this information is still incomplete.

Please address the following confirmatory items:

2. Submit the long-term core cooling analyses.

13. Analyze standard problems and submit to the NRC.

14. Provide all nodalization changes including diagrams since the approval of TRACG for ESBWR LOCA Analyses in Reference 2, include most recent changes incorporated into Rev. 2 of the DCD; Explain the statement in Reference 3 that a "Total of 5 chimneys to calculate the minimum water level." In the TRACG input decks submitted to the staff and in Figures 6.2-6 and 6.2-7, the core/chimney section is divided into only 3 rings.

19. GE needs to submit additional information on the passive containment cooling system (PCCS) vent system demonstrating that it will perform as expected.

20. Describe all design changes since the approval of TRACG for ESBWR LOCA Analyses in Reference 2 and demonstrate that the staff's conclusions would not be altered as a result of these changes.

References:

1. Letter to S.A. Hucik (GE) from W.D. Beckner (NRC), "Results of Acceptance Review for ESBWR Design Certification Application (TAC No. MC8168)," September 23, 2005

2. Letter to L.M. Quintana (GE) from W.D. Beckner (NRC), "Reissuance of Safety Evaluation Report Regarding the Application of General Electric Nuclear Energy's TRACG Code to ESBWR Loss-of-Coolant Accident (LOCA) Analyses (TAC NOS. MB6279, MB6280, MB6281, MB6282, MB6283, MB6801 and MB7255)," October 28, 2004

3. Letter from D.H. Hinds (GE) to NRC, MFN 05-096, "Summary of September 9, 2005 NRC/GE Conference Call on TRACG LOCA SER Confirmatory Items," September 20, 2005

12.1 GEH RESPONSE

2. Submit the long-term core cooling analyses.

The long-term core cooling analyses have already been submitted to the NRC through GEH letter MFN 07-377 (Reference 12-1).

13. Analyze standard problems and submit to the NRC.

Two standard problems, one integral containment test and one separate-effects test, have been selected and simulated with TRACG. The TRACG simulation results for the integral Marviken blowdown test #18 – International Standard Problem 17 (Reference 12-2) are included in Attachment A. The TRACG simulation results for the Wisconsin Flat Plate separate-effects condensation tests (References 12-3 and 12-4) are included in Attachment B.

14. Provide all nodalization changes including diagrams since the approval of TRACG for ESBWR LOCA Analyses in Reference 2, include most recent changes incorporated into Rev. 2 of the DCD; Explain the statement in Reference 3 that a "Total of 5 chimneys to calculate the minimum water level." In the TRACG input decks submitted to the staff and in Figures 6.2-6 and 6.2-7, the core/chimney section is divided into only 3 rings.

The changes made in TRACG nodalization for ESBWR LOCA analyses since the approval of the ESBWR LOCA analyses (Reference 12-5) and Rev. 2 of DCD are discussed in Sections 6A and 6B of DCD Tier 2, Rev. 4 (Reference 12-6).

As indicated in Item #16 of DCD Table 6.2-6a (Summary of ESBWR TRACG Nodalization Changes) in Reference 12-6, two individual chimneys are added besides the three super chimneys representing each of the three rings in the reactor vessel. This addition facilitates calculation of collapsed water levels in individual chimneys.

19. GE needs to submit additional information on the passive containment cooling system (PCCS) vent system demonstrating that it will perform as expected.

The ESBWR PCCS vent system, especially the vent submergence, has been re-evaluated and addressed in another GEH submittal documented in MFN 08-338 (Reference 12-7), which demonstrates that the system would adequately condense steam as required.

20. Describe all design changes since the approval of TRACG for ESBWR LOCA Analyses in Reference 2 and demonstrate that the staff's conclusions would not be altered as a result of these changes.

Table 1 summarizes all design changes that impact the LOCA analysis since the approval of TRACG for ESBWR LOCA analysis (Reference 12-5) through DCD Tier 2, Rev. 5 (Reference 12-10). Items #1 through #18 in the table describe all design changes since the approval of TRACG for ESBWR LOCA analyses (Reference 12-5) through DCD Tier 2, Rev. 2 (Reference 12-9). These were also submitted to the NRC via GEH letter MFN 05-105 (Reference 12-8). Items #19 through #28 in the table describe all design changes since DCD Tier 2, Rev. 2 through Rev. 5. The impacts of these changes on LOCA analyses have been re-analyzed and documented in Sections 6.2 and 6.3 in DCD Rev. 5 (Reference 12-10).

12.2 REFERENCES

12-1 GE Hitachi Nuclear Energy, MFN 07-377, Response to Portion of NRC Request for Additional Information Letter No. 96 – Emergency Core Cooling Systems – RAI Number 6.3-79, August 24, 2007.

12-2 Jan-Erik Marklund, Swedish Nuclear Power Inspectorate, "Data Comparison for ISP17 An International containment standard problem based on the Marviken full scale experiment Blowdown Number 18," STUDSVIK/NR-84/466, 1984.

12-3 Huhtiniemi, Ilpo K., "Condensation in the presence of non-condensable gas: Effect of surface Orientation," Ph. D. Thesis, University of Wisconsin – Madison, 1991.

12-4 I. K. Huhtiniemi and M. L. Corradini, "Condensation in the presence of non-condensable gases," Nuclear Engineering and Design, Vol. 141, 429-446, 1993.

12-5 GE Nuclear Energy, "TRACG Application for ESBWR," NEDC-33083P-A, Class III, (Proprietary), March 2005, and NEDO-33083-A, Class I (non-proprietary), October 2005.

12-6 GE Hitachi Nuclear Energy, ESBWR Design Control Document, Tier 2, Chapter 6, Engineering Safety Features. 26A6642AT, Revision 4, September 2007.

12-7 GE Hitachi Nuclear Energy, MFN 08-338, Response to Portion of NRC Request for Additional Information Letter No. 120 – Related to ESBWR Design Certification Application – RAI Number 21.6-106, April 7, 2008.

12-8 GE Energy, MFN 05-105, TRACG LOCA SER Confirmatory Items (TAC # MC8168), Enclosure 2 – Major Design Changes from Pre-Application Review Design to DCD Design, October 6, 2005.

12-9 GE Nuclear Energy, ESBWR DCD Tier2, Chapter 6, "Engineering Safety Features", Rev. 2, 26A6642AT, November 2006.

12-10 GE Hitachi Nuclear Energy, ESBWR DCD Tier2, Chapter 6, " Engineering Safety Features ", Rev. 5, 26A6642AT, May 2008.

RAI 21.6-98 Table 1. Major Design Changes from Pre-Application Review Design to DCD Rev. 5

Item	Parameter	Pre-App. Design (Ref. 1.5)	DCD Rev. 5 Design (Ref. 1.10)	DCD Rev. Posted	Reason for change	Impact on LOCA analysis	Justification for the Applicability of TRACG
1	Core Power, MW	4000	4500	0	Power uprate – improved economics.	Higher core exit and chimney void fraction.	No new phenomena introduced, power density unchanged, selected system capacities increased. TRACG applies to new design.
2	No. of Bundles	1020	1132	0	Increased to maintain power density.	Geometry change, increased shroud diameter.	No new phenomena introduced. TRACG applies to new design.
3	Change in Core Shroud Size	Base	+0.328 m	0	Increased to accommodate additional bundles.	Loss of liquid volume in downcomer (26%). Larger initial level drop.	Additional water sources included in analysis to maintain margin to core uncovery.
4	Core Lattice	F lattice w/ wide blades	N lattice, standard blades	0	Simplification – similar to current BWR cores.	No significant LOCA effect.	No new phenomena introduced. TRACG applies to new design.
5	No. of CRDs	121	269	0	Result of going back to N lattice.	No significant LOCA effect.	No new phenomena introduced. TRACG applies to new design.
6	GDCS Pool and Airspace Location	Wetwell	Drywell	0	Simplification. Additional containment pressure margin not needed.	Tested configuration for SBWR. Loss of containment pressure margin accommodated by reduced suppression pool heatup.	TRACG applicable to both configurations; testing included both.
7	PCCS	4 x 13.5 MW	6 x 11 MW	0	Increased power level.	Percent increase larger than core power increase. Reduces pool heatup.	Heat exchanger consistent with tested prototype. TRACG applicable to the larger number of PCCS units.

RAI 21.6-98 Table 1. Major Design Changes from Pre-Application Review Design to DCD Rev. 5

Item	Parameter	Pre-App. Design (Ref. 1.5)	DCD Rev. 5 Design (Ref. 1.10)	DCD Rev. Posted	Reason for change	Impact on LOCA analysis	Justification for the Applicability of TRACG
8	ICS	4 x 30 MW	4 x 33.75 MW	0	Increased power level.	Maintains 3% capacity.	Tube geometry consistent with prototype, small increase in manifold length. TRACG applicable to the longer IC manifold.
9	Pressure Relief System	12 ADS valves	10 ADS valves + 8 SRV	0	Increased relief capacity.	Minor impact on minimum water level.	TRACG critical flow model is independent of the number of valves; code is applicable to current design.
10	Containment Vents	10	12	0	Reduced blowdown mass fluxes in vents.	Minor effect on LOCA pressure and temperature.	Reduces vent flow rate, within TRACG application range.
11	Feedwater System		30 sec delay on L2; scram on LOFW; safety grade (1E) FW pump trip on FW line differential pressure.	2	Time delay on L2 to avoid unnecessary isolations and IC initiation when FW available. Early scram on LOFW helps initial level drop. FW pump trip terminates FW pumping additional mass and energy into containment via broken FW line.	Scram on LOFW is a slight benefit for small breaks. FW pump trip has no impact on LOCA analysis because loss of AC power is assumed.	TRACG control system capable of modeling design change.

RAI 21.6-98 Table 1. Major Design Changes from Pre-Application Review Design to DCD Rev. 5

Item	Parameter	Pre-App. Design (Ref. 1.5)	DCD Rev. 5 Design (Ref. 1.10)	DCD Rev. Posted	Reason for change	Impact on LOCA analysis	Justification for the Applicability of TRACG
12	Turbine Bypass Capacity	33%	110% option	0	Flexibility.	No LOCA effect, slight reduction in number of scrams/ year and improved reliability of on-site AC.	TRACG control system capable of modeling design change.
13	PCC Drain Tanks	In drywell	Eliminated; PCCS drains to GDCS pools	0	Simplification.	Tested configuration for SBWR.	TRACG applicable to new configuration.
14	Suppression Pool (SP) Volume	3610 m^3 (127486 ft^3)	4424 m^3 (156232 ft^3)	0	DW/GDCS pool & WW diameter increased to provide improved equipment clearances. Additional benefit: larger suppression pool size.	Reduces pool heatup.	No new phenomena introduced. TRACG code applicable to changed volume.
15	DW/WW Volume Ratio	1.31	1.33	0	Ratio was not exactly maintained in containment diameter increase.	Small increase in containment pressure.	No new phenomena introduced. TRACG code applicable to changed volume.
16	Spillover Connection (DW Annulus to SP)	Holes	Pipes discharging to SP at elevation of bottom horizontal vent.	2	Enhanced SP mixing.	Reduces pool heatup and wetwell pressure. Pipes are closed until after the RPV blow down to prevent any change in hydrodynamic loads.	No new phenomena introduced. Discharge location consistent with bottom horizontal vent. TRACG code applicable.

RAI 21.6-98 Table 1. Major Design Changes from Pre-Application Review Design to DCD Rev. 5

Item	Parameter	Pre-App. Design (Ref. 1.5)	DCD Rev. 5 Design (Ref. 1.10)	DCD Rev. Posted	Reason for change	Impact on LOCA analysis	Justification for the Applicability of TRACG
17	Lower DW Free Volume to Top of Active Fuel Elevation	1564 m^3 (55232 ft^3)	1190 m^3 (42024 ft^3)	2	Lower drywell volume reduced.	Improved long term LOCA response in bottom drain line and GDCS breaks.	No new phenomena introduced. TRACG code applicable to changed volume.
18	SLCS Activated on ADS	No	Yes	2	Compensate for larger initial level drop	Improves LOCA minimum water level	TRACG models are applicable to liquid flow into bypass.
19	ICS In-Line Vessel	No	One 9m^3 (318 ft^3) each train	3	Improved water level margin for AOO and SBO events.	Use of a single level logic for ECCS initiation. Increased RV water level during LOCA.	No new phenomena introduced. TRACG code applicable to changed volume.
20	SRV Capacity	124 kg/s; 126 kg/s	138 kg/s; 140.2 kg/s	3	In compliance of eighteen SRVs capacity equivalent to 102% rated nuclear boiler capacity.	Minimal impact on containment pressure and RV water level responses.	No new phenomena introduced. TRACG code applicable to increased SRV capacity.
21	Feedwater Isolation Valve Configuration	5 valves per line (1 manually-operated gate valve, 3 in-series check valves, and 1 motor-operated gate valve)	4 process-operated valves per line (2 primary-containment-isolation valves, 2 shutoff valves)	3	Resolved lack of effective isolation in the event of a design basis feedwater line in-containment rupture.	Adds rapid closure of feedwater high-energy line break. Increases RV depressurization rate. Reduces containment pressurization.	No new phenomena introduced. TRACG code applicable to new feedwater-line nodalization.

RAI 21.6-98 Table 1. Major Design Changes from Pre-Application Review Design to DCD Rev. 5

Item	Parameter	Pre-App. Design (Ref. 1.5)	DCD Rev. 5 Design (Ref. 1.10)	DCD Rev. Posted	Reason for change	Impact on LOCA analysis	Justification for the Applicability of TRACG
22	Containment Drywell-SP Connection	Spillover pipes and float valves	Spillover holes 200 mm (7.87 in) at elevation 12.37 m (40.6 ft). GDCD drain line suction elevation 18.292 m (60 ft).	3	Reducing hot feedwater overflow from DW annulus into SP, with feedwater line isolation.	Reduces peak containment pressure.	No new phenomena introduced. TRACG code applicable.
23	Main Steam Line Changes	Nominal diameter = 700 mm (28 in) upstream of MSIVs; DPVs on Main Steam Line	Nominal diameter = 750 mm (30 in) upstream of MSIVs; DPVs on Isolation Condenser lines	5	Mitigation of the stall condition by reducing average velocity, and eliminating a source for acoustic loads in the Main Steam Line.	Minimal impact on LOCA.	No new phenomena introduced. TRACG code applicable.
24	Turbine Main Steam Piping Diameter	Nominal diameter = 800 mm (32 in)	Nominal diameter = 750 mm (30 in)	5	Optimize mass flow rate through the main steam piping and reduce pressure losses.	Minimal impact on LOCA.	No new phenomena introduced. TRACG code applicable.
25	Main Steam Isolation Valve	28-in (711mm) globe valve	30-in (762mm) gate valve	5	Permitting adjusting the total main steam isolation system pressure drop at rated steam flow.	Minimal impact on LOCA.	No new phenomena introduced. TRACG code applicable to new MSIV configuration.

RAI 21.6-98 Table 1. Major Design Changes from Pre-Application Review Design to DCD Rev. 5

Item	Parameter	Pre-App. Design (Ref. 1.5)	DCD Rev. 5 Design (Ref. 1.10)	DCD Rev. Posted	Reason for change	Impact on LOCA analysis	Justification for the Applicability of TRACG
26	PCCS Vent Fan	None	One 1-HP, 727 CFM ventilation fan per PCCS vent line ending submerged in GDCD pool operational after 72 hrs.	5	Remove accumulated non-condensable gases in the PCCS tubes to greatly enhance heat transfer rate in the PCCS.	Rapidly reduces containment DW pressure when putting in service at 72 hours after a LOCA.	No new phenomena introduced. TRACG code applicable.
27	Drywell Spray Flow	0.06308 m^3/s (1000 gpm)	0.03533 m^3/s (560 gpm)	5	Optimize containment spray 72 hours after a LOCA.	Controlled depressurization of the DW, when putting in service at 72 hours after a LOCA.	No new phenomena introduced. TRACG code applicable.
28	Crosstie between FAPCS and RWCU	None	Cross-tie from FAPCS suction line to RWCU train A upstream of the non-regenerative heat exchangers	5	Rapidly reduce containment pressure and temperature 7 days after a LOCA.	Controlled depressurization and cooldown of the DW airspace, when putting in service 7 days after a LOCA.	No new phenomena introduced. TRACG code applicable.

RAI 21.6-98 Table 1. Major Design Changes from Pre-Application Review Design to DCD Rev. 5

Item	Parameter	Pre-App. Design (Ref. 1.5)	DCD Rev. 5 Design (Ref. 1.10)	DCD Rev. Posted	Reason for change	Impact on LOCA analysis	Justification for the Applicability of TRACG
29	Vacuum Breakers	2 vacuum breakers with area 0.2033 m^2	1 vacuum breaker with area 0.0967 m^2	5	The area available from the vacuum breakers assumed available for LOCA was reduced to minimize operability requirements including their numbers, reduced from 2 to 1.	The results of the parametric cases performed indicate insignificant impact on key parameters like minimum chimney level and maximum DW pressure. Separate DW-to-WW leakage path is included in LOCA analysis	No new phenomena introduced. TRACG code applicable.
30	IC steam line elevation	Elevation 22.84 m	Elevation 21.91 m	5	The IC steam supply line was modified in order to conform with the RPV design in DCD Rev. 5.	Minimal impact on Containment LOCA.	No new phenomena introduced. TRACG code applicable.

ATTACHMENT A: TRACG SIMULATION OF INTERNATIONAL STANDARD PROBLEM 17 - MARVIKEN BLOWDOWN TEST #18

A.1. Summary

The following paragraphs describe the TRACG results in comparison with the Marviken full-scale containment test – International Standard Problem (ISP) 17 (Reference A-1). The purpose is to evaluate the capability of TRACG with respect to:

- Vent clearing transient (Short-term)
- Steam/air transport through vent system (Long-term)
- Containment pressure and temperature responses (Short- and Long -term)

ISP 17 was based on the Marviken Full Scale Experiment Blowdown Test Number 18, which was to study the behavior of a large-scale pressure suppression system under LOCA conditions. The Marviken test facility is converted from a decommissioned nuclear power plant. The large pipe break is located at the bottom of the reactor vessel. The containment is compartmentalized (Figure A-1), and the Drywell (DW) is located on the top of the Wetwell (WW). The DW connects to the WW through four large steel vent pipes connecting to a common header, which in turn connects to 58 vent pipes vertically submerged in the suppression pool. For Test # 18, 28 of these vertical vent pipes were open and the rest of vent pipes were plugged during the test.

In this evaluation, TRACG calculated results are compared with the ISP17 test data. The comparisons consist of two different time frames: short term covers the period from 0 to 4.4 seconds and long term covers the period from 0 to 220 seconds.

The results of comparisons between the TRACG calculations and the measurements are summarized in the following.

(1) Vent Clearance: The TRACG results agree very well with the data for the duration of the vent clearing, and the TRACG prediction of the timing of the vent clearance is within [[ ]] second of the measurement.

(2) DW, WW, and Header Pressures: For the short-term comparisons, TRACG predictions of the DW, WW, and header pressures are within the error band (±8.1 kPa) of the data. For the long-term comparisons, the TRACG predictions of the peak DW pressure is about [[ ]] higher than the measurement, and the peak header pressure is about [[ ]] higher than the measurement, and the peak WW pressure is about [[ ]] higher than the measurement but well within the error band (±8.1 kPa) of the data.

(3) DW and WW Gas (air and steam mixture) and Pool Water Temperatures: For both the short-term and long-term comparisons, TRACG predictions of the DW gas temperature match very well with the data. The predicted long-term WW gas temperature follows the same trend as the measurement, but the peak is about [[ ]] higher than the measurement. The calculated long-term average Pool temperature agrees well with the measurement, and the calculated peak temperature is about [[ ]] higher than the measurement, which is within the maximum data error bound of ±4.3°C.

(4) Air Mass: The calculated total air mass through vents agrees very well with the computed test data. At 160 seconds, the TRACG calculated total air mass is about [[ ]] lower than the computed data, which is about [[ ]] of the initial DW air mass.

(5) At the end of the blowdown phase at 160 seconds, the TRACG calculation and computed Marviken data show that there is still a significant amount of air remaining in the DW, about 12% of the initial DW air mass.

In conclusion, the TRACG calculations agree very well with the Markiven test data, taking into consideration of the uncertainties in the measurements. Detail comparisons are presented in Figures A-6 through A-28, and discussions in Section A.5.

A.2. Data Uncertainties

The experimental data accuracies are reported in the form of maximum errors and probable errors. The maximum error calculation applied to the whole data channel with high confidence. Whereas, the probable error is defined as one standard deviation or a confidence level of 68% (Sec. 2.4, Reference A-2). Table A-1 lists the upper bound measurement errors of data documented in Reference A-2.

RAI 21.6-98 Table A-1 Data Measurement Errors

Parameter	Maximum Error	Probable Error (± 1σ)
Discharge Mass Flow Rate	± 20%	± 7%
Specific Enthalpy	+3%/-1%	N/A*
Wetwell Air Mass Flow Rate	> ± 6%	± 6%
Wetwell Steam Mass Flow Rate	± 40%	± 15%
Wetwell Water Mass Flow Rate	N/A*	N/A*
Discharge Pipe Pressure	± 90 kPa	± 50 kPa
Containment Pressure	± 8.1 kPa	± 1.2 kPa
Containment DP	± 2.1 kPa	± 2.0 kPa
Containment Temperature	± 4.3°C	± 1°C
Pool Swell Level	N/A*	N/A*
Vent Water Plug Size	N/A*	N/A*

* N/A = Not Available

A.3. TRACG Simulation Major Assumptions

(1) The heat loss from the DW and WW outer walls to the facility environment is neglected.

(2) Aluminum heat soakage is assumed to be lump parameter heat slab because in Marviken facility (aluminum is only ~1mm thick). Steel and concrete are assumed to have uniform thickness and are treated as double-sided heat slab in TRACG.

A.4. TRACG Model of Marviken Experiment

Figure A-1 shows the schematic diagram of the Marviken test facility. Figure A-2 shows the TRACG nodalization of the test facility. Table A-2 shows the initial conditions inside the containment (Table A.12, Reference A-2). The nodalization utilizes [[

]]. The nodalization also models the flow paths that connect the various regions. The DW connects to the WW by a vent system (Figure A-1), which consists of four large steel pipes, a header and 58 vertical vent pipes that submerged into the suppression pool. For Test # 18, 28 of these vertical vent pipes were open and the rest of vent pipes were plugged during the test.

The subcompartment numbers labeled in the TRACG nodalization (Figure A-2) are the same as those labeled in the Marviken test facility (Figure A-1). The nodalization for the Marviken test facility closely resembles the containment nodalization for the ESBWR LOCA analyses, consisting of [[

]]. The condensation model (Kuhn-Schrock-Peterson laminar film correlation, Sec. 6.6.11 in Reference A-3) is used in this simulation and consistent with that used in the ESBWR LOCA containment analyses in the DCD (Reference A-4).

The containment geometries, heat structures, and initial conditions are modeled to match those described in Reference A-2. The mass flow rate and enthalpy of the blowdown discharge flow rate documented in Table A.11 of Reference A-2 are used as the input boundary conditions to the TRACG model. In this simulation, the air mass flow rate from the DW through the vertical vent pipes is an internally calculated TRACG output.

A.4.1. Break Flow and Enthalpy

Figures A-3 through A-5 show the break flow rate and enthalpy histories documented in Reference A-2, which are used as input boundary conditions in the TRACG simulation. As shown in the Figures, three distinct blowdown phases can be identified. During the first 1.2 seconds the blowdown was single-phase liquid, and then transitioned into two-phase between 1.2 and 165 seconds, and finally became single-phase steam after 165 seconds. The break flow was discharged into the top of Room # 122.

A.5. TRACG Simulation Results

A.5.1. Short-term Results

The calculated TRACG short-term (0 to 4.4 seconds) results compared with the Marviken test data are given in Figures A-6 through A-15, and discussed in the following subsections.

A.5.1.1 Short-term Pressure Results

Figures A-6, A-7, and A-8 show the comparisons of the short-term pressures in the DW (Room 122), header (Room 106), and WW air space (Room 105), respectively. The TRACG pressure calculations follow closely with those of Marviken data. [[

]] The

maximum TRACG errors are within the measurement uncertainties of ±8.1 kPa reported for the containment pressure.

The TRACG header pressure calculation in Figure A-7 indicates a pressure oscillation during the initial [[ ]] seconds of the blowdown. This oscillation also shows up in the pressure differences between the DW and header in Figure A-9, and header and WW in Figure A-10. This oscillation could be attributed to the virtual-mass acceleration effect of water in the vent pipe before the vent is cleared. The experimental data in Figure A-9 also show similar oscillations.

A.5.1.2 Short-term Temperature Results

Figures A-11, A-12, and A-13 show the comparisons of the short-term gas (air and steam) mixture temperature in the DW (Room 122), header (Room 106) and WW air space (Room 105), respectively. As shown in Figure A-11, the TRACG DW gas temperature prediction follows closely with the data, well within the maximum data uncertainty of ±4.3°C. As shown in Figure A-12, the TRACG header gas temperature prediction is higher than the test measurement for the first [[ ]] seconds. The test data show a slow increase trend for the first 1.8 seconds, followed by a rapid increase trend. This could be due to water still attached to the temperature probes until the vent pipe cleared of water at 1.3 seconds (Figure A-14). As shown in Figure A-13, the measured WW gas temperature remains almost unchanged during the short-term, while the TRACG prediction indicates a gradual increase starting at [[ ]] seconds. This could be due to "*the heat transfer coefficient for the temperature transducers is quite small up to the vapor break-through the pool water surface at around 3 seconds, thus slowing down the temperature response of the probe*" (P. 45, Reference A-2).

A.5.1.3 Short-term Vent-Clearing Results

Figure A-14 shows the comparison of the average water column height in the vent pipes. The calculated TRACG results agree very well with the measurement for the duration of the vent clearing, and the timing of the vent clearance predicted by TRACG is within [[ ]] second of the measurement. As shown in Figure A-15, the calculated TRACG pool swell level is in good agreement with the measurement for the first [[ ]] seconds. The calculated TRACG maximum height of 4.8 m (relative to the vent outlet elevation) is reached at [[ ]] seconds as compared to the measured 2.9 seconds. This result is excellent according to Sec. 5.1.17 of Reference A-2, which states:

> "*The bottom of the header, which drastically changes the available cross-sectional area (of the pool), is roughly 4.8 m above the vent pipe outlet (zero point of the level scale). Therefore, not too much attention should be paid to the behavior above that level for the measured data.*"

A.5.2. Long-term Results

The calculated TRACG long-term (0 to 220 seconds) results compared with the Marviken test data are given in Figures A-16 through A-28, and discussed in the following subsections.

A.5.2.1 Long-term Pressure Results

Figure A-16 shows the comparison of the long-term DW-to-WW pressure difference (Rm. 110-105) results. Between the initial [[ ]] seconds, the TRACG calculated peak pressure difference is about [[ ]] higher than the maximum of measurement. After 60 seconds, the difference between TRACG and measured data gets smaller. Figure A-17 shows the comparison of Header-to-WW air space pressure difference. Between the initial [[ ]] seconds, the calculated TRACG peak pressure difference is about [[ ]] higher than the maximum of measurement. However, between [[ ]] seconds, the calculated pressure difference falls between the measurement maximum and minimum bounds.

Figure A-18 shows the comparison of the long-term DW pressure (Room 110) results. The calculated TRACG peak DW pressure is about [[ ]] higher than the measurement, and closely follows the trend of the measurement. Figure A-19 shows the comparison of the header pressure (Room 106) results (data not available for time < 45 seconds). The calculated TRACG peak header pressure is about [[ ]] higher than that of the measurement. However, the calculated header pressure falls within the maximum bound of the measurement between [[ ]] seconds. Figure A-20 shows the comparison of the WW pressure (Room 105) results. The calculated peak TRACG WW pressure is about [[ ]] higher than that of the measurement and well within the error band (±8.1 kPa) of the data, and follows the same trend as the measurement.

A.5.2.2 Long-term Temperature Results

Figures A-21 through A-24 show the temperature comparisons of the DW (Room 111), header (Room 106), WW air space (Room 105), and Pool, respectively.

As shown in Figure A-21, the calculated DW temperature agrees well with the measurement well within the maximum error of ±4.3°C. The slightly higher DW temperatures predicted by TRACG could be due to the slightly higher predicted air mass trapped in the DW (Figure A-26), thus resulting in less wall condensation heat transfer.

As shown in Figure A-22, the calculated header temperature follows closely with the measurement (peak error of +4°C), barely touching the upper error bound of measured data for the most of the duration.

The calculated TRACG WW gas temperature follows the same trend as the measurement, but is higher than the measurement by as much as [[ ]] as shown in Figure A-23. One possible explanation for the lower measured value is that *"there could also be some delay in the measured data due to slow reaction of probes, and in particular due to water drops attaching to the probes"* (Sec. 5.2.8, Reference A-2).

As shown in Figure A-24, the calculated TRACG average Pool temperature agrees well with the measurement. The calculated peak temperature is about [[ ]] higher than the measured value, which is within the maximum error bound of ±4.3°C.

A.5.2.3 Long-term Wetwell Air and Steam Mass Flow Results

Figures A-25 and A-26 show the comparisons of the air mass flow rate and the total air mass through the vent pipes, respectively. The Marviken data shown on these figures are not actually measured, but computed with the ideal gas law based on the measured pressures and

temperatures in the WW gas space and measured pool temperature between 0 and 55 seconds (Sec. 5.2.10, Reference A-2).

As shown in Figure A-26, the predicted total air mass by TRACG agrees very well with the revised Marviken data. At 160 seconds (end of the two-phase blowdown phase), TRACG predicts a significant amount of air still remaining in the DW, about [[ ]] of the initial DW air mass. Data also shows comparable amount of air (12% of initial amount) remaining in the DW.

Figure A-27 shows the comparison of the steam mass flow rate through the vent pipes. As shown, TRACG calculation under-estimates the initial peak steam mass flow rate by about [[ ]]. However, this is within the probable error of 15% (or 1σ) of the measurement. While near the end of blowdown, the calculated steam mass flow rate drops sharply to zero at about [[ ]] seconds later.

Figure A-28 shows the comparison of the total steam mass through the vent pipes. As shown, the calculated TRACG steam mass passing through the vents lags behind the measurement by about [[ ]] seconds. However, at the end of blowdown at 170 seconds, the total steam mass calculated by TRACG matches the measured value very well.

A.6. Conclusions

Extensive comparisons of TRACG simulation results with measured data from the Marviken blowdown test #18 have demonstrated that TRACG is able to predict both the short-term and long-term DW and WW pressure and temperature responses within the data uncertainties for most of the blowdown duration. Furthermore, TRACG is able to predict the vent clearance timing within [[ ]] seconds of measurement.

A.7. References

A-1 Committee on the Safety of Nuclear Installations, "International Standard Problems (ISP) Brief descriptions (1975-1999)," Nuclear Energy Agency, NEA/CSNI/R(2000)5, March 2000.

A-2 Jan-Erik Marklund, Swedish Nuclear Power Inspectorate, "Data Comparison for ISP17 An International containment standard problem based on the Marviken full scale experiment Blowdown Number 18," STUDSVIK/NR-84/466, 1984.

A-3 GE Hitachi Nuclear Energy, "TRACG Model Description," NEDE-32176P, Rev. 4, January 2008.

A-4 GE Hitachi Nuclear Energy, ESBWR DCD Tier2, Chapter 6, " Engineering Safety Features ", Rev. 5, 26A6642AT, May 2008.

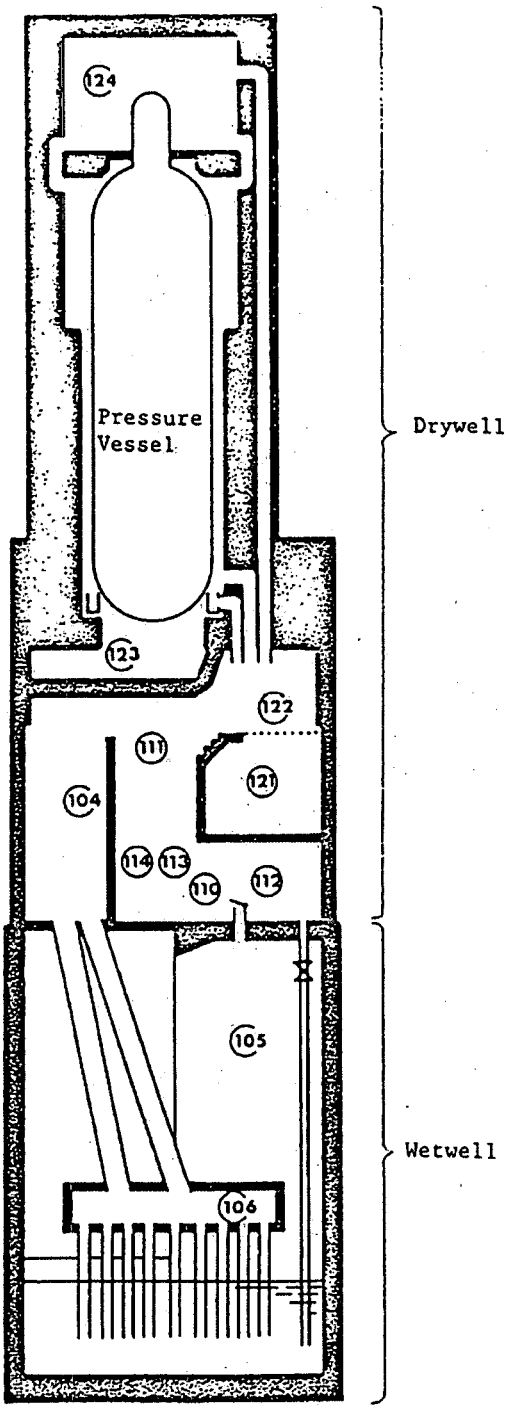

RAI 21.6-98 Figure A-1. Schematic of the Marviken Test Facility

[[ ]]

RAI 21.6-98 Figure A-2. TRACG Nodalization

RAI 21.6-98 Table A-2. TRACG Initial Conditions

Initial Containment Temperature and Pressure						
Compartment	Color Code	Temp (°C)	Humidity (g/kg)	Initial PA (bar)	Initial PV (bar)	Initial PN (bar)
DW AirSpace		61.0	12	0.994	0.051	1.045
DW AirSpace		49.5	9	0.977	0.068	1.045
DW AirSpace		21.9	4	0.904	0.141	1.045
DW AirSpace		19.0	4	0.904	0.141	1.045
POOL		16.0				
WW AirSpace		16.0		1.027	0.018	1.045

PA = partial pressure of air
PV = partial pressure of steam
PN = total pressure of mixture

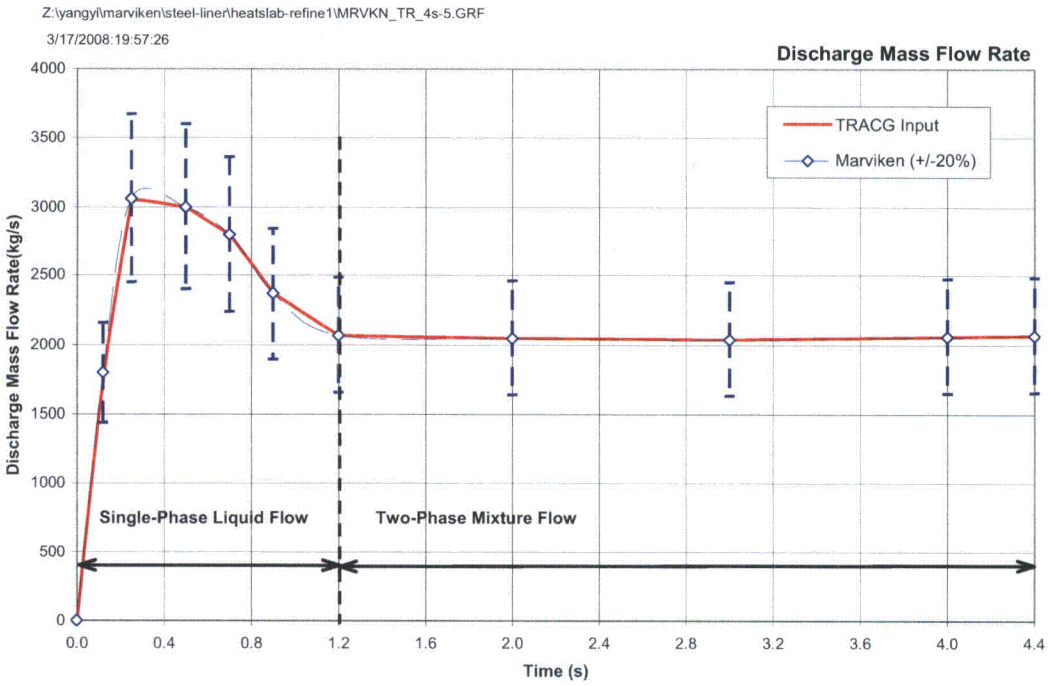

RAI 21.6-98 Figure A-3. Break Flow Rate Inputs in TRACG Simulation (4.4s)

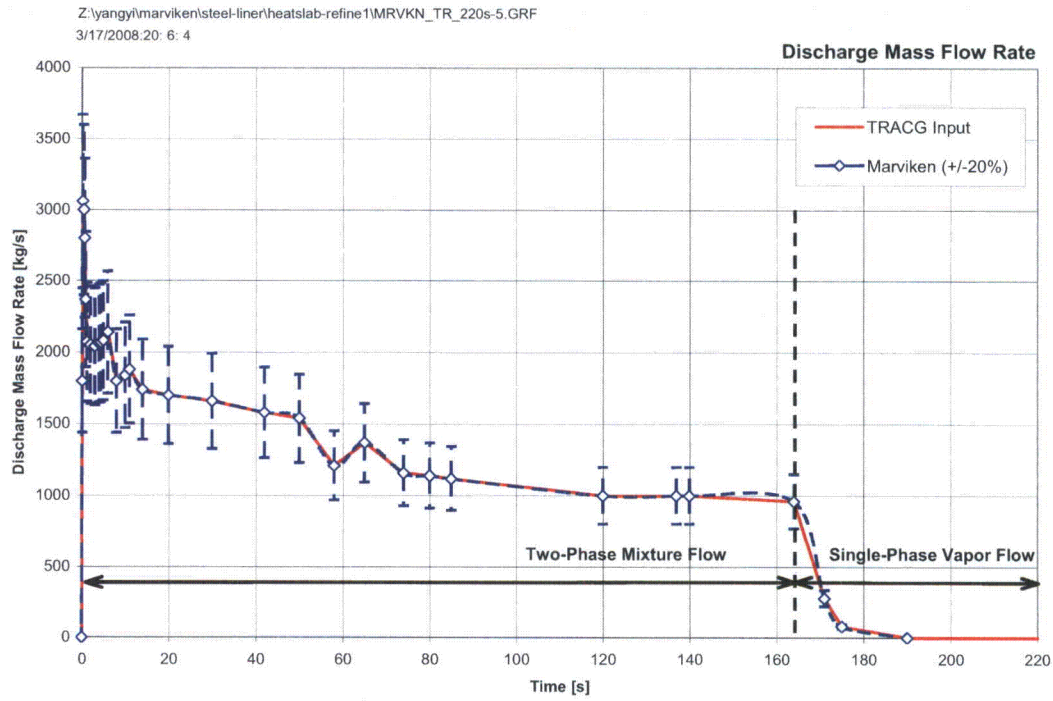

RAI 21.6-98 Figure A-4. Break Flow Rate Inputs in TRACG Simulation (220s)

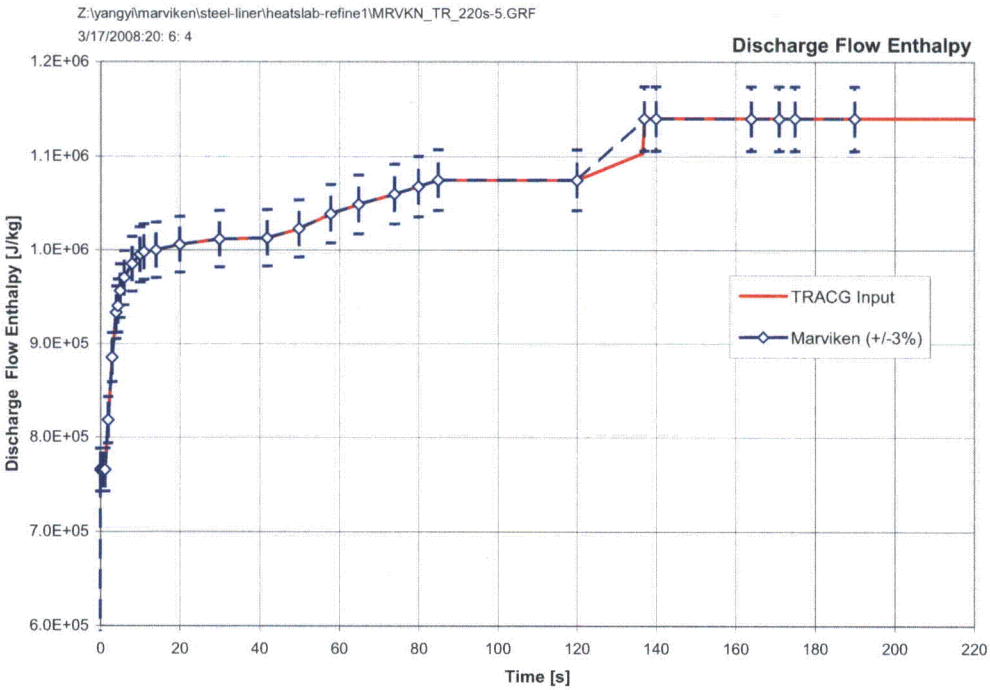

RAI 21.6-98 Figure A-5. Break Enthalpy Inputs in TRACG Simulation

[[ ]]

RAI 21.6-98 Figure A-6. DW Pressure (Rm. 122) – Short-term

[[ ]]

RAI 21.6-98 Figure A-7. Header Pressures (Rm. 106) – Short-term

[[ ]]

RAI 21.6-98 Figure A-8. WW Pressures (Rm. 105) – Short-term

[[ ]]

RAI 21.6-98 Figure A-9. DW to Header Pressures Difference (Rm. 122-106) – Short-term

[[ ]]

RAI 21.6-98 Figure A-10. Header to WW Pressures Difference (Rm. 106-105) – Short-term

[[ ]]

RAI 21.6-98 Figure A-11. DW Gas Temperature (Rm. 122) – Short-term

[[ ]]

RAI 21.6-98 Figure A-12. Header Gas Temperature (Rm. 106) – Short-term

[[ ]]

RAI 21.6-98 Figure A-13. WW Gas Average Temperature (Rm. 105) – Short-term

[[ ]]

RAI 21.6-98 Figure A-14. Water Column Height (Vent Clearing) – Short-term

[[ ]]

RAI 21.6-98 Figure A-15. Pool Swell Level – Short-term (Reference to Vent Exit Elevation)

[[ ]]

RAI 21.6-98 Figure A-16. DW-to-WW Pressure Difference (Rm.110-105) - Long Term

[[ ]]

RAI 21.6-98 Figure A-17. Header-to-WW Pressure Difference (Rm.106-105) - Long Term

[[ ]]

RAI 21.6-98 Figure A-18. DW Pressures (Rm. 110) - Long Term

[[ ]]

RAI 21.6-98 Figure A-19. Header Pressures (Rm. 106) - Long Term

[[ ]]

RAI 21.6-98 Figure A-20. WW Pressures (Rm. 105) - Long Term

[[ ]]

RAI 21.6-98 Figure A-21. DW Gas Temperatures (Rm. 111) - Long Term

[[ ]]

RAI 21.6-98 Figure A-22. Header Gas Temperatures (Rm. 106) - Long Term

[[ ]]

RAI 21.6-98 Figure A-23. WW Average Gas Temperatures (Rm. 105) - Long Term

[[ ]]

RAI 21.6-98 Figure A-24. Average Pool Temperatures - Long Term

[[ ]]

RAI 21.6-98 Figure A-25. Air Mass Flow Rate Through Vents - Long Term

[[ ]]

RAI 21.6-98 Figure A-26. Total Air Mass Through Vents - Long Term

[[ ]]

RAI 21.6-98 Figure A-27. Steam Mass Flow Rate Through Vents - Long Term

[[

]]

RAI 21.6-98 Figure A-28. Total Steam Mass Through Vents - Long Term

ATTACHMENT B: TRACG EVALUATION OF STEAM CONDENSATION IN THE PRESENCE OF NON-CONDENSABLE GASES

B.1. Summary

TRACG simulation of the University of Wisconsin Flat Plate (WFP) Steam Condensation Experiment in the Presence of Non-Condensable Gases (References B-1 and B-2) has been performed. The scope of comparison is based on the following considerations relevant to the TRACG application to ESBWR post-LOCA containment analysis:

(1) The focus is on the experimental data obtained in the vertical position of the test section since the TRACG ESBWR LOCA model treats all condensing surfaces in the containment in the vertical direction. This is justified by the fact that the measured average heat transfer coefficients (HTCs) are not sensitive to the cooling plate inclination angles as shown in Figure B-1 (prepared based on data available in Appendix C, Reference B-1).

(2) Two TRACG condensation heat transfer options are used for this evaluation. These are:

   a. Kuhn-Schrock-Peterson (K-S-P) correlation (Reference B-5) modified for Steam Condensation in Containment (Subsection 6.6.11.1 in Reference B-4), i.e., K-S-P correlation with the $f_{l\ shear}$ set equal to 1. We refer to this option as KSP_w.

   b. Minimum of "Uchida" correlation (Eq. 6.6-106 in Subsection 6.6.11.1 of Reference B-4) and KSP_w correlation. We refer to this option as Min (Uchida, KSP_w).

Comparison of TRACG-predicted average condensation heat transfer coefficients (HTC) with the experimental values, as presented in Tables B-1 and B-2 shows that TRACG with KSP_w option overpredicts the WFP data by around [[ ]], whereas TRACG with Min (Uchida, KSP_w) option overpredicts the same set of WFP data by around [[ ]]. Sensitivity study performed with these two condensation heat transfer options (KSP_w and Min (Uchida, KSP_w)) shows that the ESBWR post-LOCA peak Drywell (DW) pressure is insensitive to these options. Relevant results of this sensitivity analysis are discussed in Section B.5 of this Attachment. Therefore, use of the KSP_w option is justified for ESBWR post-LOCA containment analyses.

B.2. Introduction

The purpose of this TRACG simulation is to model the Wisconsin Flat Plate Condensation experiment in References B-1 and B-2, and to evaluate the capability of TRACG with respect to predicting the condensation heat transfer coefficient in the presence of non-condensable gases.

The WFP experiment examined the effects of surface orientation on the condensation of steam in the presence of a non-condensable gas (air). Steam and air mixture flowed downward through a rectangular channel, which is approximately 1.9m long with a cross section 0.154m x 0.154m. The condensation occurred on the inner surface of the top wall of test section. The top plate was made of aluminum and had a painted finish. A schematic diagram of the test section is shown below with British units (inch) and SI units (mm) in brackets. There are seven test stations in the WFP condensation section. TRACG nodalization uses seven cells corresponding to these seven test stations to model the condensation section.

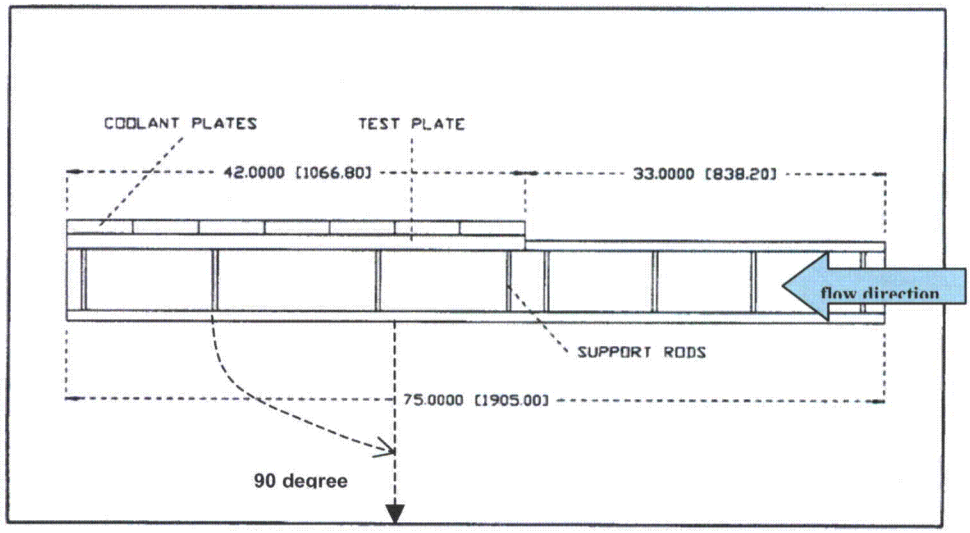

RAI 21.6-98 WFP Test Section Schematic

B.3. TRACG Simulation Approach

A one-dimensional TRACG nodalization using the Pipe component was developed to simulate the WFP condensation tests. The TRACG model uses the same geometrical data as in the WFP tests, including the pipe hydraulic diameter, flow area, cooling surface area, and flow channel inclination angle. The flow parameters of incoming air-steam mixture (temperature, air mass ratio, total pressure and velocity) and the boundary conditions used for each TRACG case are the same as those for the test. All test cases simulated with TRACG were conducted at 0.1 MPa pressure. In the TRACG simulation model, the square test section is represented by a series of connected pipes, matching both the flow area and cooled surface area as shown in the nodalization diagram below:

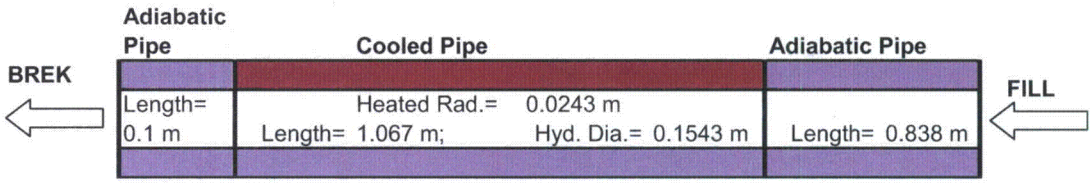

RAI 21.6-98 TRACG WFP Nodalization Diagram

The TRACG default KSP condensation model (with $f_{I}\_s=1.0$) for application to walls without shear enhancement (KSP_w) and the Min (Uchida, KSP_w) options are used for all TRACG cases in this simulation. The KSP_w and Uchida models are described in Subsection 6.6.11 of Reference B-4.

B.4. Comparisons between TRACG Results and WFP Test Data

The TRACG calculated results and WFP tests are compared and discussed in this section. The comparisons include average heat transfer coefficient, effect of air mass ratio, effect of mixture velocity and local heat transfer coefficient.

B.4.1. Average Heat Transfer Coefficient (HTC) Comparisons

The Heat Transfer Coefficient (HTC) data for WFP tests were measured by both Heat Flux Meters (HFM) and Coolant Energy Balance (CEB) methods. The averaged HTCs can be found in Appendix C of Reference B-1. In Section 6.3 of Reference B-1, it is stated that the discrepancy between the average HTC measured by the HFM method was consistently lower than the CEB by 5-10 percent. Furthermore, Reference B-1 reports the standard error of the HFM to be less than 3 percent, while the accuracy of the CEB measurement was less than 10 percent (Chapter 4, Reference B-1). Therefore, the HFM measurements are used to compare with the calculated TRACG average HTCs.

Two key parameters, which were found to have significant effect on HTC, as reported in Reference B-1, are air-steam mixture velocity and air mass ratio in the mixture. The summary of the measured and predicted average HTC comparisons with effects of air mass ratio and mixture velocity is presented in Tables B-1 and B-2 for two different TRACG options mentioned earlier. It should be noticed that for the Min (Uchida, KSP_w) option, the HTC for pure steam, i.e., air mass ratio of zero (Test Case THERM99), is the same as the KSP_w option; for higher air mass ratio, Min (Uchida, KSP_w) option selects the Uchida correlation. This is due to the nature of Uchida correlation (Equation 6.6-106 of Reference B-4), which goes to "infinity" as the air mass ratio approaches zero or pure steam. The overall comparisons with the test data show that TRACG over-predicts the average HTC for 90-degree angle (or vertical surface) by an average of [[ ]] for KSP_w option and by [[ ]] for the Min (Uchida, KSP_w) option. Comparisons of specific effects are discussed as follows:

B.4.1.1. Mixture Velocity Effect

Figure B-2 shows the effect of mixture velocity (for condensation on vertical surface) for the measured and predicted average HTC. As shown, TRACG, particularly the KSP_w option, predicts the same trend as the measured HTC versus the air-steam mixture velocity. That is, higher mixture velocity results in higher average HTC in both TRACG predictions and test data. This is due to the forced convection effect.

B.4.1.2. Air Mass Ratio Effect

Figures B-3 and B-4 show the effect of air mass ratio for the measured and predicted average HTC. As shown, TRACG predicts (with both options) the same trend as the measured HTC versus the air mass ratio for both 1 m/s and 3 m/s mixture velocities. Both the measured and predicted HTCs decrease rapidly as the air mass ratio increase. This is because the higher air mass concentration near the cooling surface impedes steam condensation on the wall. Also note that Figures B-3 and B-4 show similar trend with respect to the KSP and Uchida correlations as shown in Figure 6-38 of Reference B-4. For ready reference, Figure 6-38 of Reference B-4 is reproduced here as Figure B-5. Please note that at very small air mass ratio, less than ~0.02, the

KSP correlation yields lower HTC compared to the Uchida correlation. The opposite is true for higher air mass ratio, greater than ~0.04.

B.4.1.3. Downstream Distance from Entrance Effect

Figure B-6 compares the predicted and the measured local HTCs (for Test Case THERM83) along the flow channel downstream from entrance for vertically oriented channel. Figure B-6 shows:

- TRACG overpredicts the local HTC along the flow channel downstream from entrance. This is consistent with overprediction of average HTC shown in Tables B-1 and B-2 for Test case THERM83.
- TRACG predicts the correct trend of local HTC decreasing along the downstream from entrance.

B.5. TRACG Sensitivity Study for ESBWR Containment Analysis

The effect of Min (Uchida, KSP_w) condensation heat transfer correlation has been studied for long term (72 hours) ESBWR post-LOCA containment analysis. The bounding Main Steam Line Break with one Safety Relief Valve (SRV) failure case, discussed in the DCD (Reference B-3), has been rerun with the Min (Uchida, KSP_w) option and the results have been compared with the DCD results obtained using the KSP_w option with minor difference for film Reynolds number greater than 1000. Figure B-7 shows the comparison between the Drywell (DW) and Wetwell (WW) pressures with these two condensation heat transfer options. The results of both these options are almost identical.

The reason for this very good agreement between the containment pressures for two different options is clear from Figure B-8 where the air mass fractions near the DW wall are plotted. It is seen that after ~2 hours, the air mass fraction stays below 0.01 where the KSP_w correlation yields lower heat transfer coefficients than the Uchida correlation. Therefore, both options, KSP_w and Min (Uchida, KSP_w)), select and use the KSP_w correlation, and so the long-term containment pressures are almost the same for both options. Also, it is clear that even though TRACG simulation of WFP tests (air mass fraction much greater than 0.04) suggests that KSP_w correlation significantly over-predicts the WFP test data, these data are not very relevant to the long-term ESBWR post-LOCA containment analysis since the air mass fraction in the ESBWR DW decreases to a very small value. Most of the non-condensable move to the WW gas space. Therefore, use of the KSP_w correlation or slight modification thereof is justified for ESBWR post-LOCA containment analysis.

B.6. Conclusions

TRACG default (KSP_w) correlation generally over-predicts the WFP test HTC in the presence of non-condensable gas (air mass ratio of 0.24 or greater) for vertical plates by an average of [[ ]]. The agreement is much better, about [[ ]], for a different condensation heat transfer option, namely, Min (Uchida, KSP_w). However, TRACG sensitivity study presented in Section B.5 shows that both options produce almost the same result for the long-term post-LOCA ESBWR containment pressure. This is because during a LOCA in the ESBWR system, most of the non-condensable is displaced to the WW gas space and the non-condensable mass fraction near the DW wall is very small (less than 0.01). Therefore, use of the KSP_w correlation

or some small variation thereof is justified for the ESBWR post-LOCA containment analysis. This is also evident from the TRACG simulation results of the Marviken blowdown test #18 presented in Attachment A of this RAI response, which shows that TRACG with the default condensation heat transfer option is able to predict well both the short-term and long-term Drywell and Wetwell pressure and temperature responses.

B.6. References

B-1 I. K. Huhtiniemi, "Condensation In The Presence Of Non-Condensable Gas: Effect of Surface Orientation," Ph. D. Thesis, University of Wisconsin – Madison, August 1991.

B-2 I. K. Huhtiniemi and M. L. Corradini, "Condensation in the presence of non-condensable gases," Nuclear Engineering and Design, Vol. 141, 429-446, 1993.

B-3 GE Hitachi Nuclear Energy, ESBWR DCD Tier 2, Chapter 6, " Engineering Safety Features ", Rev. 5, 26A6642AT, May 2008.

B-4 GE Hitachi Nuclear Energy, "TRACG MODEL DESCRIPTION," NEDE-32176P, Rev. 4, January 2008.

B-5 S. Z. Kuhn, V. E. Schrock and P. F. Peterson, "Final Report on U. C. Berkeley Single Tube Condensation Studies," UCB-NE-4201 Rev. 2, August 1994.

RAI 21.6-98 Table B-1. Summary of Measured and Predicted (KSP_w) Average HTCs

[[						

]]

RAI 21.6-98 Table B-2. Summary of Measured and Predicted (Min (Uchida, KSP_w))

Average HTCs

[[						

]]

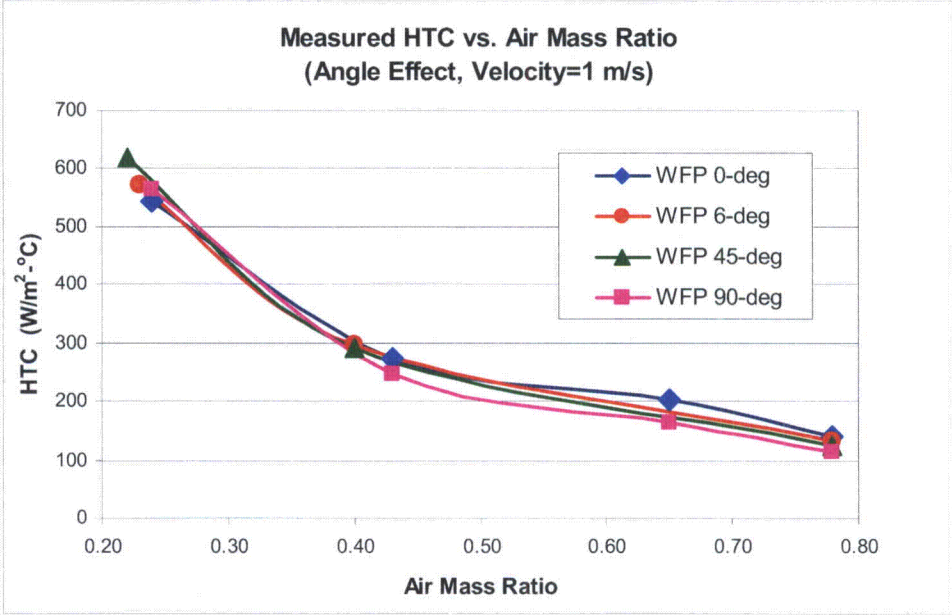

RAI 21.6-98 Figure B-1. Measured Average HTC – Effect of Air Mass Ratio and Inclination Angle

[[ ]]

RAI 21.6-98 Figure B-2. Average HTC – Effect of Mixture Velocity at Air Mass Ratio of 0.65

[[ ]]

RAI 21.6-98 Figure B-3. Average HTC – Effect of Air Mass Ratio at 1 m/s Mixture Velocity

[[ ]]

RAI 21.6-98 Figure B-4. Average HTC – Effect of Air Mass Ratio at 3m/s Mixture Velocity

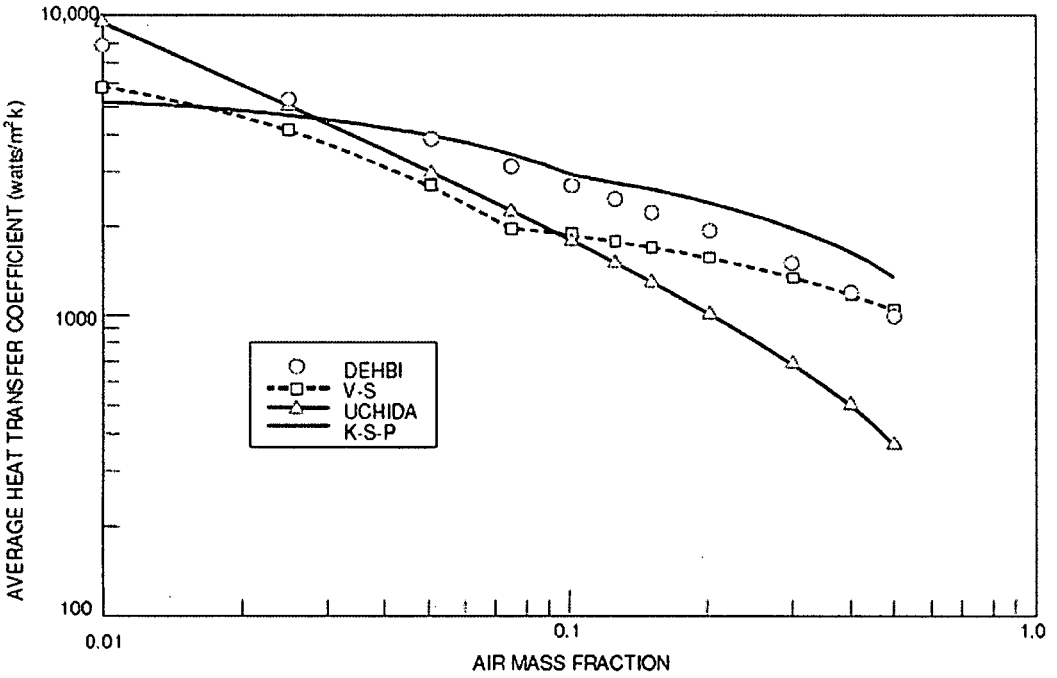

RAI 21.6-98 Figure B-5. Comparison of Average Heat Transfer Coefficients Predicted by Four Correlations under Containment Conditions

[[ ]]

RAI 21.6-98 Figure B-6. Local HTC (For Test Case THERM83) – Distance from Entrance

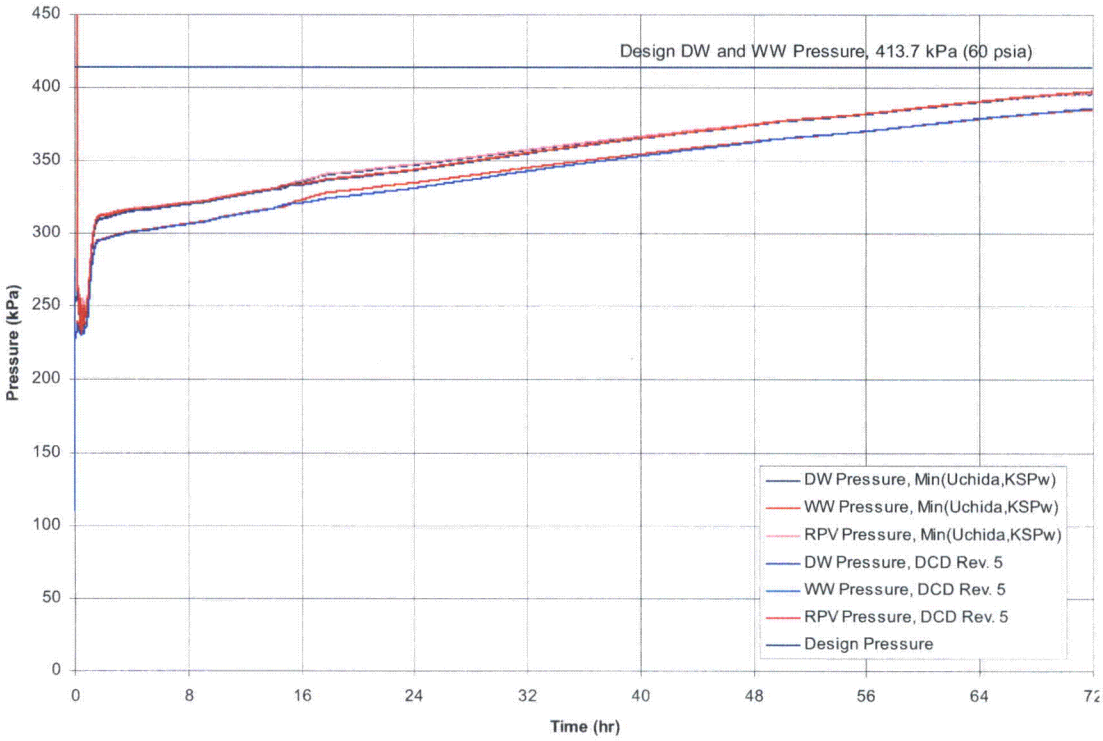

RAI 21.6-98 Figure B-7. Comparison of ESBWR Bounding MSLB Containment Pressures for Two Options of Condensation Heat Transfer Correlations.

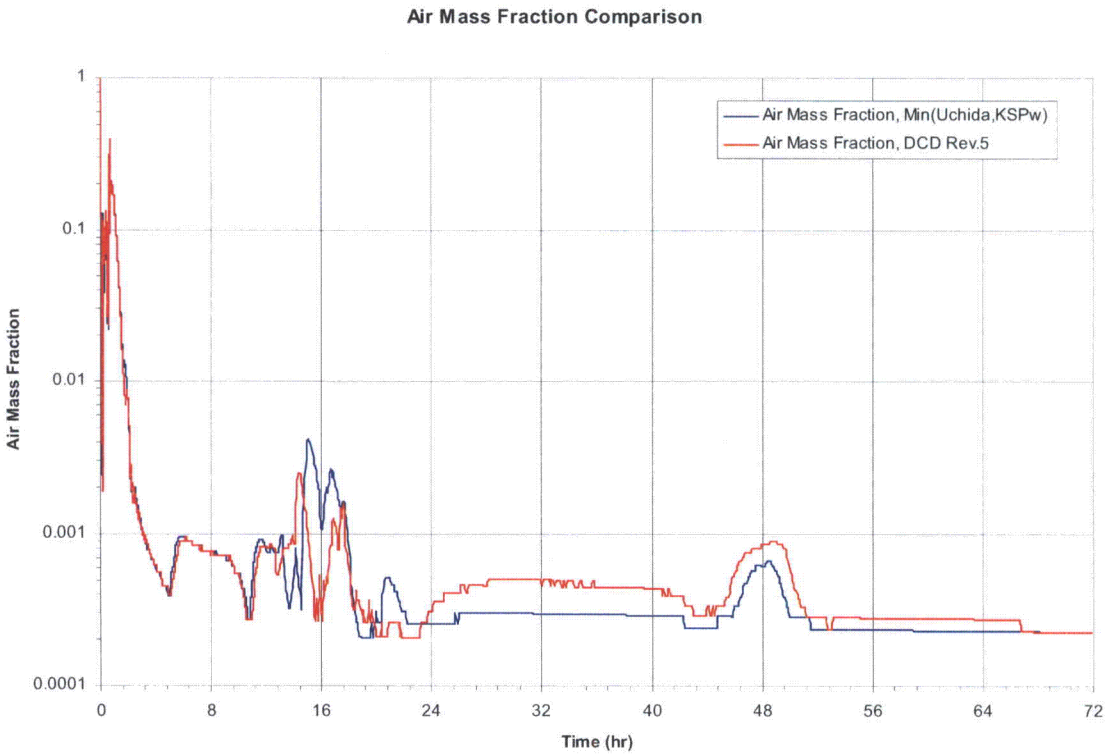

RAI 21.6-98 Figure B-8. Comparison of Non-condensable (Air) Mass Fractions in ESBWR Containment (DW) after MSLB for Two different Condensation Heat Transfer Options.

DCD Impact

No DCD changes will be made in response to this RAI.

13.0 NRC RAI 21.6-96 S02

The PCCS is not over capacity starting at about 3 hours; include the response in a licensing document & Code qualification assessment and justification.

Part A: GEH's response to RAI 21.6-96 Supplement 1 states that "For the long-term Passive Containment Cooling System (PCCS) operation, the PCCS is over capacity starting at about 3 hours. Under this overcapacity condition, the PCCS regulates the heat removal rate to match the decay heat by accumulating non-condensable (NC) gases in the lower part of the PCCS tubes."

[a] The statement that "the PCCS is over capacity starting at about 3 hours" is misleading. Both GEH's TRACG and the staff's MELCOR results show that the PCCS does not operate at overcapacity: energy removal rate from the PCCS is below the decay heat generation leading to continuous containment pressurization and heat up for 72 hours after a LOCA.

Each PCCS is designed to remove 11 MW at design conditions stated in ESBWR DCD Tier 2 Rev. 5 Table 6.2-10. It may appear that six PCCS would be able to remove 66 MW which is significantly higher than the decay power (e.g., 29 MW at 24 hours and 21 MW at 72 hours). (See ESBWR DCD Tier 2 Rev. 5 Figure 6.2-14c1.) The PCCS is unable to remove the design capacity power of 66 MW and arrest the containment pressurization during the first 72 hours after a LOCA because it operates at containment conditions which are less favorable than its design conditions. An example is that the design conditions include that the operation of PCCS at 100 percent steam environment but the presence of non-condensables in the drywell adversely affects the steam condensation rate, and thus, the efficiency of PCCS.

Please clarify the statement "the PCCS is over capacity starting at about 3 hours."

[b] Explain what physical conditions force the PCCS to regulate the heat removal rate to match the decay heat.

[c] Update the DCD or a topical report incorporated by reference as appropriate to provide this technical description.

[d] NRC TRACG Inspection 12/15/08 to 12/19/08. The response to RAI 21.6-96 S01 provided assessment comparisons for TRACG04 V53 and TRACG04 V40 against test data. Because some assessment results were degraded (compared to the earlier versions) while some cases were improved, please provide an additional column with qualification justification in the tables listed in RAI 21.6-96 S01. Since the latest version of TRACG04P Level-2 code V5711 was used for DCD safety analysis, provide a similar assessment for V5711 to RAI21.6-96 S01.

13.1 GEH RESPONSE

(a) The statement, "the Passive Containment Cooling System (PCCS) is over capacity starting at about 3 hours", simply means that the PCCS has more than enough capacity (surface area) to remove all the decay heat at 3 hours into the postulated accident. The reason it does not remove more heat than the decay heat and depressurize the system is because of its self-regulating characteristics explained in (b) below.

(b) The PCCS is self-regulating because of the feedback between heat removal, condenser pressure and noncondensible gas holdup within the condenser. If the heat removal in the condenser starts to increase beyond that required to condense the steam generated by decay heat, the pressure in the condenser starts to fall. The reduction in condenser pressure reduces the flow of noncondensible gases out of the condenser to the vent. This results in increased holdup of noncondensibles in the condenser tubes and a reduction in the heat removal, until the condensation rate equalizes with the steam inflow. If the heat removal in the condenser drops, the reverse process occurs. The condenser pressurizes and drives out noncondensibles until the heat transfer is restored to match the condensation of the steam flow rate. This regulating behavior of the PCCS has been demonstrated convincingly in the PANDA integral system tests. The reason for the slow increase in containment pressure over 72 hours is mainly due to direct heat addition to the wetwell through leakage and heat transfer from the walls.

(c) The requested information, description stated in Item (a) and Item (b), will be included in the Licensing Topical Report (LTR) NEDE-33440P Revision 1. This LTR is referred in the ESBWR DCD Tier 2, Section 6.2.9 as Reference 6.2-11. ESBWR DCD Tier 2, Section 6.2.2.3 will be revised as noted in the attached markup.

(d) The following 6 TRACG cases were excluded in the assessments performed with the latest Version 5711 of the TRACG04P code.

- Case GIRH1 in GIRAFFE Helium Test
- Case M10b in PANDA Transient Test (M-Series)
- Case P04 and Case P06 in PANDA Transient Test (P-Series)
- Case TE1CE2 and Case TE1CE2_70 in PANDA Exploratory Test

Please note that cases for the test facility are all included where multiple cases are needed to provide the assessment. The reduced set of cases covers all the test facilities. Results from the assessment using the latest TRACG04P Version 5711 Level 2 code are presented in Tables 21.6-96 S02-1 through 21.6-96 S02-17 and Figures 21.6-96 S02-1 through 21.6-96 S02-18. The numbering sequences of the tables and figures are unchanged from what was presented in the response to RAI 21.6-96 S01, MFN 08-644. In general, results from TRACG04P Version 5711 Level 2 do not show any significant deviation from the test data and the previous TRACG version results with the exception of the PANTHERS Isolation Condenser (IC) Performances Tests under Component Performance Tests and One-Sixth Scale Boron Mixing Test under Integral Systems Tests.

For the PANTHERS IC Performances Tests under Component Performance Tests, different behaviors are observed in Test T12 case. Two peaks are predicted in the Inlet Pressure Transient and Heat Transfer as shown in Figure 21.6-96S02-2a and Figure 21.6-96 S02-3a. The earlier pressure rise in the TRACG04P Version 5711 Level 2 prediction of Test T12 relative to test data is attributed to entrainment and possibly dissolution of non-condensable gas in the drain flow in the test. Gas dissolution is not modeled in TRACG and entrainment under the conditions produced in the IC test facility may be under predicted. Greater retention of noncondensable gases in the condenser tubes in the TRACG simulation would cause a more rapid increase in the pressure required for condensation of

the inlet steam flow. This behavior is similar to that seen in analyses performed with previous versions of TRACG. The noncondensable gas holdup calculated by TRACG is sensitive to calculation parameters such as the condensate velocity and interfacial shear. The initial drop in pressure seen in Figure 21.6-96S02-2a is due to a momentary increase in the calculated noncondensable gas entrainment resulting in a sharply reduced gas holdup. This calculation has shown some sensitivity to the time step size used in the TRACG calculations. A sensitivity study was conducted by reducing the maximum time step size by half. The results are shown in Table 21.6-96S02-5, Figure 21.6-96S02-2 and Figure 21.6-96 S02-3. The resulting calculations show pressure and heat transfer trajectories close to the previous results. The peak pressure and timing of the peak are not significantly altered. This shows that while some of the details of this transient are sensitive to the time step size, the overall behavior of the transient calculated by TRACG is not affected.

For the One-Sixth Scale Boron Mixing Test, results for the cases using the TRACG04P Version 5711 code provide better agreement with the data than any other code version that has been used so far to analyze this test, see Figure 21.6-96S02-6 through Figure 21.6-96 S02-13. This study was re-done with a better simulation of the facility using air and water. Previous calculations had simulated an equivalent steam-water condition.

In all, the conclusions drawn from previous submittals (listed below) remain valid.

1. GE Hitachi Nuclear Energy, NEDC-32725P, "TRACG Qualification for SBWR," Revision 1 August 2002.
2. GE Hitachi Nuclear Energy, NEDC-33080P, "TRACG Qualification for ESBWR," Revision 0, August 2002.
3. MFN 04-059, Dated June 2, 2004, "Update of ESBWR TRACG Qualification for NEDC-32725P and NEDC-33080P Using the 9-Apr-2004 Program Library Version of TRACG04."

RAI 21.6-96 S02 Table 21.6-96 S02-1

Summary of TRACG Results for the Toshiba Low Pressure Void Fraction Tests

[[

]]

RAI 21.6-96 S02 Table 21.6-96 S02-2
Summary of TRACG Results for the Ontario Hydro Void Fraction Tests

[[ ]]

RAI 21.6-96 S02 Table 21.6-96 S02-3

Summary of TRACG Results for the PANTHERS PCC SS Steam-Air Tests

[[								

]]

RAI 21.6-96 S02 Table 21.6-96 S02-4

Summary of TRACG Results for the PANTHERS PCC SS Pure Steam Tests

[[				

]]

RAI 21.6-96 S02 Table 21.6-96 S02-5

Summary of TRACG Results for the PANTHERS IC Tests

[[				

]]

RAI 21.6-96 S02 Table 21.6-96 S02-6

Summary of TRACG Results for the PANDA PCC Tests

[[				

]]

RAI 21.6-96 S02 Table 21.6-96 S02-7

Summary of TRACG Results for the Suppression Pool Stratification Test

(PSTF Test 5807-29)

[[					

]]

RAI 21.6-96 S02 Table 21.6-96 S02-8

Summary of TRACG Results for the GIST Test (Test C01A)

[[						

]]

RAI 21.6-96 S02 Table 21.6-96 S02-9

Summary of TRACG Accuracy for GIRAFFE Helium Tests

[[						

]]

RAI 21.6-96 S02 Table 21.6-96 S02-10

Summary of TRACG Results for the GIRAFFE Systems Interactions Test

[[						

RAI 21.6-96 S02 Table 21.6-96 S02-10

Summary of TRACG Results for the GIRAFFE Systems Interactions Test

[[						

]]

RAI 21.6-96 S02 Table 21.6-96 S02-11

Summary of TRACG Results for the PSTF MARK III Test 5703-01

[[						

]]

RAI 21.6-96 S02 Table 21.6-96 S02-12

Summary of TRACG Results for the 4T MARK II Test 5101-34

[[						

]]

RAI 21.6-96 S02 Table 21.6-96 S02-13

Summary of TRACG Results for the PANDA M-Series

[[						

]]

RAI 21.6-96 S02 Table 21.6-96 S02-14

Summary of TRACG Results for the PANDA P-Series

[[						

]]

RAI 21.6-96 S02 Table 21.6-96 S02-15

Summary of TRACG Results for the Dodewaard Startup Test

[[					

]]

RAI 21.6-96 S02 Table 21.6-96 S02-16

Summary of TRACG Results for the CRIEPI Low Pressure Tests

[[					

]]

RAI 21.6-96 S02 Table 21.6-96 S02-17

Summary of TRACG Results for the SIRIUS Two-Phase Instability Tests

[[					

]]

[[ ]]

RAI 21.6-96 S02 Figure 1. Comparison of TRACG and PANTHERS Inlet Pressure for Test 54
(Figure 4.1-28, Ref. 3)

[[ ]]

RAI 21.6-96 S02 Figure 2. Comparison of TRACG and PANTHERS Inlet Pressure Transient for Test 12

(Reduced maximum time step size)

(Figure 4.2-6, Ref. 3)

[[ ]]

RAI 21.6-96 S02 Figure 2a. Comparison of TRACG and PANTHERS Inlet Pressure Transient for Test 12
(Figure 4.2-6, Ref. 3)

[[ ]]

RAI 21.6-96 S02 Figure 3. Comparison of TRACG and PANTHERS Heat Transfer for Test 12

(Reduced maximum time step size)
(Figure 4.2-7, Ref. 3)

[[ ]]

RAI 21.6-96 S02 Figure 3a. Comparison of TRACG and PANTHERS Heat Transfer for Test 12

(Figure 4.2-7, Ref. 3)

[[ ]]

RAI 21.6-96 S02 Figure 4. TRACG Suppression Pool Nodalization
(Suppression Pool Stratification Tests)

[[ ]]

RAI 21.6-96 S02 Figure 5. Final Pool Temperature Comparison, TRACG04 Version 53, TRACG04 Version 5711 Level 2.
(Suppression Pool Stratification Tests)

[[ ]]

RAI 21.6-96 S02 Figure 6. Channel at 41-in. Center: Well-Mixed Model
(Boron Mixing Tests, Figure 5.4-3, Ref. 3)

[[ ]]

RAI 21.6-96 S02 Figure 7. Channel at 55-in. Middle: Well-Mixed Model
(Boron Mixing Tests, Figure 5.4-4, Ref. 3)

[[.]]

RAI 21.6-96 S02 Figure 8. Channel at 41-in. Periphery: Well-Mixed Model
(Boron Mixing Tests, Figure 5.4-5, Ref. 3)

[[ ]]

RAI 21.6-96 S02 Figure 9. Bypass at 41-in. Center: Well-Mixed Model
(Boron Mixing Tests, Figure 5.4-6, Ref. 3)

[[ ]]

RAI 21.6-96 S02 Figure 10. Bypass at 55-in. Middle: Well-Mixed Model
(Boron Mixing Tests, Figure 5.4-7, Ref. 3)

[[ ]]

RAI 21.6-96 02 Figure 11. Bypass at 41-in. Periphery: Well-Mixed Model
(Boron Mixing Tests, Figure 5.4-8, Ref. 3)

[[ ]]

RAI 21.6-96 S02 Figure 12. Lower Plenum at 14-in. Middle: Well-Mixed Model
(Boron Mixing Tests, Figure 5.4-9, Ref. 3)

[[ ]]

RAI 21.6-96 S02 Figure 13. Lower Plenum Center: Well-Mixed Model
(Boron Mixing Tests, Figure 5.4-10, Ref. 3)

[[ ]]

RAI 21.6-96 S02 Figure 14. DW Pressure Response
(PSTF Mark III Test 5703-01, Figure 5.5-5, Ref. 3)

[[ ]]

RAI 21.6-96 S02 Figure 15 DW Pressure Response
(4T/Mark II Test 5101-34, Figure 5.6-5, Ref. 3)

[[ ]]

RAI 21.6-96 S02 Figure 16. WW Pressure Response
(4T/Mark II Test 5101-34, Figure 5.6-6, Ref. 3)

[[ ]]

RAI 21.6-96 S02 Figure 17. Steam Flow to PCC3 for Test E2 –
Power Reduced 50%
(PANDA Exploratory Tests, Figure 6.4-18, Ref. 3)

Note: Case TE1CE2 and Case TE1CE2_70 in PANDA Exploratory Test for Natural Circulation and Flow Oscillation Tests are eliminated from V5711 level 2 code assessment.

[[ ]]

RAI 21.6-96 S02 Figure 18. Steam Flow to PCC3 for Test E2
Power Reduced 70%
(PANDA Exploratory Tests, Figure 6.4-18, Ref. 3)

Note: Case TE1CE2 and Case TE1CE2_70 in PANDA Exploratory Test for Natural Circulation and Flow Oscillation Tests are eliminated from V5711 level 2 code assessment.

DCD Impact

ESBWR DCD Tier 2, Subsection 6.2.2.3 will be revised as noted in the Enclosure 3 markup.

LTR NEDE-33440P Table 1.1 will be revised as shown in the attached markup. A new Section 13 will be added to contain this response to RAI 21.6-96 S02 in its entirety.

14.0 NRC RAI 6.2-98 S01

RAI 6.2-98 was a followup to RAI 6.2-53 (MFN 06-215). The intent of these RAIs was to understand the TRACG calculation for the bounding scenario. ESBWR DCD Tier 2 provides limited information that is insufficient to understand the analyses. These RAIs focused on key phenomena-the trapping and transient distribution of noncondensable gases in the drywell and subsequent transport to the wetwell.

(A) The limiting design basis accident changed from feed water line break (FWLB) to main steam line break (MSLB) as given in ESBWR DCD Tier 2 Revision 3. As a result, in RAI 6.2-141, the staff requested GEH to revisit RAIs that were affected by this change, specifically RAI 6.2-98. However, the GEH's response to RAI 6.2-98 was based only on the FWLB accident. The analyses results of the FWLB accident are important because of their closeness to that of the MSLB accident and the fact that FWLB is the second limiting accident. Please provide the analyses results of the MSLB accident.

(B) The addition of a double pipe connection, which was not modeled previously (MFN 06-215), significantly increased the transfer of nitrogen trapped in the GDCS during the GDCS period and subsequently released to the drywell and then to the wetwell. This modeling improvement reduced the amount of holdup of nitrogen in the GDCS from a ~10-12% of the total in the previous modeling to a ~ 5% of the total in the current modeling. The holdup of nitrogen of 5% of the total appears to result from the TRACG's inability to model mixing of gases in the GDCS tank open volume. Please (1) explain whether you chose the nodalization to minimize the nitrogen holdup in the GDCS pools and (2) quantify the effect of using a well mixed atmosphere in the GDCS pools open volume.

(C) As shown on Figure 6.2-98-5, the noncondensable gas holdup in the drywell head region at 72 hours resulting in a pressure of 50 KPa is significant. Please (1) provide the mass of noncondensables held up in the drywell head region and (2) quantify the effect on the drywell pressure, if the noncondensables held up in the drywell head and GDCS pools were transferred to the wetwell.

(D) After the opening of the DPVs, the long-term containment responses from FWLB accident to MSLB accidents are expected to be similar. However, the results show that they differ. Please (1) identify and justify the nodalization differences between FWLB and MSLB accidents and (2) explain the differences in results.

(E) During a phone call with the staff on September 24, 2007, GEH discussed a potential design change to add a drywell gas recirculation system to the PCCS which will start operating three days after the initiation of a LOCA to improve the PCCS's ability to remove thermal energy from the containment. In your response, please address the effect of the drywell gas recirculation system and any other systems that you plan to credit in your analyses.

14.1 GEH RESPONSE

The containment responses to a postulated main steam line break (MSLB) and feedwater line break (FWLB) are discussed in the following paragraphs and figures.

The bounding cases (DCD Tier 2, Revision 4, Figures 6.2-13a1 to 6.2-14d3) are used for these discussions. These cases assume a single failure of one depressurization valve (DPV) and bounding conditions (DCD Tier 2, Revision 4, Table 6.2-6), and assume 100% double-ended break.

(A) The change in limiting design basis accident from FWLB to MSLB is discussed in this section.

(A1) General Discussions [MSLB – Bounding Conditions]

(A1.1) Nodalization

Referring to the TRACG nodalization (Figures 6.2-98S01-1 and 6.2-98S01-2), the broken main steam line is located at Level 34 and discharges steam into the drywell (DW) at this elevation. Two pipes (per Gravity-Driven Cooling System (GDCS) airspace) are used to simulate the connection between the GDCS pool airspace and the DW (RAI 6.2-98 S01 Figure 6.2-98 S01-2), to purge the residual non-condensable (NC) gases in this airspace. For the NC gases, the nitrogen properties are used in these TRACG calculations.

(A1.2) Pressure Responses

RAI 6.2-98 S01 Figure 6.2-98 S01-3 shows the reactor pressure vessel (RPV), DW and wetwell (WW) pressures, and RAI 6.2-98 S01 Figure 6.2-98 S01-3a shows the same responses in short-term time scale.

Following the postulated loss-of-coolant accident (LOCA), the DW pressure increases rapidly leading to the clearing of the Passive Containment Cooling System (PCCS) and main vents. At approximately 79 seconds, the DW pressure reaches a peak value of 250 kPa (36.3 psia). This peak pressure is below the design pressure of 413.7 kPa (60 psia) with large margin. During this blowdown period, a significant amount of NC gas is purged into the WW and pressurizes the WW. The RPV continues to depressurize due to the break flow and the Automatic Depressurization System (ADS) flows. At approximately 0.2 hours, the RPV pressure drops below the pressure point at which the GDCS water is allowed to inject into the downcomer by gravity head. The subcooled GDCS water continues flowing into the RPV and reduces the steaming from the RPV and the DW pressure. At approximately 0.48 hours, the DW pressure drops below the WW pressure, causing the openings of vacuum breakers and allowing some NC gases to flow back into the DW. Consequently, the system pressures drop to a value of approximately 217 kPa.

Subsequently, the decay heat overcomes the subcooling of the GDCS water and steaming resumes (at ~ 0.66 hours, RAI 6.2-98 S01 Figure 6.2-98 S01-3a). The resumption of RPV steaming causes the DW pressure to increase again starting from 0.66 hours.

(A1.3) Level and Heat Removal Responses

RAI 6.2-98 S01 Figure 6.2-98 S01-4 shows the downcomer collapsed level, and RAI 6.2-98 S01 Figure 6.2-98 S01-5shows the GDCS pool water levels. After the initiation of the GDCS flow, the GDCS pool water level drops and consequently the downcomer collapsed level rises.

At approximately 17.1 hours, the downcomer water level swells up to the DPV elevation. This level swell causes a surge of DPV flow from the downcomer into the DW annulus.

The addition of subcooled downcomer water condenses extra steam in the DW annulus and sets off a brief pressure reduction in the DW annulus region (RAI 6.2-98 S01 Figure 6.2-98 S01-3a). Because the pressure is lower in the DW annulus than those the DW head and GDCS pool airspace, the NC gases hidden in these airspaces start to move back to the DW annulus (Figures 6.2-98S01-12 and 6.2-98S01-13).

For the rest of the transient, the downcomer collapsed level maintains an equilibrium position below the elevation of the DPVs (stub tube elevation at 21.91 meters). The corresponding GDCS pool equilibrium level is approximately 21.4 meters.

RAI 6.2-98 S01 Figure 6.2-98 S01-6 compares the total heat removal by the PCCS with the decay heat. From 6 to 30 hours, approximately 90 to 95% of the decay heat is removed by the PCCS and discharged to the Isolation Condenser (IC) Passive Containment Cooling (PCC) pools, which are outside of the containment. The residual decay heat (approximately 5 to 10% not removed by the PCCS) corresponds to the reduction in RPV steaming rate. This reduction is due to that a small portion of the decay heat that is used to heat up the incoming cooler GDCS water. RAI 6.2-98 S01 Figure 6.2-98 S01-7 compares the GDCS pool water temperature with the downcomer water temperatures. In this design, the hot PCCS condensate (~105 °C) drains to the GDCS pools and mixes with the remaining water (for the MSLB case, ~ 1000 m^3) in the pools. The GDCS water injected into the RPV during the MSLB transient is at a temperature considerably lower than that for the PCCS condensate. After 60 hours, the mixture temperature approaches an equilibrium temperature of 100 °C (RAI 6.2-98 S01 Figure 6.2-98 S01-7).

RAI 6.2-98 S01 Figure 6.2-98 S01-8 shows the IC/PCC pool water level. The IC/PCC pool water level drops due to boiloff by the decay heat. At 35 hours, the pool level drops below the elevation of 29.6 m, (or top one-quarter portion of the PCCS condenser tube length uncovered). The connection valves open to allow the water from the dryer/separator storage pools to flow into the IC/PCC pools. This increase in PCCS condenser tube coverage causes a small increase in PCCS condensation power (RAI 6.2-98 S01 Figure 6.2-98 S01-6).

(A1.4) NC Gas Responses

RAI 6.2-98 S01 Figure 6.2-98 S01-9 through _RAI 6.2-98 S01 Figure 6.2-98 S01-13 show the NC gas pressures in the DW annulus, lower DW, air gap between the RPV and the reactor shield wall, the DW head airspace, and the GDCS pool airspace. Most of the initial NC gases in the DW annulus are purged into the WW within 3 hours. It takes approximately 24 hours to purge most of the NC gases in the DW head airspace (RAI 6.2-98 S01 Figure 6.2-98 S01-12). It takes approximately 20 hours to purge most of the NC gases in the GDCS pool airspaces (RAI 6.2-98 S01 Figure 6.2-98 S01-13).

Figures 6.2-98S01-14 through 6.2-98S01-16 show the NC gas mass profiles in the DW head airspace, GDCS pool airspace and in the WW. Figures 6.2-98S01-14 and 6.2-98S01-15 show that there is essentially no NC gas remaining in the DW head and GDCS airspaces, after 24 hours into the transient. Significant increase in the total WW NC gas mass occurs in the first 3 hours (RAI 6.2-98 S01 Figure 6.2-98 S01-16), during this time period basically all the initial NC gases in the DW annulus are purged into the WW. The second step increase in the total WW NC gas mass occurs form 18 to

20 hours, corresponding to the purging of the remaining NC gas in the DW head and GDCS pool airspaces. The increase in WW NC gas after 20 hours corresponds to the radiolytic gases generated in the core and purged into the WW via the PCCS. The total NC gas mass in the WW at 72 hours is 15043 kg.

(A1.5) Suppression Pool and WW Responses

RAI 6.2-98 S01 Figure 6.2-98 S01-17 shows the water levels in the DW annulus and suppression pool. At 72 hours, the DW annulus collapsed level reaches to approximately 5 meters below the RPV bottom. The suppression pool level rises to 10.51 meters (reference to RPV bottom), due to the condensation of steam through the main vents during the blowdown and the early part of LOCA transient.

Figures 6.2-98S01-18 and 6.2-98S01-19 show the suppression pool water temperatures at different elevations in Ring 7 (next to the horizontal vents) and Ring 8 (away from the horizontal vents). Shortly after the blowdown period, the suppression pool stratification model prevents any mixing in the bottom three levels (Levels 25, 26 and 27) in the suppression pool. (The stratification model sets the flow areas to zero in the radial direction at these 3 levels when there is no discharge from the vent or safety-relief valve (SRV) discharge line to the lower level). RAI 6.2-98 S01 Figure 6.2-98 S01-19 shows that the water temperatures in these levels (in Ring 8) remain constant for the 72 hours transient after the initial heatup from the blowdown. After the blowdown, the pool surface temperatures (Level 29 in Rings 7 and 8) increase an additional 5°K as the result of the energy/steam in the PCCS vent flow and the increase in the WW air temperatures (Figures 6.2-98S01-20 and 6.2-98S01-21). The long-term pool surface temperature is 77°C.

Figures 6.2-98S01-20 and _6.2-98S01-21 show the WW gas temperatures at different elevations in Ring 7 (next to the vacuum breakers and leakage) and Ring 8 (away from the vacuum breakers). Air temperatures at Levels 29 and 30 follow closely with pool surface water temperatures. The increase for the gas temperature at the top WW corner next to the leakage path (Level 31, Ring 7) is larger than for other temperatures due to the inflow of hotter gas from the DW via the leakage path and the gas stratification model. The WW gas stratification model applies a large value of loss coefficient (100000) at the axial faces (Rings 7 and 8, between Levels 30 and 31) and restricts the mixing between the cells at Levels 30 and 31.

RAI 6.2-98 S01 Figure 6.2-98 S01-22 shows the WW total and NC gas pressures in Ring 7.

(A1.6) PCCS Inlet Conditions

RAI 6.2-98 S01 Figure 6.2-98 S01-23 shows the total mixture and NC gas mass flows at the PCCS inlet, and RAI 6.2-98 S01 Figure 6.2-98 S01-24 shows the mass flows with enlarged time scale. RAI 6.2-98 S01 Figure 6.2-98 S01-25 shows the moisture content at the PCCS inlet. The moisture content is calculated as (1 – void fraction) at the top of the DW next to the PCCS inlet. The calculated results show that there are no significant water droplets at the PCCS inlet location during this transient.

(A1.7) Effect of MSLB Steam Discharge Location (Level 34 Versus Level 23)

In the analyses prior to DCD Tier 2, Revision 3, the MSLB steam flow was assumed to discharge at Level 23 (in the DW region below the RPV bottom) and to force the NC gases in the DW to transfer into the WW. Parametric cases were performed to assess the impact of the discharge location for the steam break flow, at Level 23 versus at Level 34 (the same elevation as the main steam line). The results of these parametric studies show that the simulation with MSLB steam discharged at Level 34 generates slightly higher long-term DW pressure than that discharged at Level 23. These results were discussed in response to RAI 6.2-53 S01 (MFN 02-215, Supplement 1).

Based on these parametric studies, the broken main steam line for MSLB is simulated at Level 34 and discharges steam into the DW at this elevation.

(A1.8) Effect of 1-Pipe Connection Versus 2-Pipe Connection

In the analyses prior to DCD Tier 2, Revision 3, the TRACG nodalization used 1-pipe connection (per GDCS airspace) to simulate the flow path between the GDCS pool airspace and the DW. The TRACG nodalization was later modified to use 2-pipe connection (per GDCS airspace) to further promote the purging of the residual NC gas in the GDCS airspace. Parametric cases (using MSLB case) were performed to assess the effectiveness of 1-pipe versus 2-pipe connection. Results of these parametric studies show that the 2-pipe connection essentially purges all NC gas remaining in the GDCS pool airspace. Consequently, the calculated long-term DW pressure for MSLB is higher with 2-pipe connection than that with 1-pipe connection. These results were discussed in response to RAI 6.2-53 S01 (MFN 02-215, Supplement 1).

Based on these parametric studies, the TRACG nodalization is revised with 2-pipe connection (per GDCS airspace) for all breaks to maximize the calculated long term DW pressure.

(A1.9) Effect of Nitrogen Versus Air in the Containment

In the analyses prior to DCD Tier 2, Revision 4, the TRACG nodalization used air properties for the NC gases inside the containment. Parametric cases (using the MSLB bounding case as base case) were performed to assess the impact of nitrogen versus air properties. Results of these parametric studies show that the difference in the calculated maximum DW pressure at 72 hours is small (+0.53 kPa for nitrogen) comparing to the margin to the design pressure.

Based on these parametric studies, the TRACG nodalization is revised (in DCD Tier 2, Revision 4) with nitrogen properties for the NC gases for all breaks to maximize the calculated long-term DW pressure.

(A1.10) Effect of One DPV Failure Versus One SRV Failure

The MSLB bounding case assumes a single failure of one DPV. Parametric case with a single failure of one SRV was performed, to assess the impact of one DPV failure versus one SRV failure. Comparison of these two cases shows that the failure of one DPV generates higher long-term DW pressure. The calculated peak DW pressure for the case with a single failure of one DPV is 0.79 kPa higher at 72 hours than that for the case with one SRV failure.

(A2) General Discussions [FWLB – Bounding Conditions]

The containment responses to a postulated FWLB are discussed in the following paragraphs and figures. The bounding case (DCD Tier 2, Revision 4, Figures 6.2-13a1 to 6.2-13d3) is used for these discussions. This case assumes a single failure of one DPV and bounding conditions (DCD Tier 2, Revision 4, Table 6.2-6), and assumes 100% double-ended break.

(A2.1) Nodalization

Figures 6.2-98S01-1 and _6.2-98S01-2 show the TRACG nodalizations for the RPV and containment. DCD Tier 2, Revision 4, Figure 6.2-8b shows the nodalization for the feedwater line system. Two pipes (per GDCS airspace) are used to simulate the connection between the GDCS pool airspace and the DW (RAI 6.2-98 S01 Figure 6.2-98 S01-2), to purge the residual NC gases in this airspace. For the NC gases, the nitrogen properties are used in these TRACG calculations.

In the analyses prior to DCD Tier 2, Revision 4, the FWLB assumes a single failure of one SRV. Result of parametric study on the MSLB bounding case (see discussion in Paragraph A1.10 of this response) shows that the calculated peak DW pressure for the case with a single failure of one DPV is 0.79 kPa higher at 72 hours than that for the case with one SRV failure. The assumption of a single failure of one DPV is also used in the FWLB case to maximize the calculated containment pressure.

(A2.2) Pressure Responses

RAI 6.2-98 S01 Figure 6.2-98 S01-26 shows the RPV, DW and WW pressures, and RAI 6.2-98 S01 Figure 6.2-98 S01-27 and _ RAI 6.2-98 S01 Figure 6.2-98 S01-28 show the DW and WW pressures at different time scales.

Following the postulated LOCA, the DW pressure increased rapidly leading to the clearing of the PCCS and main vents. The DW pressure increase is terminated at approximately 70 seconds (RAI 6.2-98 S01 Figure 6.2-98 S01-27), when most of the NC gases in the DW annulus have been purged into the WW (RAI 6.2-98 S01 Figure 6.2-98 S01-32). The peak DW pressure prior to the GDCS flow initiation for this case is approximately 318 kPa (46.1 psia) (RAI 6.2-98 S01 Figure 6.2-98 S01-28), and occurred at 347 seconds, shortly after the opening of DPVs. This peak pressure is below the design pressure of 60 psia with large margin.

The GDCS flow initiates at approximately 507 seconds (DCD Tier 2, Revision 4, Table 6.2-7d). The subcooled GDCS water continues flowing into the RPV, reduces the steaming from the RPV and the DW pressure. At approximately 800 seconds, the DW pressure drops below the WW pressure, causing the openings of vacuum breakers and allowing some NC gases to flow back into the DW. Consequently, the system pressures drop to a value of approximately 260 kPa (RAI 6.2-98 S01 Figure 6.2-98 S01-28).

Subsequently, decay heat overcomes the subcooling in the GDCS water and steaming resumes (at ~ 1900 seconds, RAI 6.2-98 S01 Figure 6.2-98 S01-28). The resumption of RPV steaming causes the DW pressure to increase again starting from 2500 seconds. The DW pressure reaches the long-term peak of 351 kPa (51 psia) at 72 hours (RAI 6.2-98 S01 Figure 6.2-98 S01-26).

After 2500 seconds, the DW pressure is higher than the WW pressure. The PCCS takes steam/NC gas mixture from the DW and purges the NC gases into the WW. Most of the NC gases that returned to the DW due to the vacuum breaker openings are purged back into the WW in approximately 3 hours (RAI 6.2-98 S01 Figure 6.2-98 S01-31).

(A2.3) Level and Heat Removal Responses

RAI 6.2-98 S01 Figure 6.2-98 S01-29 compares the total heat removal by the PCCS with the decay heat. After the first 6 hours, the PCCS condensers are able to remove all the decay heat with some margin to spare. From this point on, all the decay heat generated by the core is transferred to the IC/PCC pools, which are located outside of the containment.

RAI 6.2-98 S01 Figure 6.2-98 S01-30 shows the IC/PCC pool water level. The IC/PCC pool water level drops due to boiloff by the decay heat. At 34.1 hours, the pool level drops below the elevation of 29.6 m, (or top one-quarter portion of the PCCS condenser tube length uncovered). The connection valves open to allow the water from the Dryer/Separator storage pools to flow into the IC/PCC pools.

(A2.4) NC Gas Responses

Figures 6.2-98S01-31 through 6.2-98S01-33 show the NC gas pressures in the DW annulus, the DW head airspace and the GDCS pool airspace. RAI 6.2-98 S01 Figure 6.2-98 S01-33 shows that most of the NC gases in the DW annulus are purged into the WW within 100 seconds. At approximately 800 seconds, some NC gases flows back to the DW annulus (RAI 6.2-98 S01 Figure 6.2-98 S01-33) after the opening of the vacuum breakers.

To maximize the calculated DW pressure during the post-GDCS draindown period, two pipes are used in the TRACG nodalization to simulate the connection between the GDCS airspace and the DW, to purge the residual NC gases in this airspace (see discussion in Paragraph A1.8 of this response). These two pipes are connected at the top two axial levels in the GDCS airspace (L35 and L34, RAI 6.2-98 S01 Figure 6.2-98 S01-2), one pipe per level (per GDCS airspace).

For MSLB, in which case the GDCS pool level stays above L33 (i.e., no air mass is stored in L33), the two-pipe model works effectively to purge the NC gas masses stored in the top two levels to minimal values in a few hours. For breaks other than MSLB, the GDCS pool level may drop into L33 during the draindown period and a small amount of NC gas mass remains in this bottom level. Since the pressure margins for the non-MSLB breaks are more than 10% higher than that for the MSLB (DCD Tier 2, Revision 4, Table 6.2-5,), this small amount of NC gas remaining in the GDCS airspace for non-MSLB breaks would not change the conclusion that MSLB is the limiting break.

Figures 6.2-98S01-34 through _6.2-98S01-36 show the NC gas mass profiles in the DW head airspace, the GDCS pool airspace and the WW. RAI 6.2-98 S01 Figure 6.2-98 S01-31 shows that there is essentially no NC gas remaining in the DW annulus region, after 3 hours into the transient. Significant increase in the total WW NC gas mass occurs in the first 3 hours (RAI 6.2-98 S01 Figure 6.2-98 S01-36), during this time period basically all the initial NC gases in the DW annulus are purged into the WW. The increase in WW NC gas after 12 hours corresponds to the radiolytic gases generated

in the core and purged into the WW via the PCCS. The total NC gas mass in the WW at 72 hours is 14324 kg.

RAI 6.2-98 S01 Figure 6.2-98 S01-34 shows the NC gas mass profiles in the GDCS airspace. Initially, the GDCS water level is located at L34 (Level 34, DCD Tier 2, Revision 3, Figure 6.2-7), and the gas space includes L34 and L35 with initial NC gas masses stored in these levels. For the FWLB, the water level drops after the initiation of GDCS flow and drops to the pool bottom (L33) in approximately 4 hours. This creates a new bottom layer of gas space, which is approximately 6 meters below the connection pipes, to store NC gas mass. NC gas masses stored in the top 2 levels (L34 and L35) are purged to the minimal values in a few hours, by the connection pipes. At 72 hours, a total of 680 kg of NC gas is stored in the bottom two levels (L33 and L34). This amount is less than 5% of the total NC gas mass inside the containment (DW and WW).

It should be noted that for the MSLB the GDCS pool level stays above L33 (i.e., no NC gas mass is stored in L33). And, NC gas masses stored in the top 2 levels (L34 and L35) are purged to the minimal values in a few hours, through the connection pipes.

RAI 6.2-98 S01 Figure 6.2-98 S01-35 shows the DW head airspace NC mass. The total NC gas mass in the DW head airspace at 72 hours is 30 kg. This amount is approximately 0.2% of the total NC gas mass inside the containment (DW and WW).

(A2.5) Effect of Residue NC Gas Mass on the DW Pressure

At 72 hours, the total NC gas masses in the WW, GDCS airspace and DW head airspace are, 14324 kg, 680 kg and 30 kg. There is essentially no NC gas remaining in the DW annulus region. The total NC gas in these regions is 15034 kg. If the residue NC gas masses in the GDCS airspace and DW head airspace are purged completely into the WW, the DW pressure would increase by the NC gas mass ratio of (15034/14324 = 1.05).

For the FWLB case, the impact of residue NC gas mass is an increase of 5% in the calculated DW pressure. For the bounding FWLB case, the maximum DW pressure at 72 hours would increase from 351.7 kPa (DCD Tier 2, Revision 4, Table 6.2-5) to 369.3 kPa. The margin to design pressure of 45.3 psig would reduce from 19.9% to 14.2%.

The above assessment shows that the MSLB is still the limiting break.

(A2.6) Suppression Pool and WW Responses

RAI 6.2-98 S01 Figure 6.2-98 S01-37 compares the water levels in the DW annulus and suppression pool. The DW annulus water level rises due to the break flow discharges from the RPV and from the broken feedwater piping (from the feedwater heaters). In approximately 10 hours, the DW annulus water level reaches the quasi-equilibrium elevation of 9 meters. At this elevation, the DW annulus water level is approximately 3 meters below the spillover holes. The hot water in the DW annulus will remain in the DW and not enters into the suppression pool via the spillover holes.

Figures 6.2-98S01-38 through _6.2-98S01-40 show the DW gas temperature, WW gas temperature and suppression pool surface temperature.

(A2.7) Downcomer Level and FWLB Break Flow

RAI 6.2-98 S01 Figure 6.2-98 S01-41 shows the two-phase level in the RPV downcomer, and RAI 6.2-98 S01 Figure 6.2-98 S01-41a shows the two-phase level with enlarged time scale. The FWLB elevation is located at 18.915 meters (from the RPV bottom). RAI 6.2-98 S01 Figure 6.2-98 S01-41a shows that the two-phase level swells above the break elevation from 0.5 to 2.0 hours. During this time period, the downcomer two-phase mixture over-spills from the RPV into the DW annulus. RAI 6.2-98 S01 Figure 6.2-98 S01-42 shows the FWLB flow from the RPV. RAI 6.2-98 S01 Figure 6.2-98 S01-43 compares the downcomer liquid temperature (at L16) with the DW annulus vapor temperature. The FWLB elevation is located at L16 (RAI 6.2-98 S01 Figure 6.2-98 S01-1) and the GDCS injection is located at L10 (8.4 meters below the break elevation). The injected GDCS water mixes with the downcomer fluid. The subcooling of this mixture reduces as it moves upward towards the break elevation.

(A2.8) PCCS Inlet Conditions

RAI 6.2-98 S01 Figure 6.2-98 S01-44 shows the total mixture and air mass flows at the PCCS inlet, and RAI 6.2-98 S01 Figure 6.2-98 S01-45 shows the mass flows with enlarged time scale. 6.2-98S01-45a shows the moisture content at the PCCS inlet. This is calculated as (1–void fraction) at the top of the DW next to the PCCS inlet. The calculated results show that there are no water droplets at the PCCS inlet location during this transient.

(B) The NC gas holdup in the DW head and GDCS pool airspaces and effect of a well-mixed atmosphere in the GDCS open volume is discussed in this section.

(B1) Double Pipe Connection

Two pipes (per GDCS airspace) are used to simulate the connection between the GDCS pool airspace and the DW (RAI 6.2-98 S01 Figure 6.2-98 S01-2). This nodalization is selected to minimize the NC gas holdup in the DW head and GDCS pool airspaces. Parametric studies (using MSLB case) were performed earlier (response to RAI 6.2-53 S01, MFN 02-215, Supplement 1) to evaluate the effectiveness of the double pipe connection. The results show that there are essentially no NC gases remaining in the DW head and GDCS airspaces for the MSLB with double pipe connection. The current results (Paragraph A1.4 in this response) also show the same effect on the purging of NC gases.

The two pipes are connected at the top two axial levels in the GDCS airspace (L35 and L34, RAI 6.2-98 S01 Figure 6.2-98 S01-2), one pipe per level (per GDCS airspace). For MSLB, in which case the GDCS pool level stays above L33 (i.e., no air mass is stored in L33), the two-pipe model works effectively to purge the NC gas masses stored in the top two levels to minimal values in a few hours. For breaks other than MSLB, the GDCS pool levels drop into L33 (the pool level is approximately 6 meters below the lower connection pipes) during the draindown period and a small amount of NC gas mass remains in this bottom level. Since the pressure margins for the non-MSLB breaks are more than 10% higher than that for the MSLB (DCD Tier 2, Revision 4, Table 6.2-5), this small amount of NC gas remaining in the GDCS airspace for non-MSLB breaks would not change the conclusion that MSLB is the limiting break.

For the bounding FWLB (Paragraphs B2.4 and B2.5), the holdup NC gas mass is approximately 5% of the total NC gas mass in the containment. The impact of this holdup gas on the calculated DW pressure at 72 hours is a reduction of 5% in pressure margin (i.e., from 19.9% to 14.2%).

(B2) Effect of Well-Mixed Atmosphere in the GDCS Open Volume

A well-mixed atmosphere in the GDCS airspace that is opened to the DW annulus would eliminate the hideout volumes for the NC gases. The effect is a complete purging of NC gases from these hideout volumes and maximizing the calculated DW pressure.

For the MSLB, there are essentially no NC gases remaining in the DW head and GDCS airspaces (Paragraph A1.4). The calculated DW pressure accounts for the effect that all NC gases have been purged into the WW.

For the bounding FWLB (Paragraphs B2.4 and B2.5), the remaining NC gas mass in the DW head and GDCS airspace is approximately 5% of the total NC gas mass in the containment. The impact of this amount of holdup gas on the calculated DW pressure at 72 hours is an increase of 5% in DW pressure, or a reduction of 5% in pressure margin (i.e., from 19.9% to 14.2%).

(C)The NC gas holdup in the DW head and effect of transferring NC gas from the DW head and GDCS airspaces to the WW is discussed in this section.

(C1) NC Gas Mass

The NC gas mass profiles in the DW head, GDCS airspace and WW are discussed in Paragraph A1.4 and RAI 6.2-98 S01 Figure 6.2-98 S01-14 through _16 for the bounding MSLB case.

The NC gas mass profiles in the DW head, GDCS airspace and WW are discussed in Paragraph A2.4 and RAI 6.2-98 S01 Figure 6.2-98 S01-34 through 36 for the bounding FWLB case.

(C2) Effect of Residue NC Gas in the Holdup Volumes on the DW Pressure

For the bounding MSLB, there are essentially no NC gases remaining in the DW head and GDCS airspaces (Paragraph A1.4). The calculated DW pressure accounts for the effect that all NC gases have been purged into the WW.

For the bounding FWLB break (Paragraphs B2.4 and B2.5), the remaining NC gas mass in the DW head and GDCS airspace is approximately 5% of the total NC gas mass in the containment. The impact of this amount of holdup gas on the calculated DW pressure at 72 hours is an increase of 5% in DW pressure, or a reduction of 5% in pressure margin (i.e., from 19.9% to 14.2%).

(D) After the opening of the DPVs, the long-term containment responses from FWLB accident to MSLB accidents are expected to be similar. However, the results show that they differ. Please (1) identify and justify the nodalization differences between FWLB and MSLB accidents and (2) explain the differences in results.

(D1) Nodalization

The MSLB and the FWLB use the same nodalizations for the RPV and containment (Paragraphs A1.1 and A2.1). The differences between these two cases are the modeling of the break pipes (DCD Tier 2, Revision 4, Figure 6.2-8 for MSLB and Figure 6.2-8b for FWLB).

The difference in the DW pressures between these two cases is explained in the following paragraph.

(D2) Differences in LOCA Transient

The key factors that affect the long-term DW pressure are the suppression pool surface temperature, the NC gas hideout and the WW gas temperature. The suppression pool surface temperature affects the partial steam pressure in the WW, and consequently the DW pressure. Figures 6.2-98S01-46 to _6.2-98S01-48 compare the DW pressures, suppression pool surface temperatures and WW gas temperatures from these two cases.

During the blowdown period, the steam blowdown from the DW into the suppression pool via the main vents heats up the suppression pool water. The heatup in the suppression pool surface in the MSLB case is higher than that in the FWLB case (RAI 6.2-98 S01 Figure 6.2-98 S01-47). The same temperature difference is maintained (more or less) for the rest of the 72 hours transient. At 72 hours, the pool surface temperatures for the MSLB and FWLB are 76.7°C and 70.1°C, respectively. The corresponding partial steam pressures are 41.3 kPa and 31.3 kPa. The difference in the partial steam pressure between these two cases is 10.0 kPa. The impact of higher suppression pool surface temperature is 10 kPa on the long-term DW pressure in the FWLB case.

RAI 6.2-98 S01 Figure 6.2-98 S01-48 compares the WW gas temperature at the top of WW. As a result of higher suppression pool surface temperature, the WW gas temperature is a few degrees higher in the MSLB case than that in the FWLB case. At 72 hours, the WW gas temperatures are 116.3°C (389.4°K) and 112.9°C (386.0°K), respectively. The difference in the WW gas temperature is 3.4°C (3.4°K) between these two cases. The ratio of (3.4°K/389.4°K) is approximately 1%. The impact of higher WW gas temperature is +1% on the long-term DW pressure in the FWLB case, or 3.5 kPa.

For the bounding FWLB case (Paragraphs B2.4 and B2.5), the remaining NC gas mass in the DW head and GDCS airspace is approximately 5% of the total NC gas mass in the containment. The impact of this amount of holdup gas on the calculated DW pressure at 72 hours is an increase of 5% in DW pressure, or 17.6 kPa.

RAI 6.2-98 S01 Figure 6.2-98 S01-46 compares the DW pressures from these two cases. For the MSLB case, essentially all NC gases remaining in the DW head and GDCS airspaces (Paragraph A1.4) are purged into the WW after 20 hours. The calculated DW pressure in the MSLB case accounts for the effect that all NC gases have been purged into the WW. After 20 hours, the calculated DW pressures from these two cases are very similar in trend. The DW pressure in the MSLB case is higher than that in the FWLB case. The pressure difference is more or less constant through out the rest of the transient.

At 72 hours, the difference in DW pressure between these two cases is (384.6 kPa – 351.7 kPa) or 32.9 kPa (DCD Tier 2, Revision 4, Table 6.2-5). The calculated DW pressure is lower in the FWLB case is due to the lower suppression pool surface temperature, lower WW gas temperature and some hideout NC gas. The combined effect of these factors on the long-term DW pressure is an increase of (10.0 + 3.5 + 17.6) or 31.7 kPa. Accounting for this combined effect, the calculated DW pressure in the FWLB case agree very well with that calculated in the MSLB case.

It should be noted that approximately 41% of the difference in the DW pressures is due to the differences in the suppression pool surface and WW gas temperatures. These temperature differences are results of response to different blowdown transient from different break size and location.

(E) The effect of the DW gas recirculation system and any other systems that may be credited in the long-term containment pressure and temperature analyses will be provided in a future RAI response.

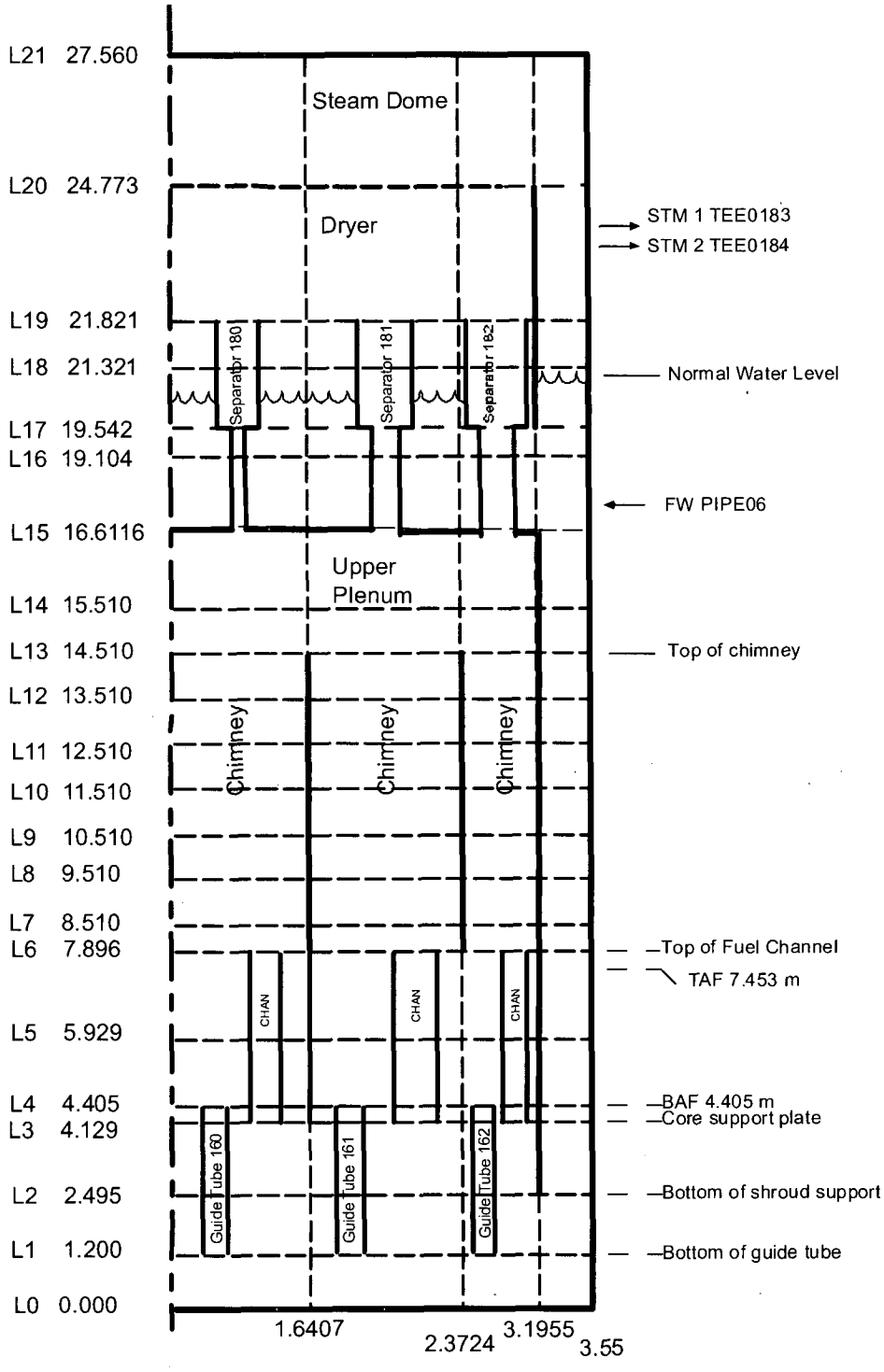

RAI 6.2-98 S01 Figure 6.2-98 S01-1. DCD TRACG Nodalization of the ESBWR RPV

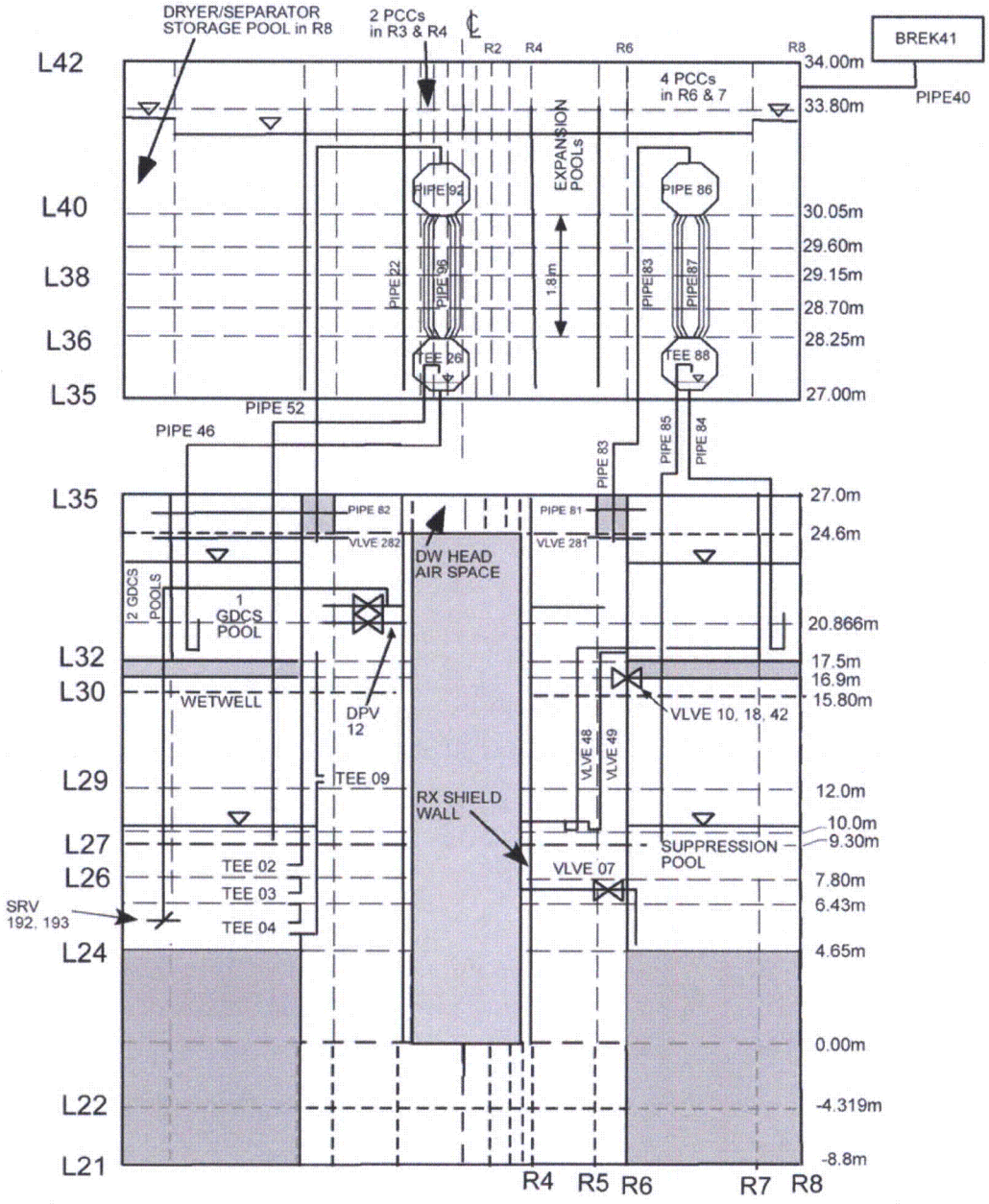

RAI 6.2-98 S01 Figure 6.2-98 S01-2. DCD TRACG Nodalization of the ESBWR Containment

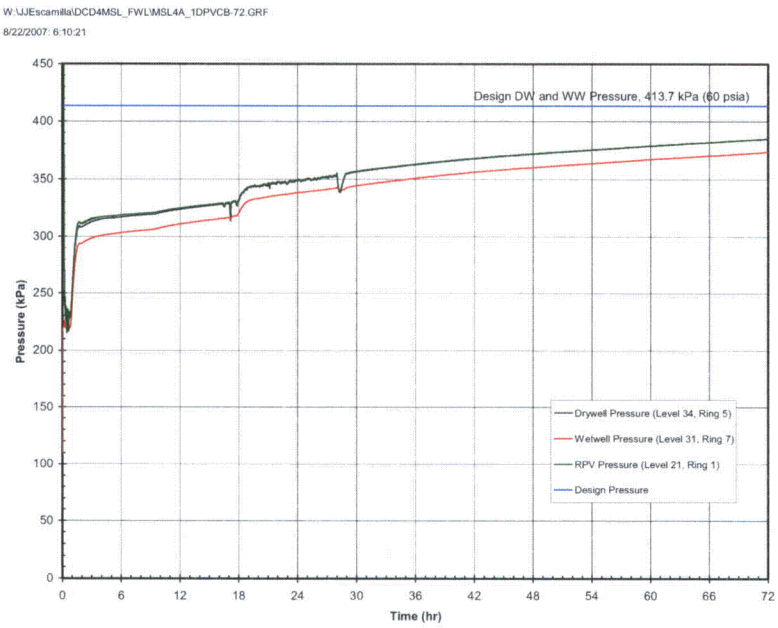

RAI 6.2-98 S01 Figure 6.2-98 S01-3. Containment Pressure Response (72 Hours)

(MSLB: MSL4A_1DPVCB-72)

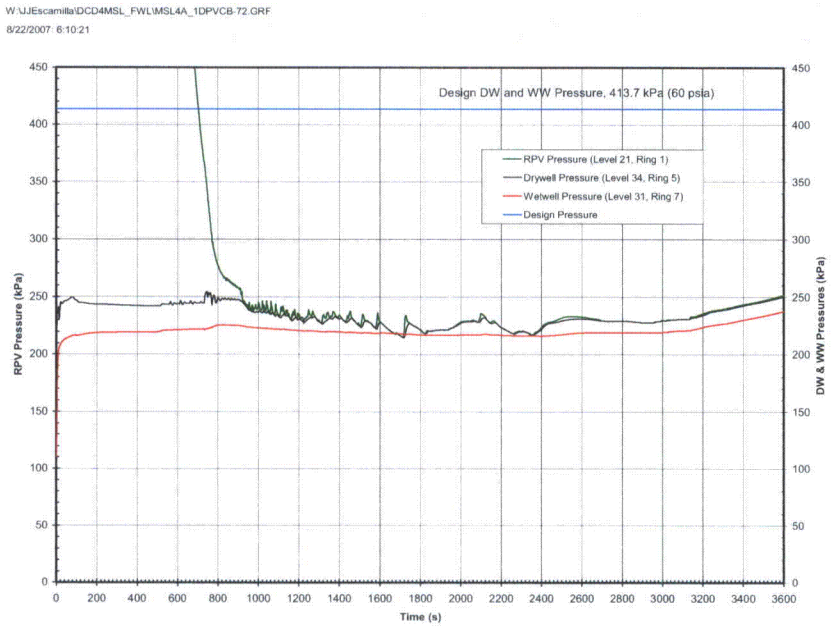

RAI 6.2-98 S01 Figure 6.2-98 S01-3a. Containment Pressure Response (Short-Term Time Scale) (3600 Seconds)

(MSLB: MSL4A_1DPVCB-72)

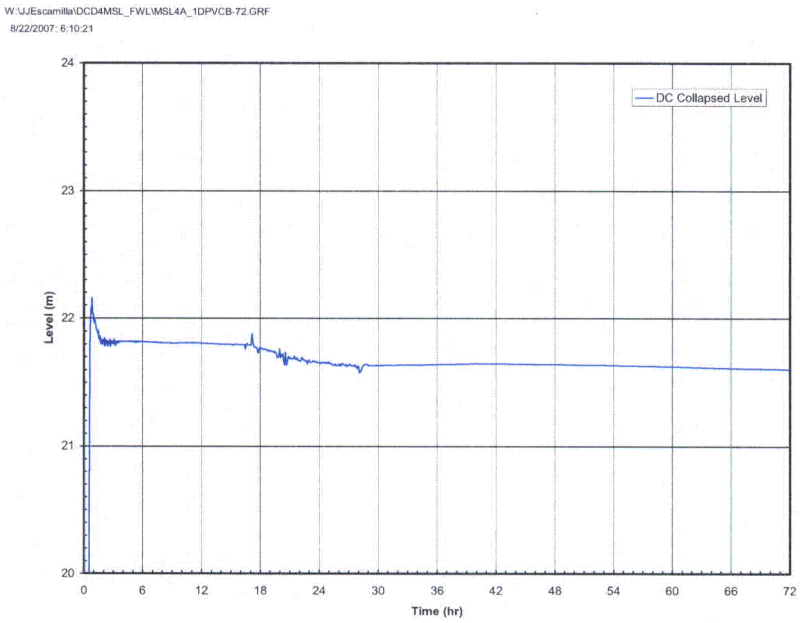

RAI 6.2-98 S01 Figure 6.2-98 S01-4. Downcomer Collapsed Level (72 Hours)

(MSLB: MSL4A_1DPVCB-72)

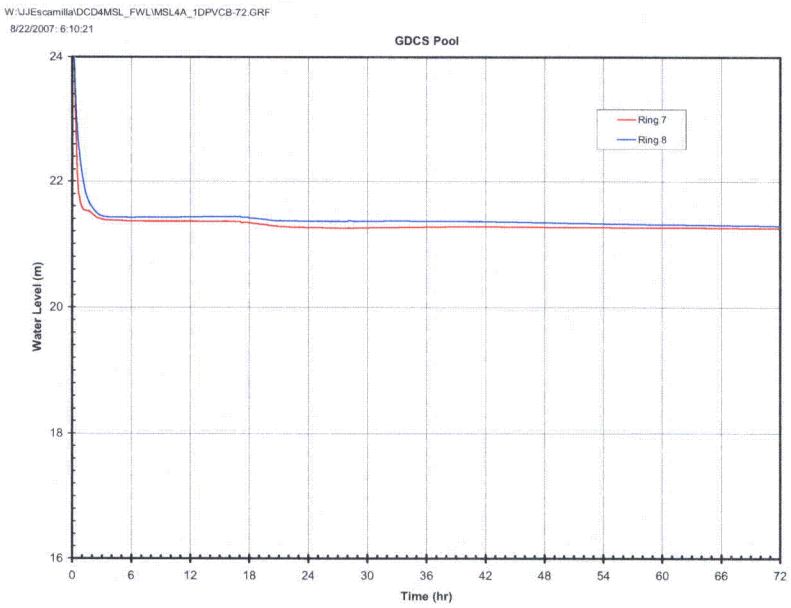

RAI 6.2-98 S01 Figure 6.2-98 S01-5. GDCS Pool Levels (72 Hours)

(MSLB: MSL4A_1DPVCB-72)

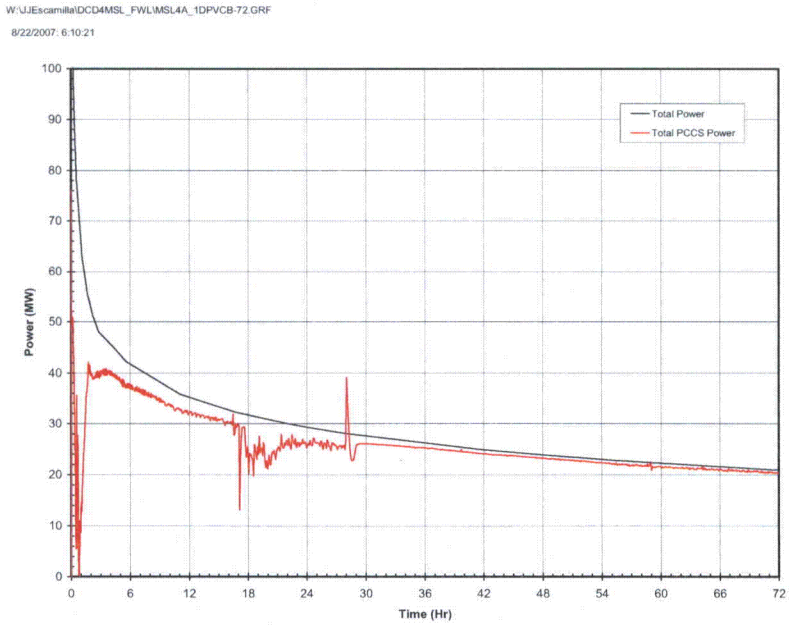

RAI 6.2-98 S01 Figure 6.2-98 S01-6. PCCS Heat Removal versus Decay Heat (72 Hours)

(MSLB: MSL4A_1DPVCB-72)

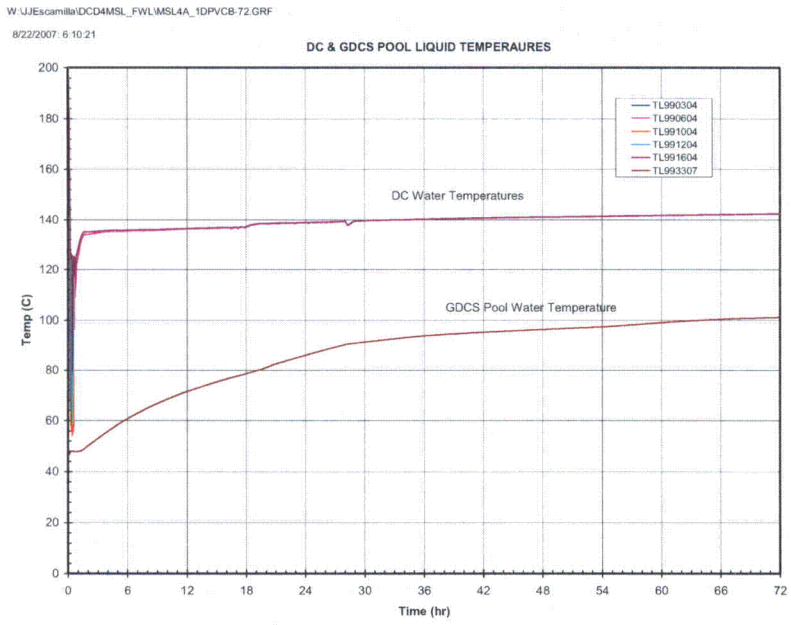

RAI 6.2-98 S01 Figure 6.2-98 S01-7. GDCS Pool Water Temperature (72 Hours)

(MSLB: MSL4A_1DPVCB-72)

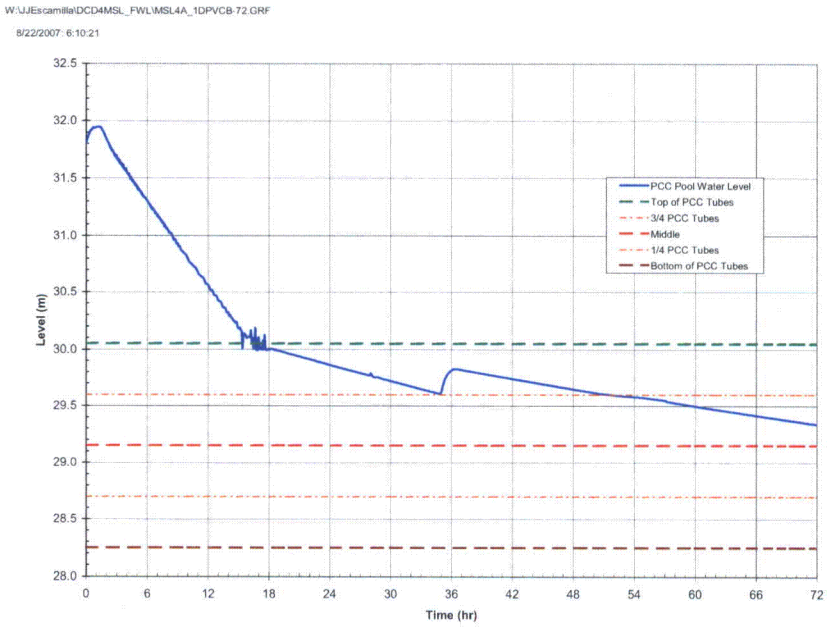

RAI 6.2-98 S01 Figure 6.2-98 S01-8. IC/PCC Pool Water Level (72 Hours)

(MSLB: MSL4A_1DPVCB-72)

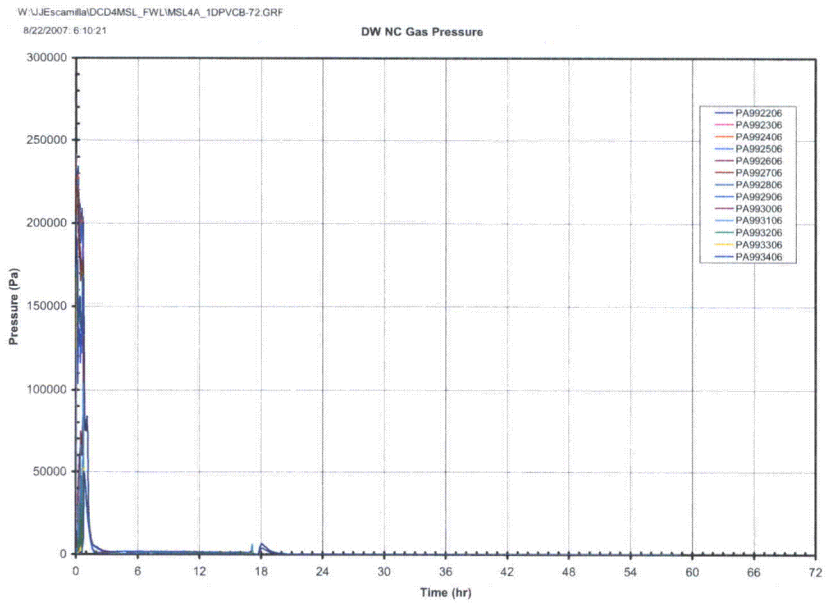

RAI 6.2-98 S01 Figure 6.2-98 S01-9. DW Annulus NC Gas Pressures (Level 23 - Second Level from Bottom, Level 34 - Top) (72 Hours)

(MSLB: MSL4A_1DPVCB-72)

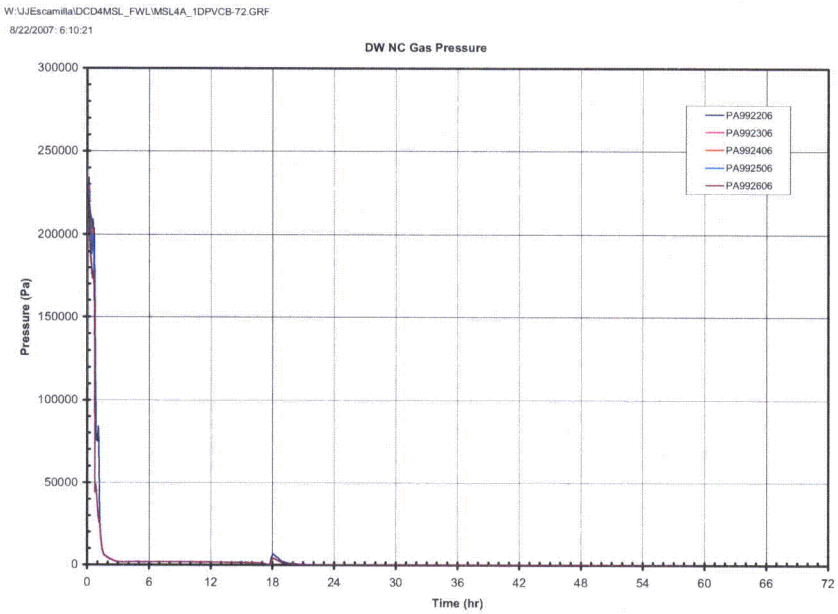

RAI 6.2-98 S01 Figure 6.2-98 S01-10. Lower DW NC Gas Pressures
(Level 23 - Second Level from DW Bottom)
(72 Hours)

(MSLB: MSL4A_1DPVCB-72)

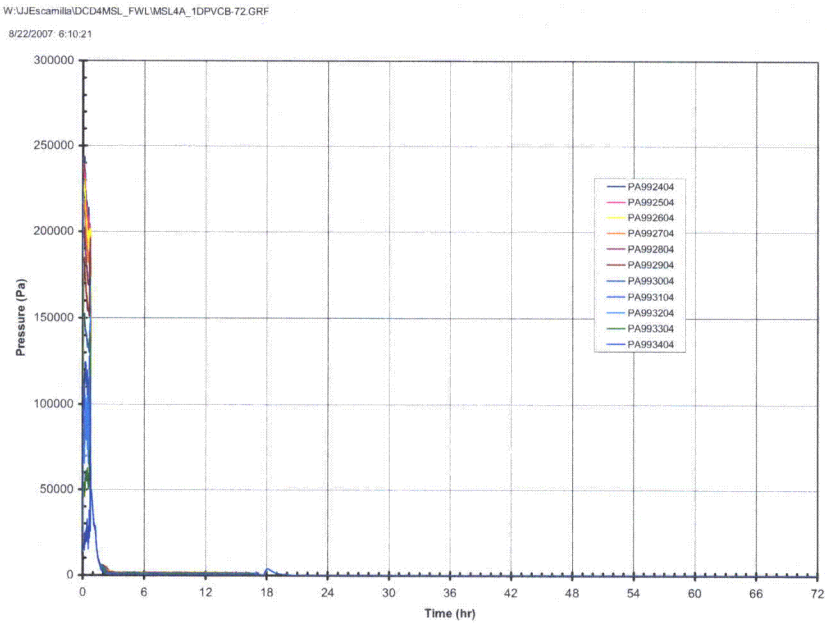

RAI 6.2-98 S01 Figure 6.2-98 S01-11. DW-Reactor Shield Wall NC Gas Pressures
(Level 24 - Bottom, Level 34 - Top)
(72 Hours)

(MSLB: MSL4A_1DPVCB-72)

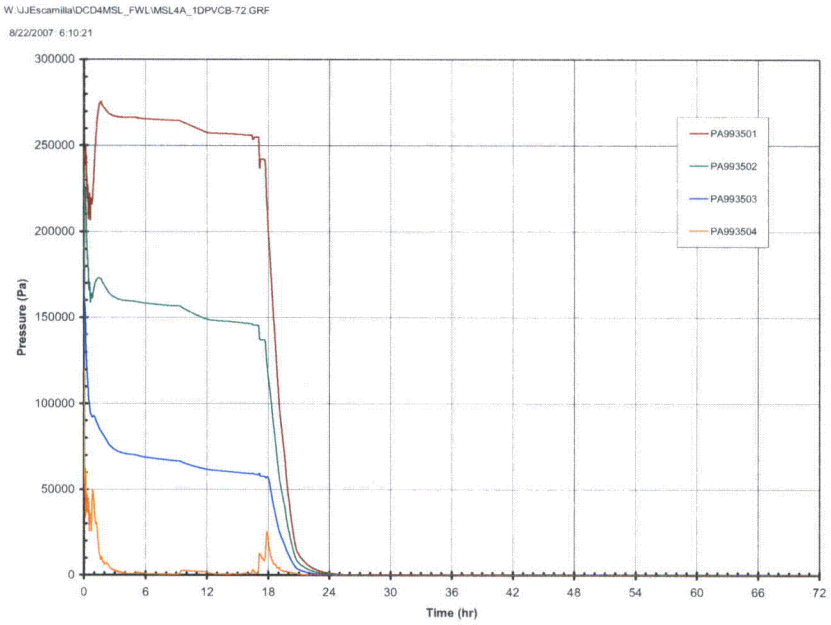

RAI 6.2-98 S01 Figure 6.2-98 S01-12. DW Head NC Gas Pressures
(Level 35 - DW Head)
(72 Hours)

(MSLB: MSL4A_1DPVCB-72)

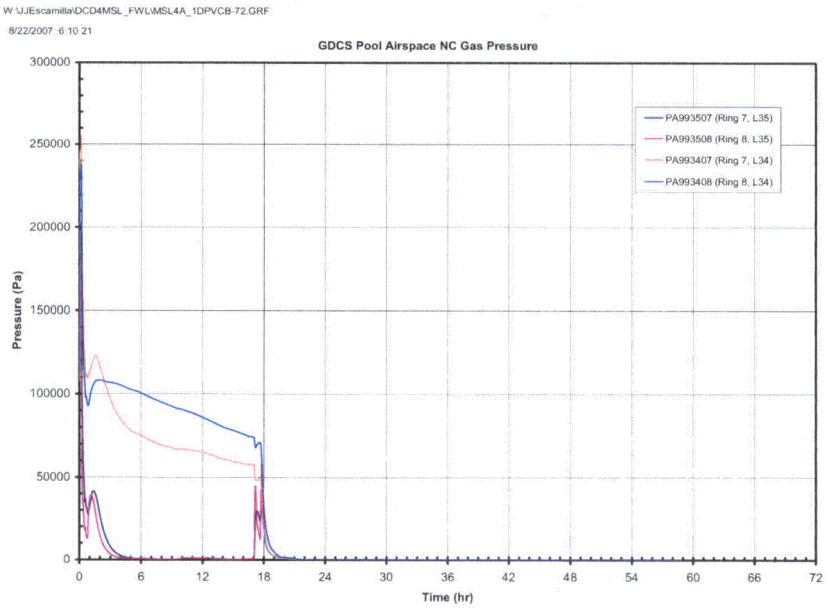

RAI 6.2-98 S01 Figure 6.2-98 S01-13. GDCS Pool Airspace NC Gas Pressures
(72 Hours)

(MSLB: MSL4A_1DPVCB-72)

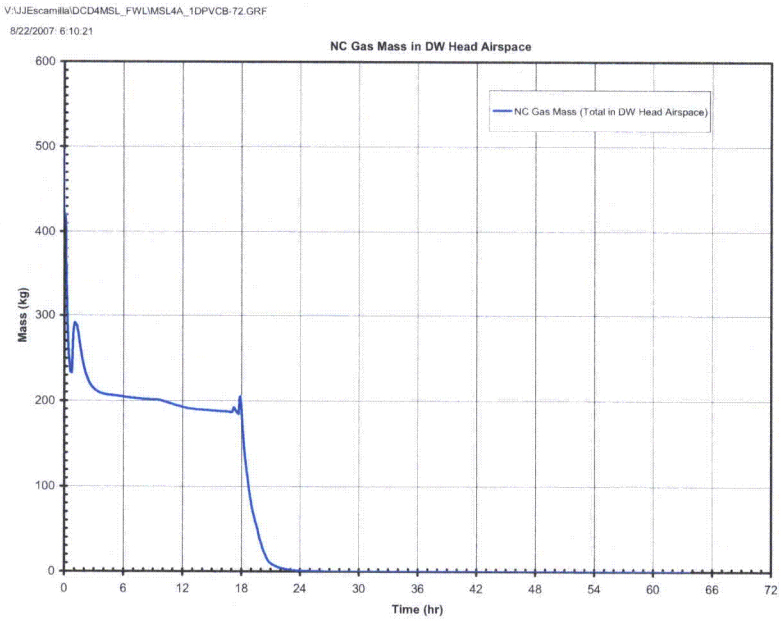

RAI 6.2-98 S01 Figure 6.2-98 S01-14. NC Gas Mass Profile in the DW Head Airspace (72 Hours)

(MSLB: MSL4A_1DPVCB-72)

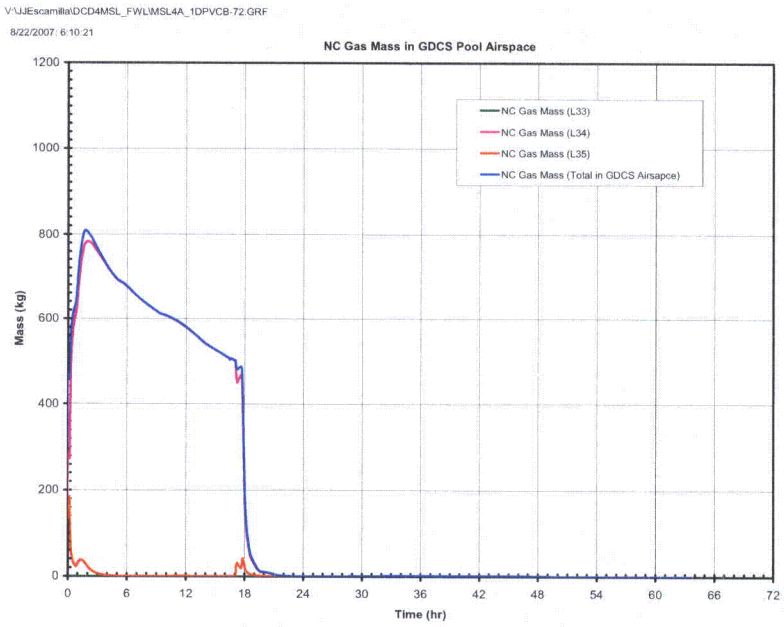

RAI 6.2-98 S01 Figure 6.2-98 S01-15. NC Gas Mass Profiles in the GDCS Pool Airspace (72 Hours)

(MSLB: MSL4A_1DPVCB-72)

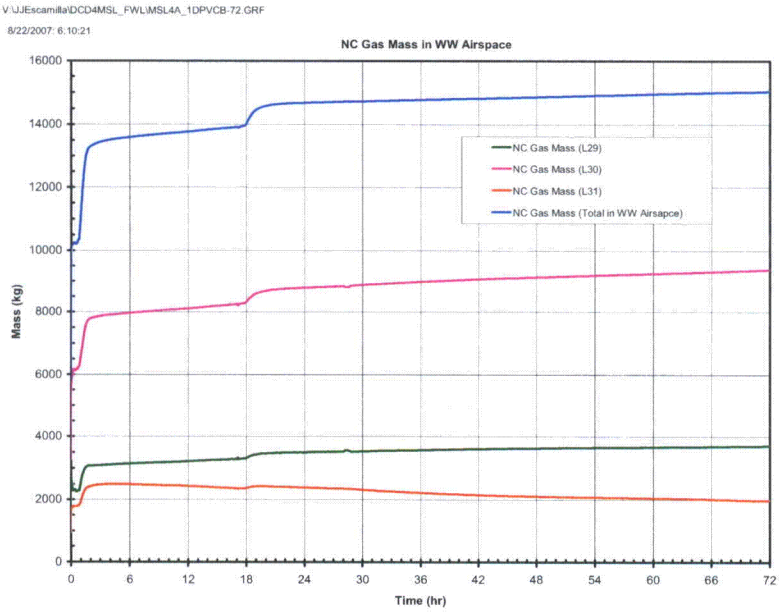

RAI 6.2-98 S01 Figure 6.2-98 S01-16. NC Gas Mass Profiles in the WW (72 Hours)

(MSLB: MSL4A_1DPVCB-72)

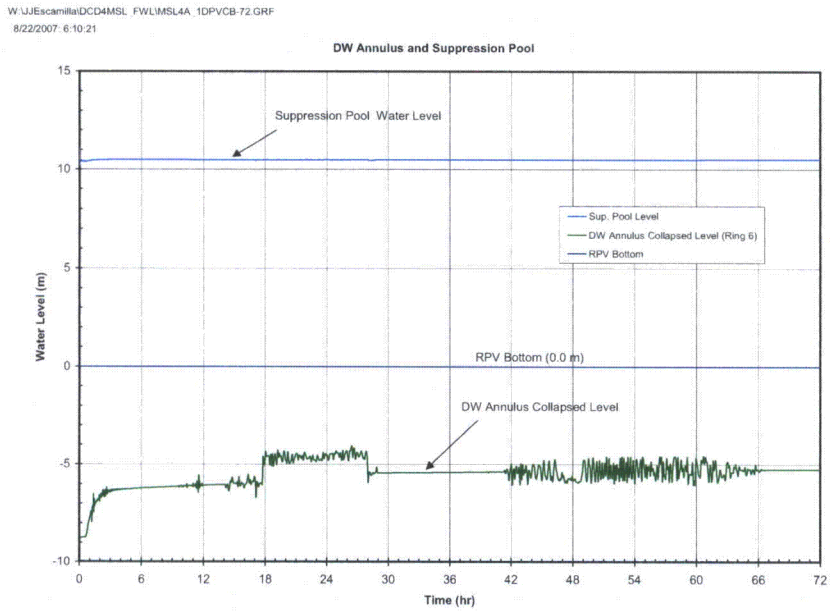

RAI 6.2-98 S01 Figure 6.2-98 S01-17. DW Annulus and Suppression Pool Levels (72 Hours)

(MSLB: MSL4A_1DPVCB-72)

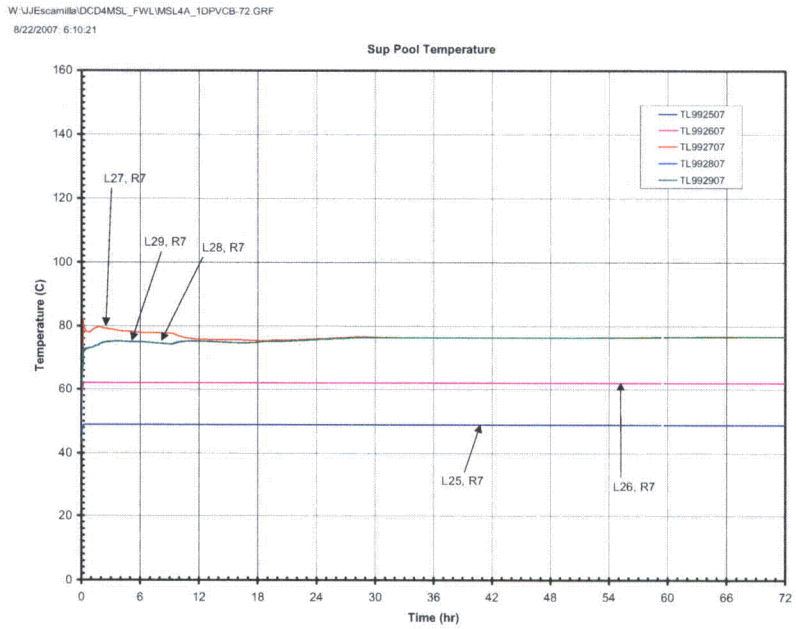

RAI 6.2-98 S01 Figure 6.2-98 S01-18. Suppression Pool Water Temperatures
(at Ring 7)
(72 Hours)

(MSLB: MSL4A_1DPVCB-72)

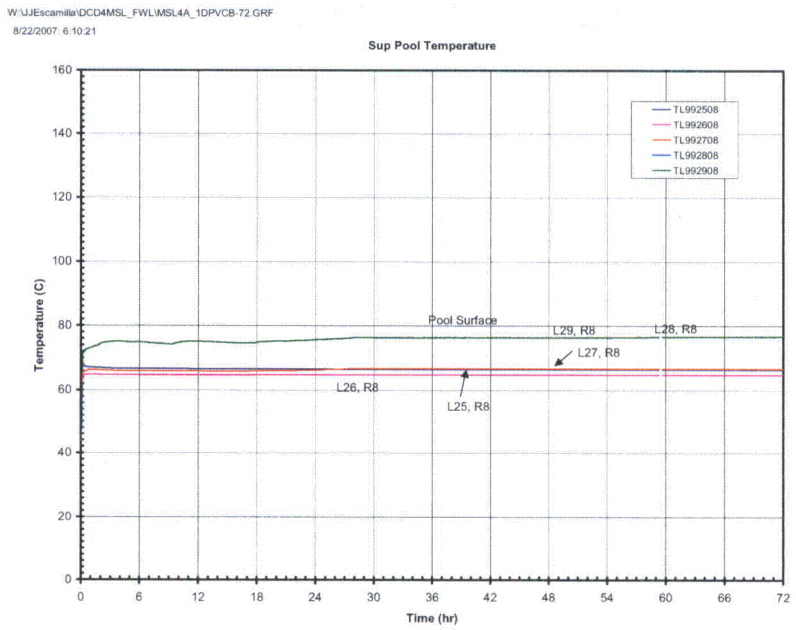

RAI 6.2-98 S01 Figure 6.2-98 S01-19. Suppression Pool Water Temperatures
(at Ring 8)
(72 Hours)

(MSLB: MSL4A_1DPVCB-72)

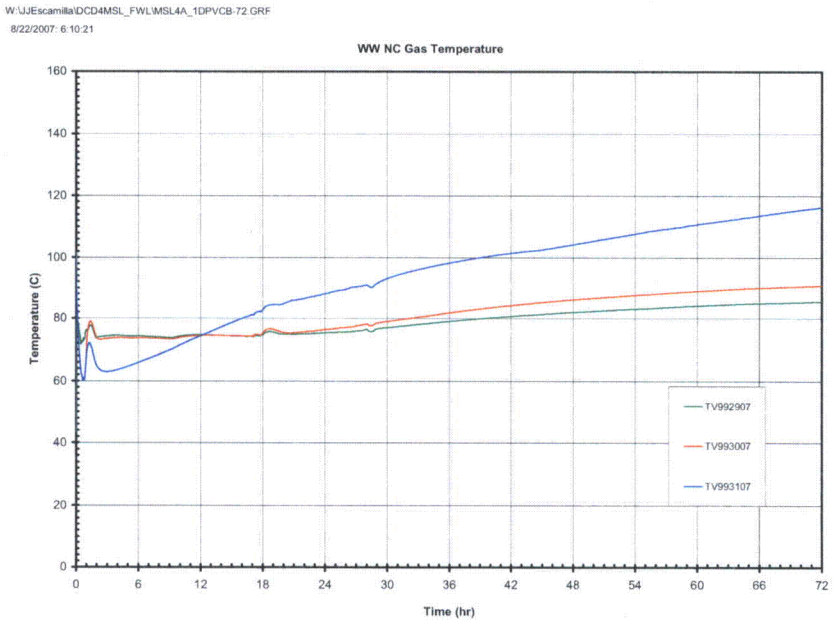

RAI 6.2-98 S01 Figure 6.2-98 S01-20. WW NC Gas Temperatures
(at Ring 7)
(72 Hours)

(MSLB: MSL4A_1DPVCB-72)

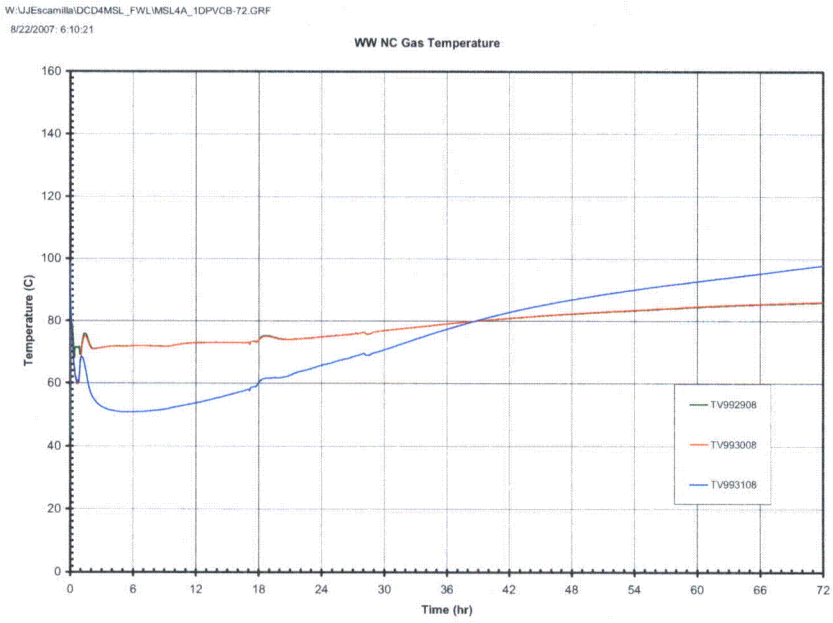

RAI 6.2-98 S01 Figure 6.2-98 S01-21. WW NC Gas Temperatures
(at Ring 8)
(72 Hours)

(MSLB: MSL4A_1DPVCB-72)

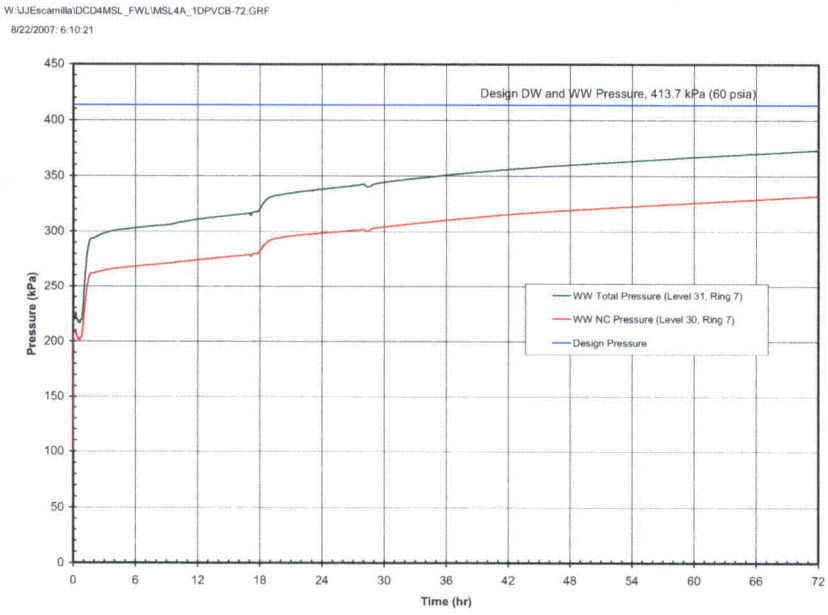

RAI 6.2-98 S01 Figure 6.2-98 S01-22. WW NC Gas Pressure
(in Ring 7)
(72 Hours)

(MSLB: MSL4A_1DPVCB-72)

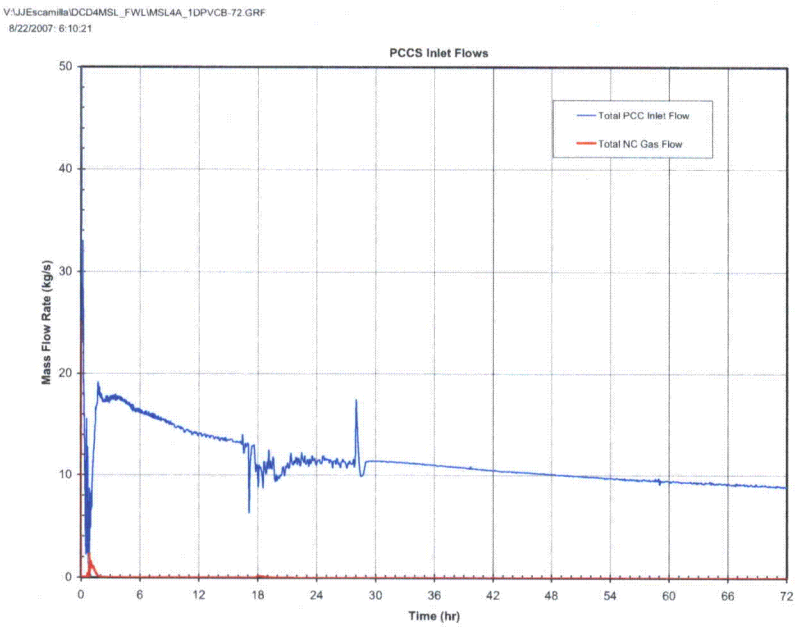

RAI 6.2-98 S01 Figure 6.2-98 S01-23. Total Mixture and NC Gas Mass Flows at the PCCS Inlet
(72 Hours)

(MSLB: MSL4A_1DPVCB-72)

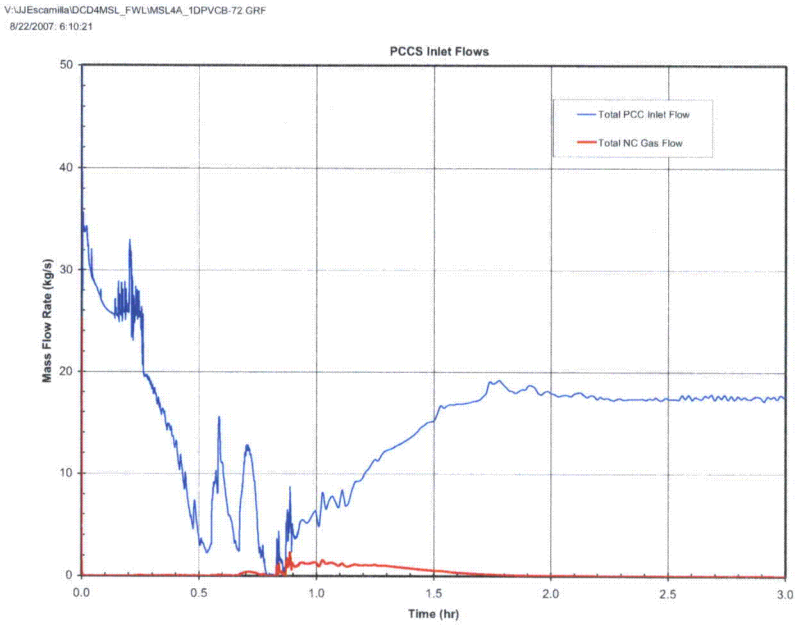

RAI 6.2-98 S01 Figure 6.2-98 S01-24. Total Mixture and NC Gas Mass Flows at the PCCS Inlet

(3 Hours)

(MSLB: MSL4A_1DPVCB-72)

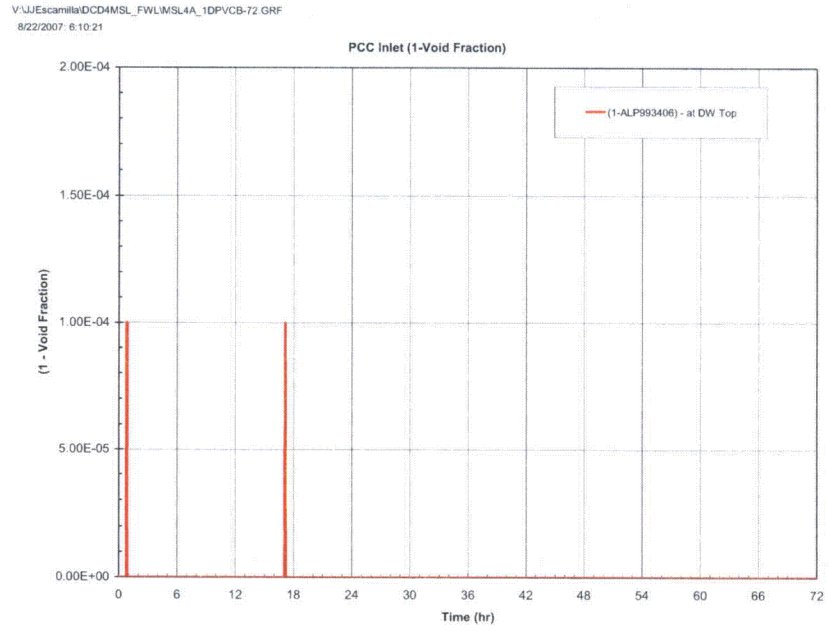

RAI 6.2-98 S01 Figure 6.2-98 S01-25. Mixture Content at the PCCS Inlet

(72 Hours)

(MSLB: MSL4A_1DPVCB-72)

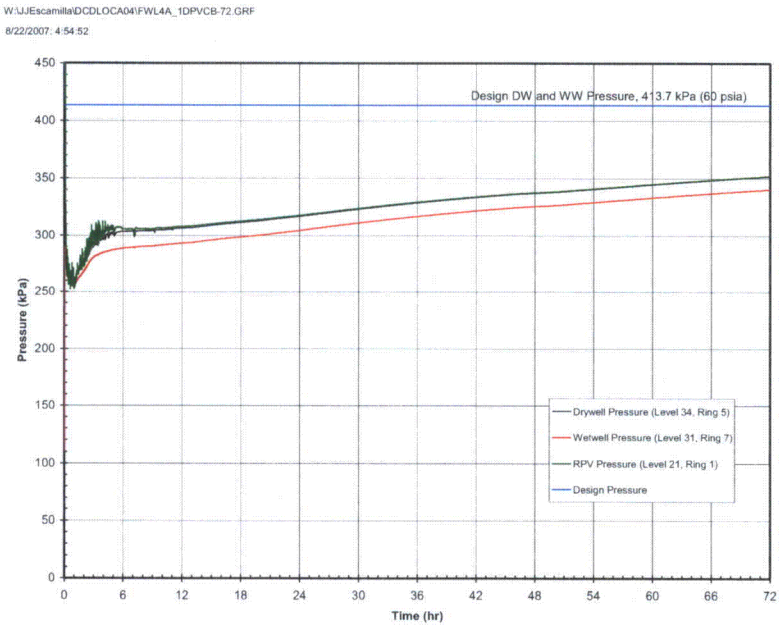

RAI 6.2-98 S01 Figure 6.2-98 S01-26. Containment Pressure Response (72 Hours)

(FWLB: FWL4A_1DPVCB-72)

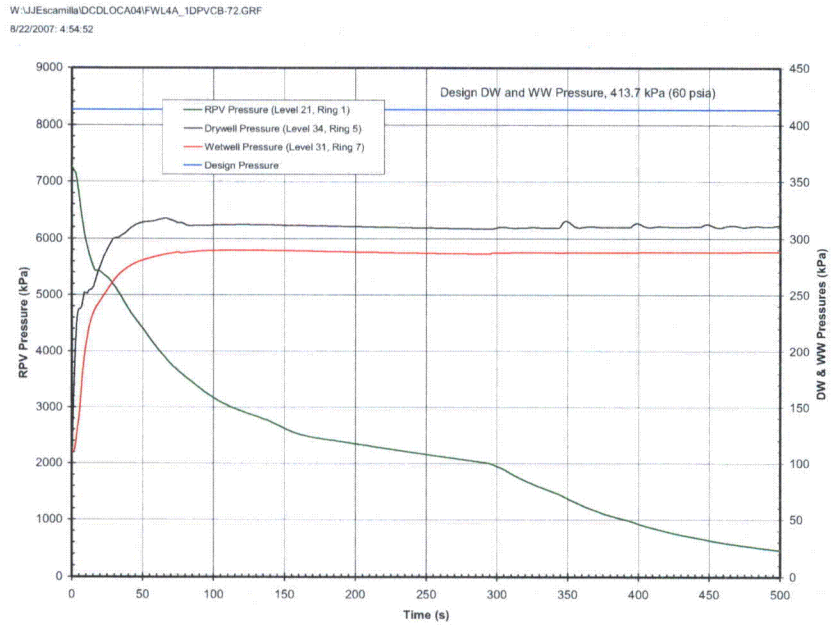

RAI 6.2-98 S01 Figure 6.2-98 S01-27. Containment Pressure Response (500 Seconds)

(FWLB: FWL4A_1DPVCB-72)

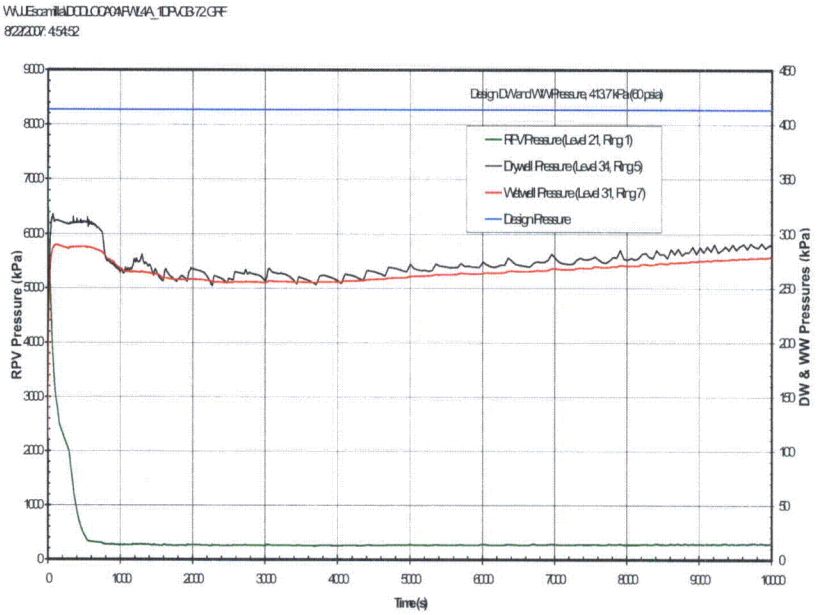

RAI 6.2-98 S01 Figure 6.2-98 S01-28. Containment Pressure Response (10000 Seconds)

(FWLB: FWL4A_1DPVCB-72)

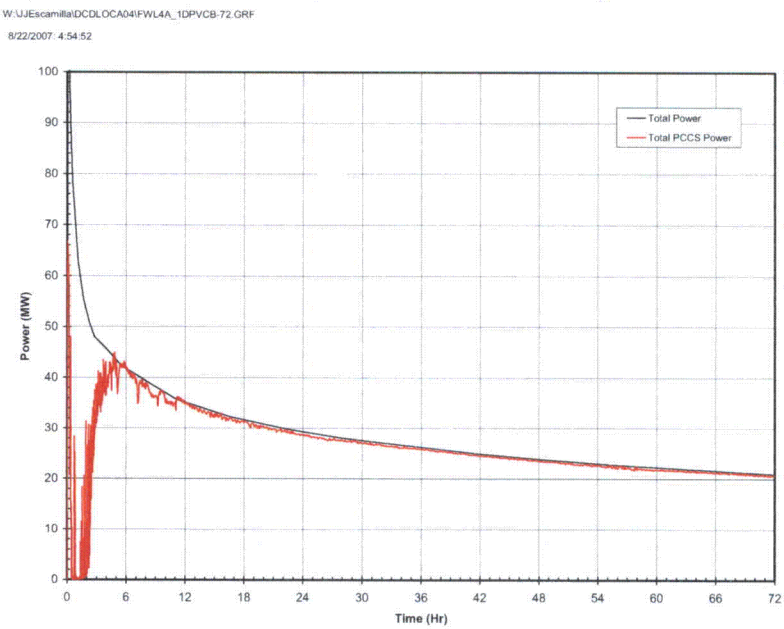

RAI 6.2-98 S01 Figure 6.2-98 S01-29. PCCS Heat Removal versus Decay Heat (72 Hours)

(FWLB: FWL4A_1DPVCB-72)

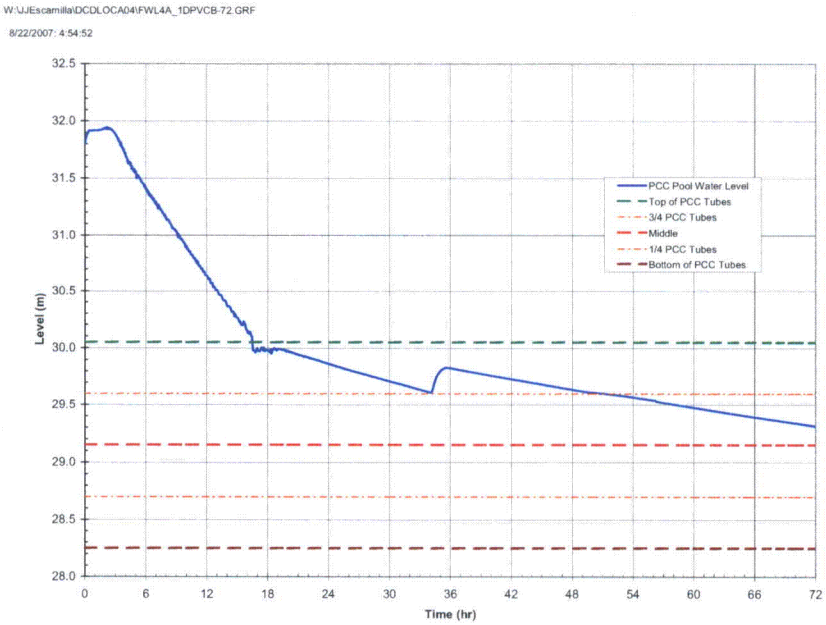

RAI 6.2-98 S01 Figure 6.2-98 S01-30. IC/PCC Pool Water Level (72 Hours)

(FWLB: FWL4A_1DPVCB-72)

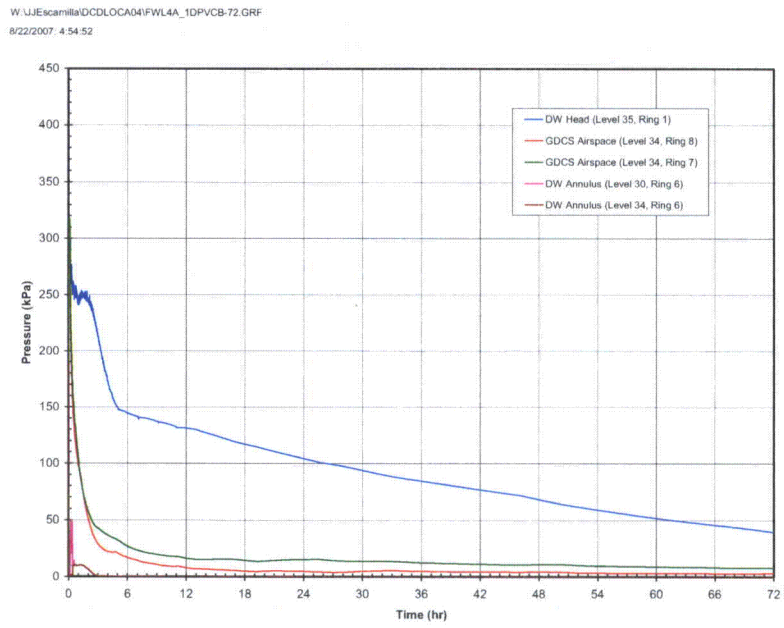

RAI 6.2-98 S01 Figure 6.2-98 S01-31. DW and GDCS NC Gas Pressures (72 Hours)

(FWLB: FWL4A_1DPVCB-72)

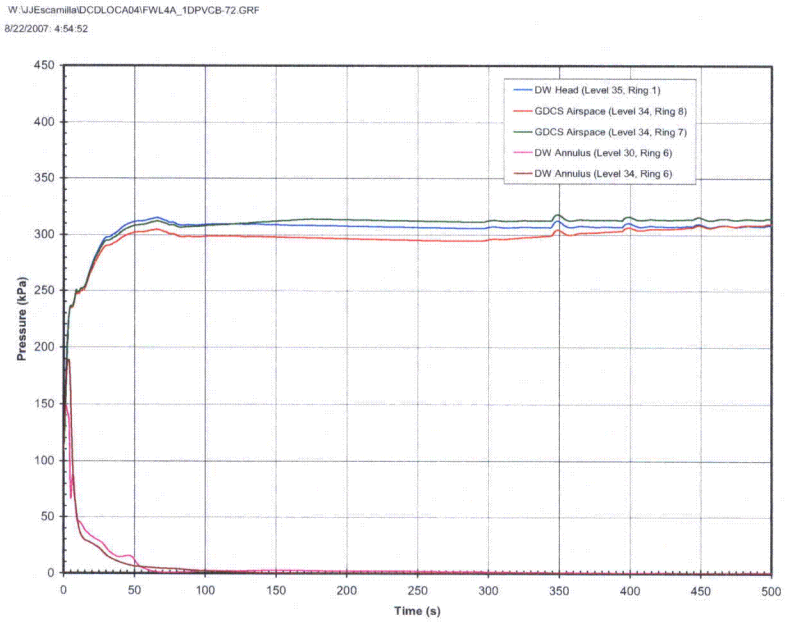

RAI 6.2-98 S01 Figure 6.2-98 S01-32. DW and GDCS NC Gas Pressures (500 Seconds)

(FWLB: FWL4A_1DPVCB-72)

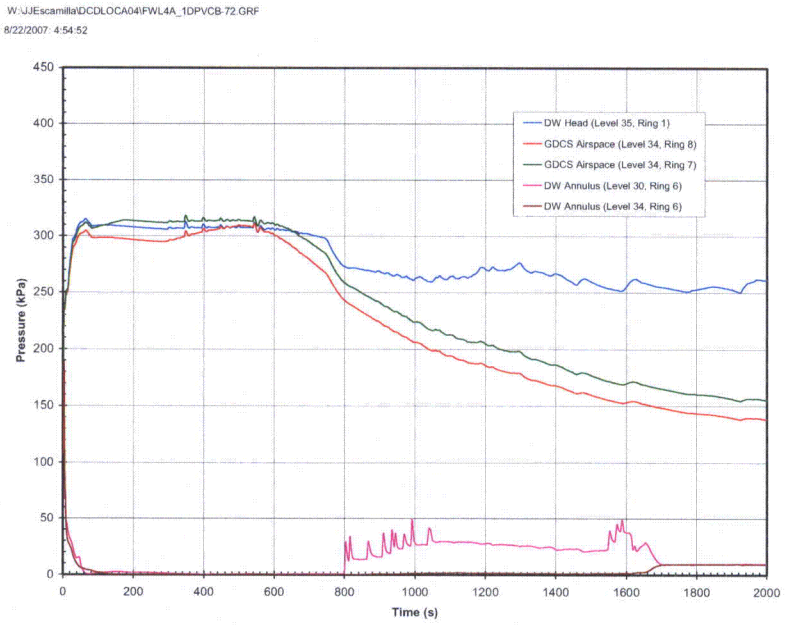

RAI 6.2-98 S01 Figure 6.2-98 S01-33. DW and GDCS NC Gas Pressures (2000 Seconds)

(FWLB: FWL4A_1DPVCB-72)

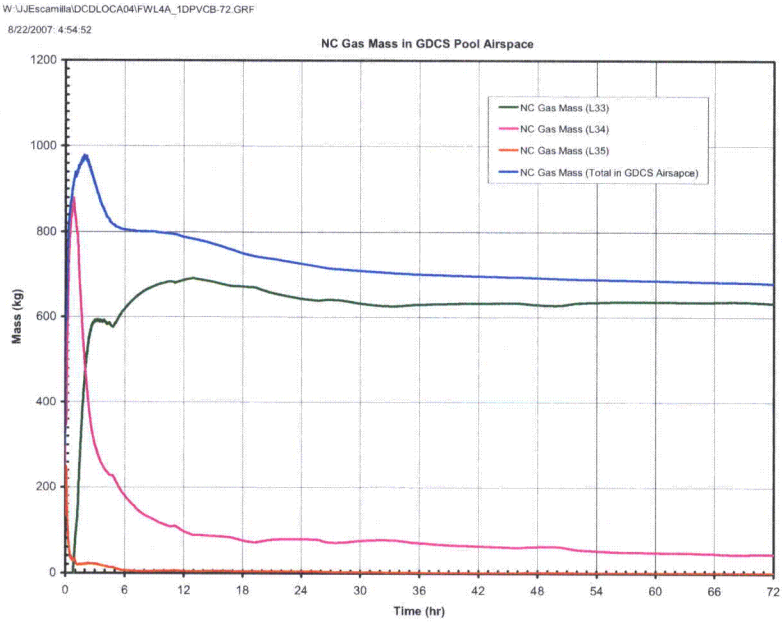

RAI 6.2-98 S01 Figure 6.2-98 S01-34. NC Gas Mass Profiles in the GDCS Airspace (72 Hours)

(FWLB: FWL4A_1DPVCB-72)

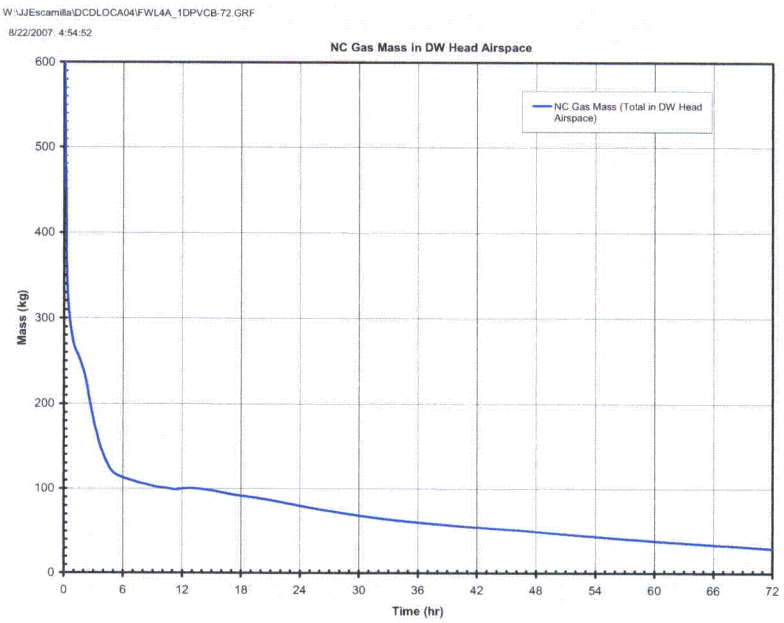

RAI 6.2-98 S01 Figure 6.2-98 S01-35. NC Gas Mass Profiles in the DW Head Airspace (72 Hours)

(FWLB: FWL4A_1DPVCB-72)

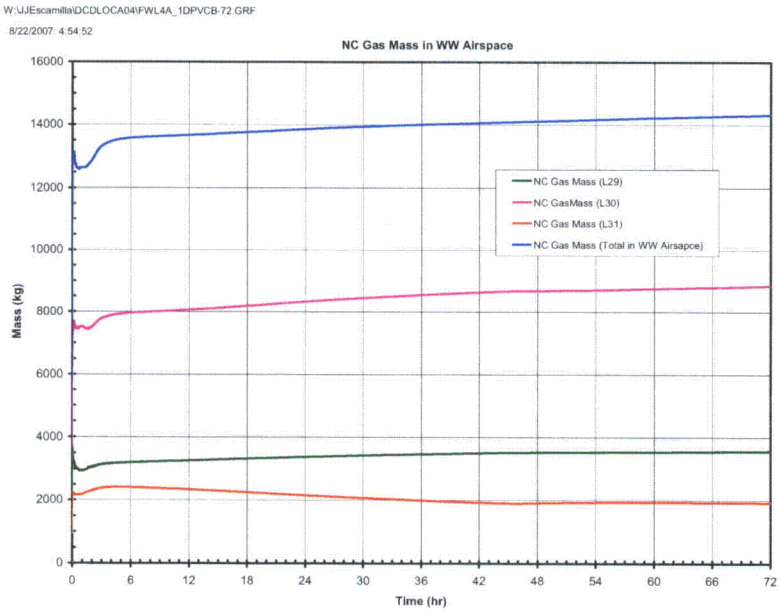

RAI 6.2-98 S01 Figure 6.2-98 S01-36. NC Gas Mass Profiles in the WW (72 Hours)

(FWLB: FWL4A_1DPVCB-72)

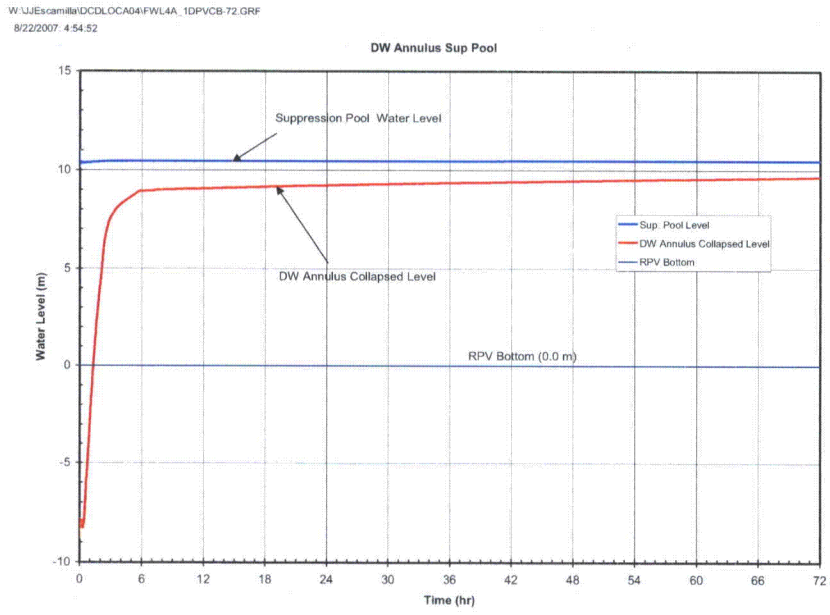

RAI 6.2-98 S01 Figure 6.2-98 S01-37. DW Annulus and Suppression Pool Levels (72 Hours)

(FWLB: FWL4A_1DPVCB-72)

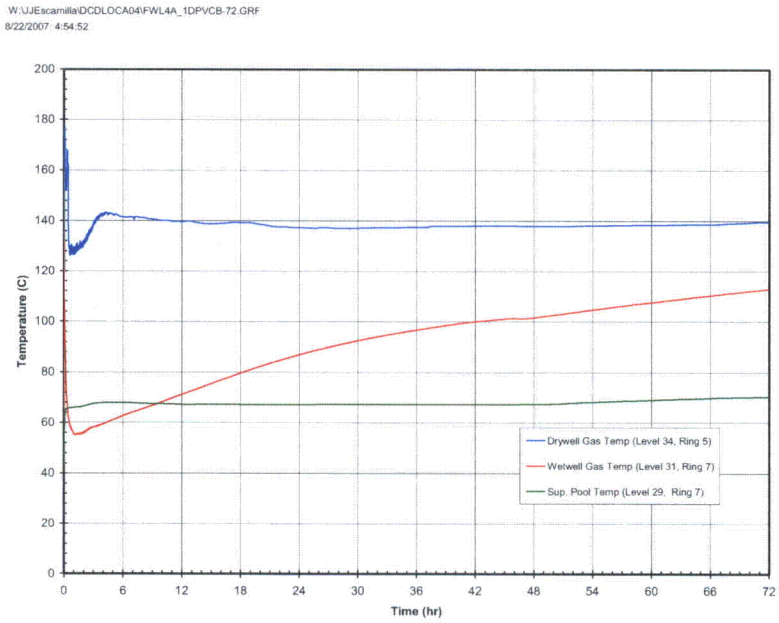

RAI 6.2-98 S01 Figure 6.2-98 S01-38. Containment Temperatures (72 Hours)

(FWLB: FWL4A_1DPVCB-72)

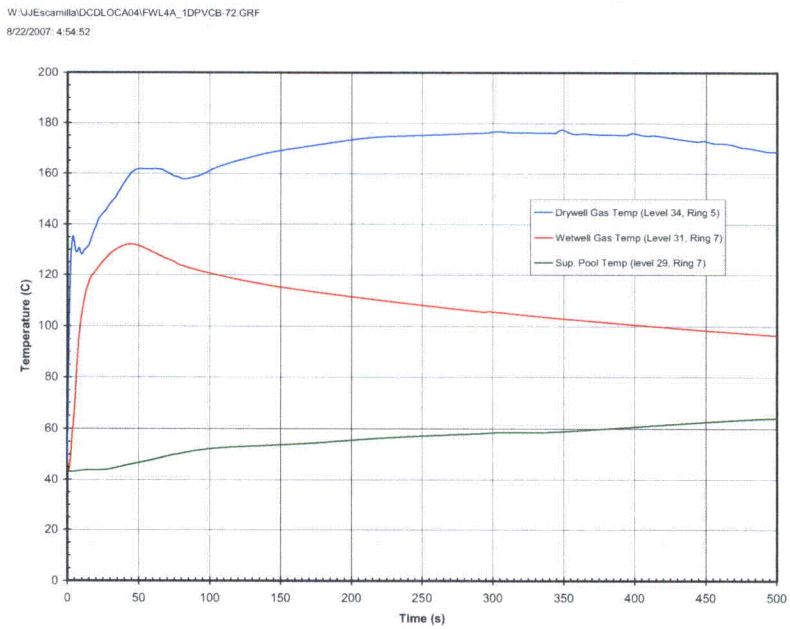

RAI 6.2-98 S01 Figure 6.2-98 S01-39. Containment Temperatures (500 Seconds)

(FWLB: FWL4A_1DPVCB-72)

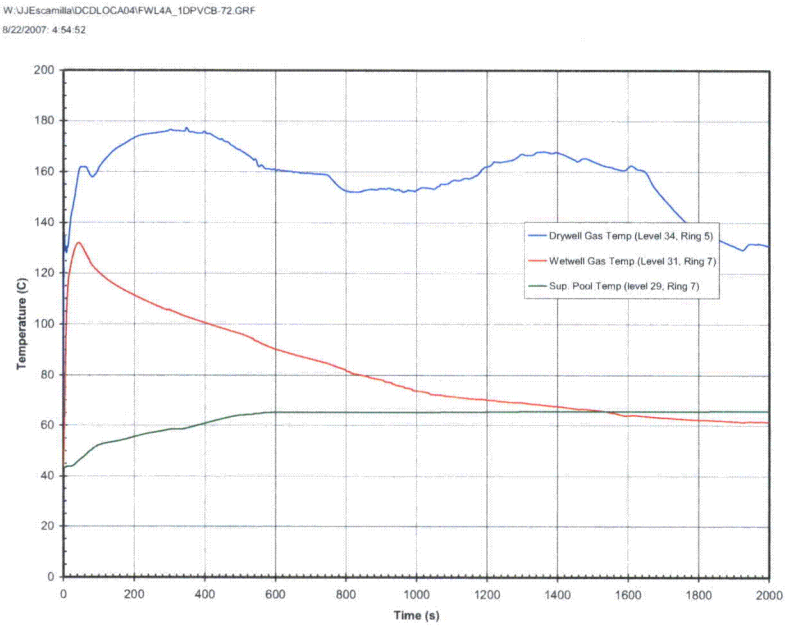

RAI 6.2-98 S01 Figure 6.2-98 S01-40. Containment Temperatures (2000 Seconds)

(FWLB: FWL4A_1DPVCB-72)

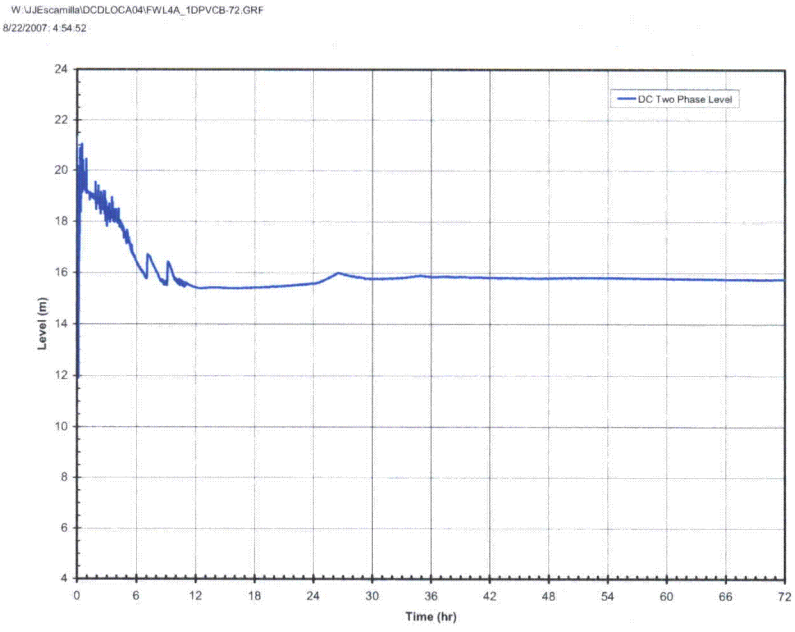

RAI 6.2-98 S01 Figure 6.2-98 S01-41. Two-Phase Level in the RPV Downcomer (72 Hours)

(FWLB: FWL4A_1DPVCB-72)

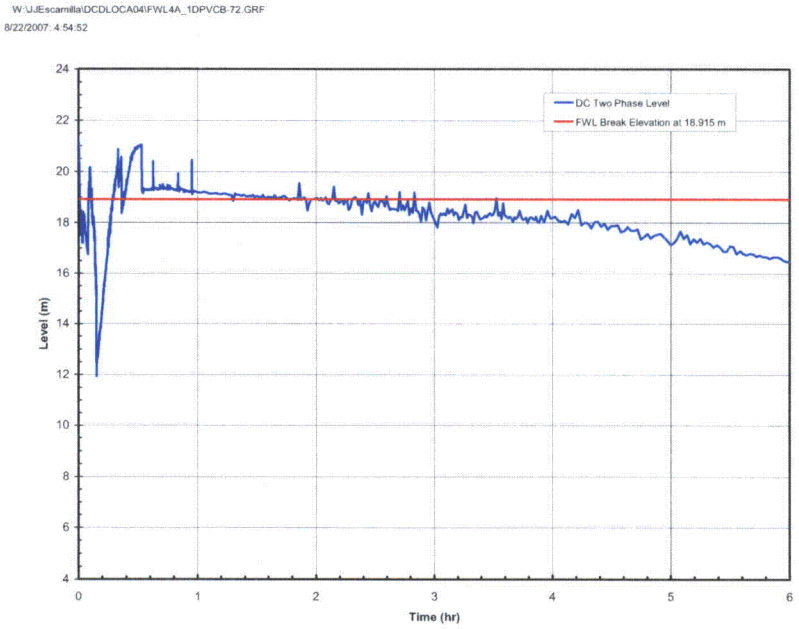

RAI 6.2-98 S01 Figure 6.2-98 S01-41a. Two-Phase Level in the RPV Downcomer (6 Hours)

(FWLB: FWL4A_1DPVCB-72)

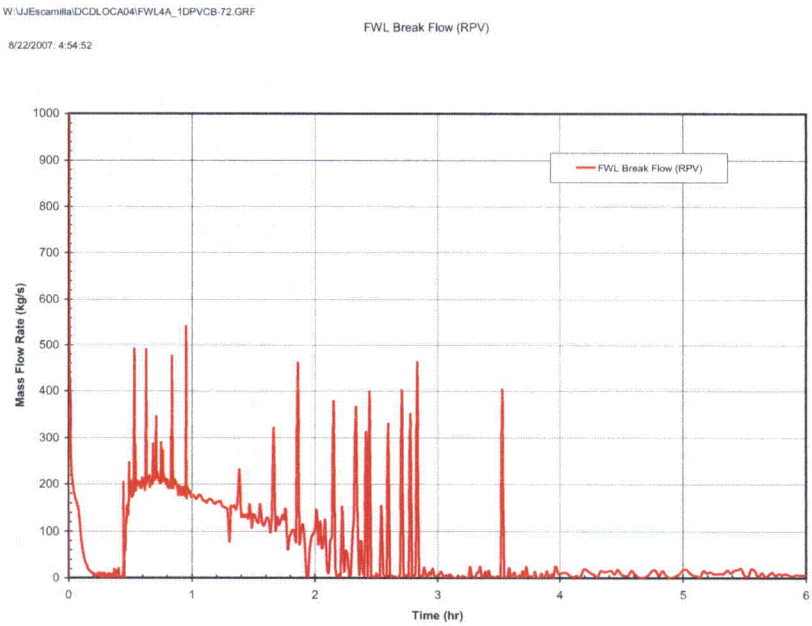

RAI 6.2-98 S01 Figure 6.2-98 S01-42. FWLB Break Flow from the RPV (6 Hours)

(FWLB: FWL4A_1DPVCB-72)

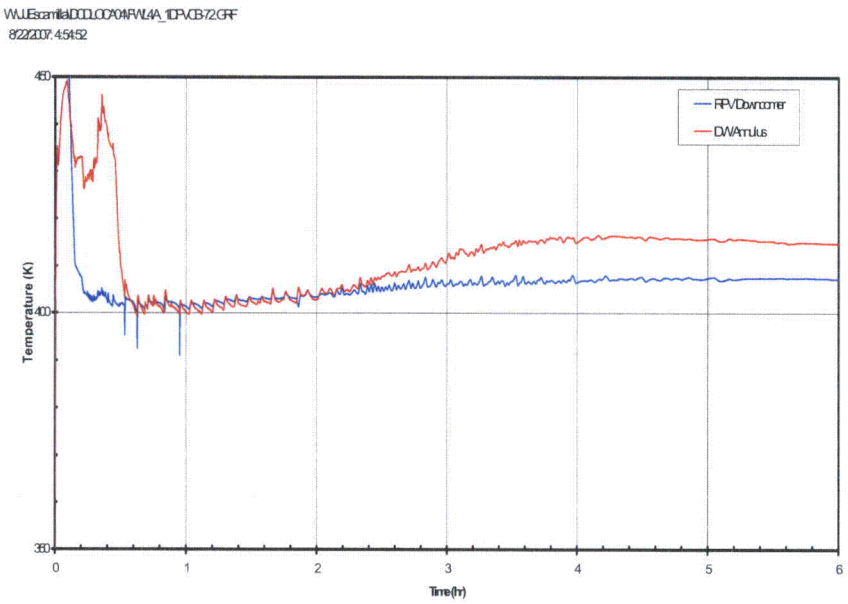

RAI 6.2-98 S01 Figure 6.2-98 S01-43. Temperatures in the RPV Downcomer and DW Annulus

(6 Hours)

(FWLB: FWL4A_1DPVCB-72)

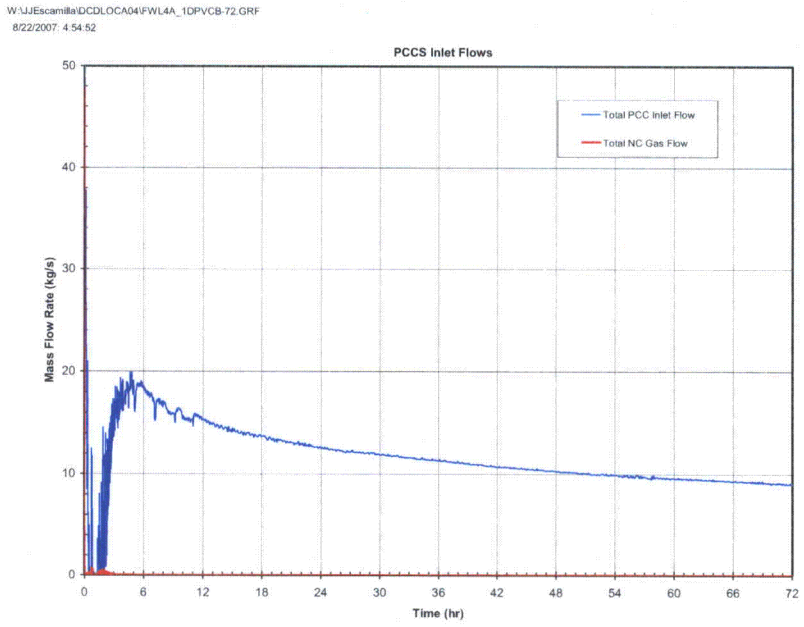

RAI 6.2-98 S01 Figure 6.2-98 S01-44. Total Mixture and NC Gas Mass Flows at the PCCS Inlet

(72 Hours)

(FWLB: FWL4A_1DPVCB-72)

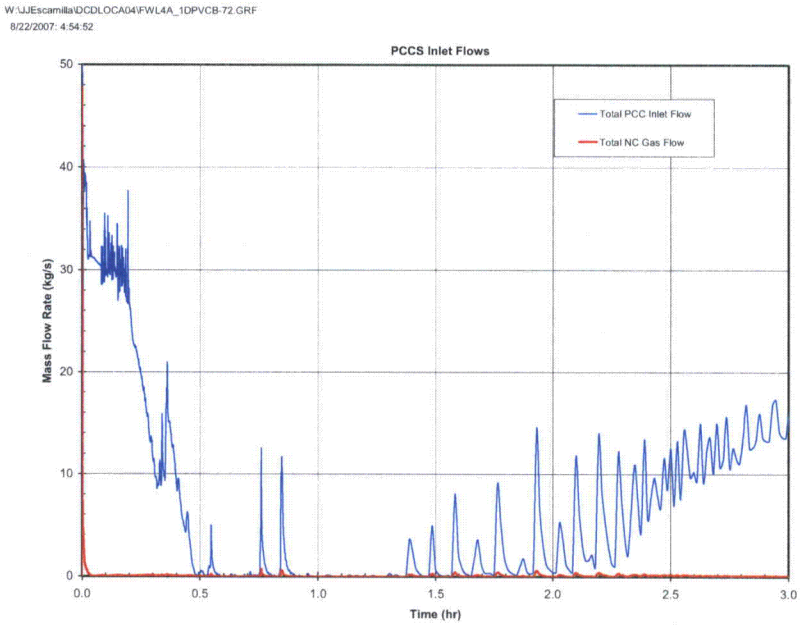

RAI 6.2-98 S01 Figure 6.2-98 S01-45. Total Mixture and NC Gas Mass Flows at the PCCS Inlet

(3 Hours)

(FWLB: FWL4A_1DPVCB-72)

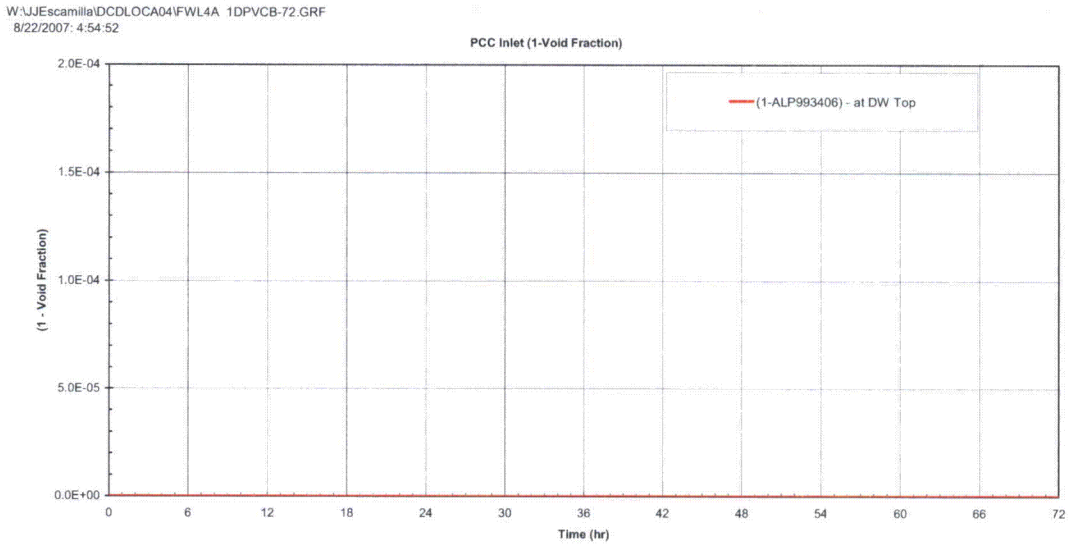

RAI 6.2-98 S01 Figure 6.2-98 S01-45a. Moisture Content at the PCCS Inlet

(72 Hours)

(FWLB: FWL4A_1DPVCB-72)

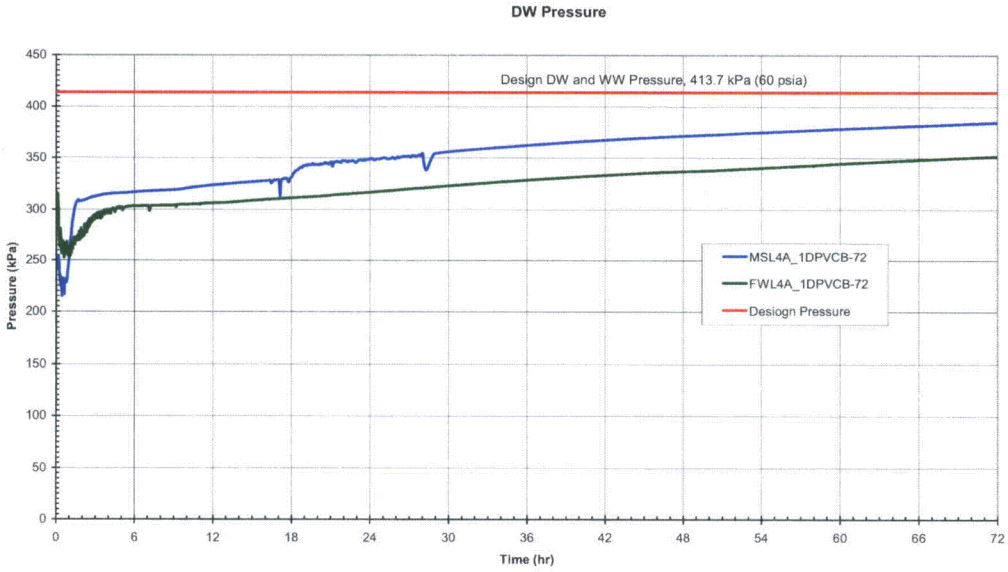

RAI 6.2-98 S01 Figure 6.2-98 S01-46. Comparison of DW Pressures – MSLB versus FWLB (72 Hours)

(MSLB: MSL4A_1DPVCB-72; FWLB: FWL4A_1DPVCB-72)

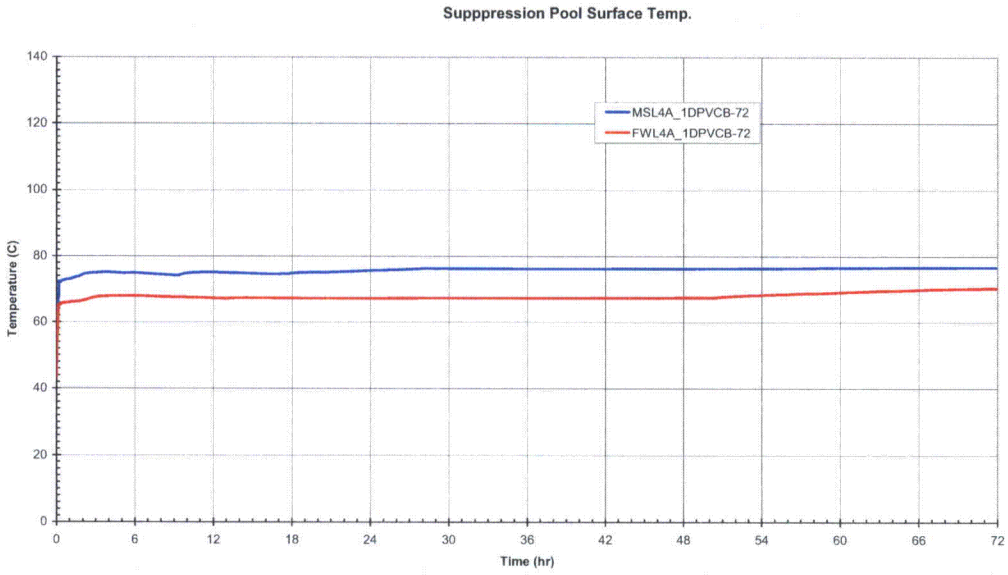

RAI 6.2-98 S01 Figure 6.2-98 S01-47. Comparison of Suppression Pool Surface Temperatures MSLB versus FWLB (72 Hours)

(MSLB: MSL4A_1DPVCB-72; FWLB: FWL4A_1DPVCB-72)

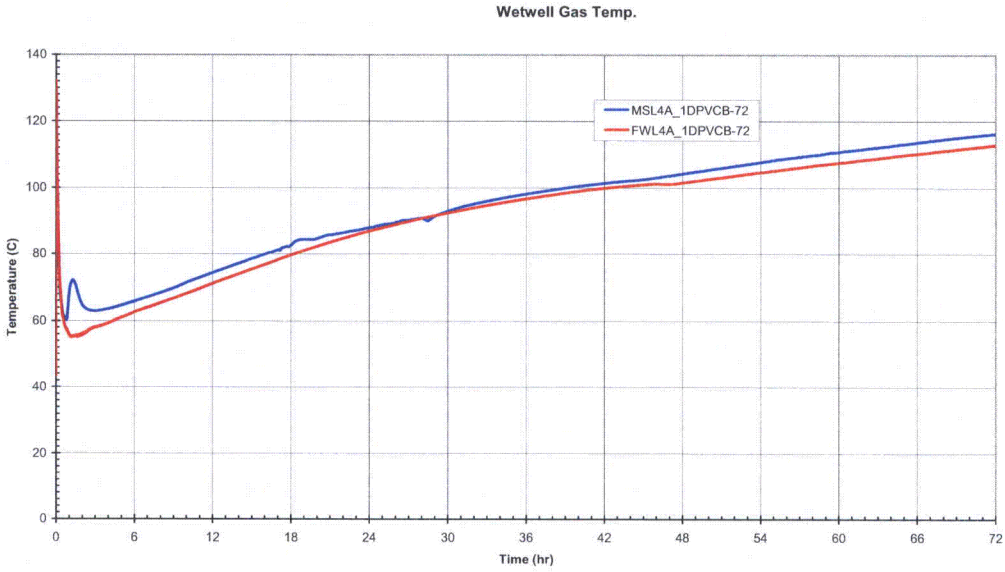

RAI 6.2-98 S01 Figure 6.2-98 S01-48. Comparison of WW Gas Temperatures
MSLB versus FWLB
(72 Hours)

(MSLB: MSL4A_1DPVCB-72; FWLB: FWL4A_1DPVCB-72)

15.0 NRC RAI 6.2-98 S01 REVISION 1

RAI 6.2-98 was a follow up to RAI 6.2-53 (MFN 06-215). The intent of these RAIs was to understand the TRACG calculation for the bounding scenario. ESBWR DCD Tier 2 provides limited information that is insufficient to understand the analyses. These RAIs focused on key phenomena-the trapping and transient distribution of noncondensable gases in the drywell and subsequent transport to the wetwell.

(E) During a phone call with the staff on September 24, 2007, GEH discussed a potential design change to add a drywell gas recirculation system to the PCCS, which will start operating three days after the initiation of a LOCA to improve the PCCS's ability to remove thermal energy from the containment. In your response, please address the effect of the drywell gas recirculation system and any other systems that you plan to credit in your analyses.

15.1 GEH RESPONSE:

(E) At three days after the initiation of a loss-of-coolant accident (LOCA), several mitigating measures would be in place to reduce the containment pressure and temperature, and to maintain them at reduced levels well below design limits. These measures are (1) to provide Isolation Condenser (IC)/Passive Containment Cooling (PCC) pool makeup water to improve the PCC condenser efficiency, (2) to activate the PCC vent fans (drywell gas recirculation system) to enhance the heat exchanger efficiency by removing the accumulation of non-condensable (NC) gases from the PCC condensers and circulating these gases to the Gravity-Driven Cooling System (GDCS) pool space and back to the drywell (DW), and (3) to take credit of the Passive Autocatalytic Recombiner System (PARS) in the analyses after three days. The effects of these measures on the containment pressure response have been analyzed and the key results are discussed in the response to RAI 6.2-139 (MFN 08-357, dated April 19, 2008). The response to RAI 6.2-139 also describes the PCC vent fan system, including functional arrangement and schematic diagram.

The following paragraphs provide additional discussions on the transient distribution of NC gases in the DW and GDCS pool space and subsequent transport to and from the wetwell (WW), before and after the activation of the PCC vent fans.

(1) Description of the Cases

The base case for this evaluation is a guillotine break in the main steam line under bounding conditions. For all cases described in this response, the steam bypass leakage area between the DW and WW is assumed to be the nominal value of 1 cm^2, with a single depressurization valve (DPV) failure-to-open occurrence. The following paragraphs discuss the effect of the PCC vent fans, based on an assumption of a nominal bypass leakage area of 1 cm^2. After the activation of PCC vent fans and IC/PCC pool refilling at 72 hours following a LOCA, the DW pressure drops to and remains at or below the value of WW pressure. The impact of steam bypass leakage on the containment pressure becomes very small or non-existent. Consequently, the effect of the PCC vent fans for the case with bypass leakage area of 2 cm^2 (licensing basis) is expected to be similar to those discussed below that assume a bypass leakage area of 1 cm^2.

From 0 to 72 hours following a LOCA, the analyses assume no credit from the PARS, PCC vent fans, or any other active systems. This part of the analyses is described in DCD Revision 3, Section 6.2, as the Main Steam Line Break bounding case ("MSL3_1DPVCB_NL2Pa-72").

From three to seven days following a LOCA, the analyses continue from the above calculation with no credit from the PARS. However, the IC/PCC pools are continuously refilled starting at 72 hours following a LOCA with 201 gpm of water at 100°F. Two cases are performed, one case with six PCC vent fans, (i.e., one PCC vent fan for each of the six PCC vent lines), and the other case with four PCC vent fans, (i.e., one PCC vent fan for each of the first four PCC vent lines, no vent fan for the other two PCC vent lines).

For these two cases, the PCC vent fans discharge the NC gases into the DW annulus. The effect of PCC vent fan discharge location on the DW pressure is discussed in Item (4) below. The effect of additional credit from the PARS on the DW pressure is discussed in Item (5) below.

(2) Discussions of the Key Transient Responses

RAI 6.2-98S01R01 Figure 6.2-98S01R01-1 and RAI 6.2-98S01R01 Figure 6.2-98S01R01-2 show the pressure and NC gas mass responses in the DW and WW from 0 to seven days (0 to 168 hours). RAI 6.2-98S01R01 Figure 6.2-98S01R01-3 shows the NC gas mass responses in the DW head and GDCS gas spaces from 0 to seven days (0 to 168 hours).

The key transient responses from 0 to 72 hours are discussed in Item (A1) of the response to RAI 6.2-139 (MFN 08-357, dated April 19, 2008). During the first three days of the transient, the IC/PCC pool level drops due to boil-off by the decay heat. At the end of 72 hours, the IC/PCC pool water covers about 65% of the PCC condenser tube length. At 72 hours, the PCC vent fans and the IC/PCC pool refilling are initiated. The PCC vent fans remove the accumulated NC gases from the bottom portion of the PCC condenser tubes and discharge them into the DW. The IC/PCC pool refilling continuously increases the portion of the PCC condenser tube that is covered by the IC/PCC pool water. Both actions enhance the PCC condenser heat removal rate, condensing more DW steam. As a result, the DW pressure drops rapidly shortly after the activation of these actions (RAI 6.2-98S01R01 Figure 6.2-98S01R01-1). Shortly after 72 hours, the DW pressure drops below the WW pressure, resulting in vacuum breaker (VB) openings and reversed leakage flow (i.e., from the WW to the DW). The gas mixture (mostly NC gases) flows back from the WW to the DW through the VBs and leakage path (RAI 6.2-98S01R01 Figure 6.2-98S01R01-4). This continued relocation of NC gases from the WW to the DW results in continued pressure reduction in the WW (RAI 6.2-98S01R01 Figure 6.2-98S01R01-1).

Transient Responses for the Case using Six PCC Vent Fans

Prior to 72 hours, there is a very small amount of NC gases remaining in the DW, DW head, and GDCS gas spaces (RAI 6.2-98S01R01 Figure 6.2-98S01R01-2 and RAI 6.2-98S01R01 Figure 6.2-98S01R01-3). After 72 hours, the gas mixture (mostly NC gases) flows from the WW to the DW through the VBs and the leakage path. While inside the DW, the NC gases mix with the steam (from the DPVs and break pipe) in the DW and enters into the PCC condensers. The PCC condensers condense the steam and the condensate drains to the GDCS pools. The PCC vent fans remove the NC gases accumulation from the bottom of the

PCC condenser tubes, discharging them back into the DW (instead of purging the NC gases into the WW). This process results in steady accumulation of NC gases in the DW, DW head, and GDCS gas spaces. Correspondingly, the NC gas mass in the WW is reduced by the same amount that is transferred to the DW. The WW and DW pressures (RAI 6.2-98S01R01 Figure 6.2-98S01R01-1) decrease as the NC gas mass in the WW is reduced (and by the increased steam mixture flow through the PCC condensers caused by the increased differential pressure across the PCC condensers). The pressure reduction is proportional to the total amount of NC gases that are removed from the WW (and the differential pressure across the PCC condensers).

With the operation of PCC vent fans, the PCC condenser heat removal capacity depends on the steam mixture flow rate and the NC gas mass fraction at the inlet of the PCC condensers. For a fixed flow rate, the heat removal capacity is reduced as the PCC condenser inlet NC gas fraction is increased. The inlet NC gas fraction is increased as the amount of NC gas mass in the DW is increased. After 144 hours, the DW NC gas mass reaches a quasi-equilibrium level. At this level, the PCC condenser heat removal capacity matches the steaming rate into the DW. As a result, the DW pressure also reaches a quasi-equilibrium level at about 310 kPa (RAI 6.2-98S01R01 Figure 6.2-98S01R01-1).

RAI 6.2-98S01R01 Figure 6.2-98S01R01-5 shows the comparison between the decay heat and the PCC condenser heat removal rate for the case using six PCC vent fans. The six PCC condenser units are modeled as two separate components in the TRACG model; one component models two PCC condenser units and the other one models four PCC condenser units. This figure shows heat removal rates for the total and for the individual components. The heat loads are evenly distributed among these PCC components. At 72 hours, there is a surge of heat removal rate due to the initiation of PCC vent fans and IC/PCC pool refilling (negligible contribution from the refilling in such a short period of time).

Transient Responses for the Case using Four PCC Vent Fans

This case is analyzed using four PCC vent fans, (i.e., one PCC vent fan for each of the first four PCC vent lines, no vent fan for the other two PCC vent lines). RAI 6.2-98S01R01 Figure 6.2-98S01R01-1 to RAI 6.2-98S01R01 Figure 6.2-98S01R01-3 show the pressure and NC gas mass responses. RAI 6.2-98S01R01 Figure 6.2-98S01R01-6 shows the comparison between the decay heat and the PCC condensers heat removal rate for the case using four PCC vent fans.

The pressure drop responses are similar in pattern to that for the case using six PCC vent fans. At 72 hours, the DW and WW pressures drop rapidly shortly after the activation of the PCC vent fans and IC/PCC pool refilling. From 72 to 168 hours, the DW pressure remains at or below the WW pressure (RAI 6.2-98S01R01 Figure 6.2-98S01R01-1). During this time period, there are no PCC vent fans or pressure difference (DW – WW) to drive the steam gas mixture flowing through the component that models the two PCC condenser units with no PCC vent fans. As a result, NC gases are accumulated inside the PCC condenser tubes and shuts off these two PCC condenser units. The heat removal capacity of the two PCC components decreases to zero shortly after 72 hours (RAI 6.2-98S01R01 Figure 6.2-98S01R01-6).

Consequently, the four PCC components pick up the total heat load from the decay heat (RAI 6.2-98S01R01 Figure 6.2-98S01R01-6). On the basis of per unit of PCC in the four PCC component case, the heat load for the case using four PCC vent fans is about 50% higher than that for the case using six PCC vent fans. To achieve higher heat removal rate, the inlet NC gas mass fraction is necessary to remain at a lower value, and therefore lower NC gas mass can be stored in the DW. RAI 6.2-98S01R01 Figure 6.2-98S01R01-2 shows that the total amount of NC gas mass that can be redistributed back into the DW. This amount is proportional to the total PCC vent fan capacity. Similarly, the overall pressure reduction (RAI 6.2-98S01R01 Figure 6.2-98S01R01-1) is proportional to the total PCC vent fan capacity, because it depends on the total amount of NC gases that are removed from the WW and the pressure differential developed across the PCC condensers.

(3) Effect of Total PCC Vent Fan Capacity

Item (2) in this response discusses the transient responses for the cases using six PCC vent fans and using four PCC vent fans. The total amount of NC gas mass that can be redistributed back into the DW is proportional to the total PCC vent fan capacity (RAI 6.2-98S01R01 Figure 6.2-98S01R01-2). Similarly, the overall pressure reduction (RAI 6.2-98S01R01 Figure 6.2-98S01R01-1) is proportional to the total PCC vent fan capacity, because it depends on the total amount of NC gases that are removed from the WW and the pressure differential developed across the PCC condensers.

(4) Effect of PCC Vent Fan Discharge Location

The key transient responses discussed in Items (2) and (3) are from cases where the PCC vent fans discharge to the DW annulus. Parametric cases have been performed to assess the effect of PCC vent fan discharge location (Figure 6.2-139-4 in the response to RAI 6.2-139 (MFN 08-357, dated April 19, 2008). The results show that there is a small improvement in the pressure response if the PCC vent fan discharge is relocated from the DW annulus to the GDCS pool compartment since some amount of NC gases is forced to reside in the GDCS pool space.

(5) Effect of PARS After the Activation of PCC Vent Fans

The key transient responses discussed in Items (2) and (3) are from cases with the PCC vent fans activated after 72 hours, but with no credit from the PARS. Parametric cases have been performed to assess the effect of PARS after the activation of PCC vent fans (Figure 6.2-139-5 in the response to RAI 6.2-139 (MFN 08-357, dated April 19, 2008)). When PARS is credited, the credit is simulated as the rate of production of NC gases equal to the rate of their recombination by the PARS. The results show that there is a small improvement in the pressure response when PARS is credited.

DCD Impact:

No DCD changes will be made in response to this RAI.

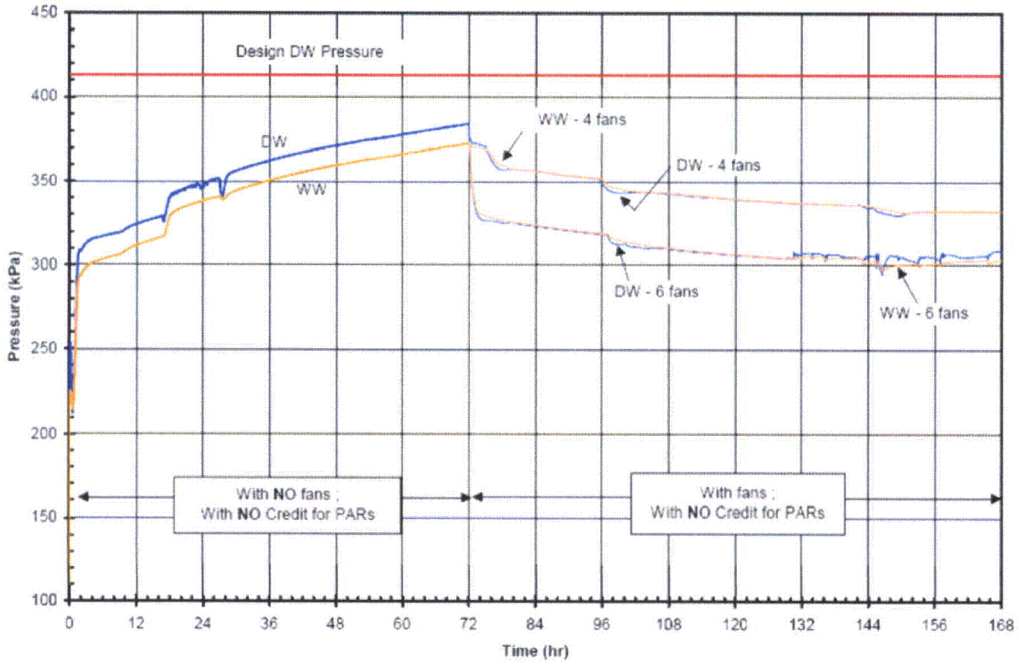

RAI 6.2-98S01R01 Figure 6.2-98S01R01-1. Pressure Responses in DW and WW

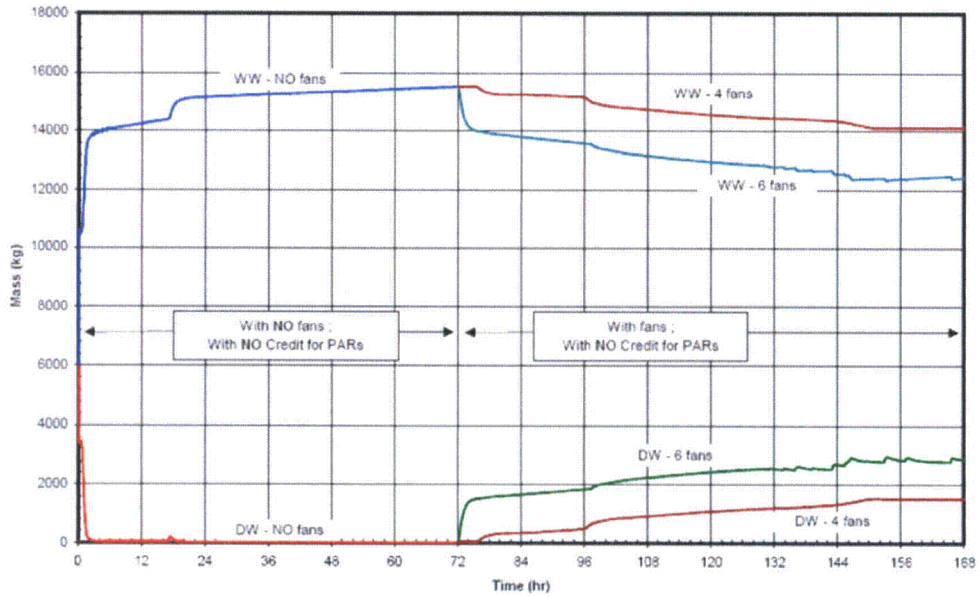

RAI 6.2-98S01R01 Figure 6.2-98S01R01-2. NC Gas Mass Responses in DW and WW

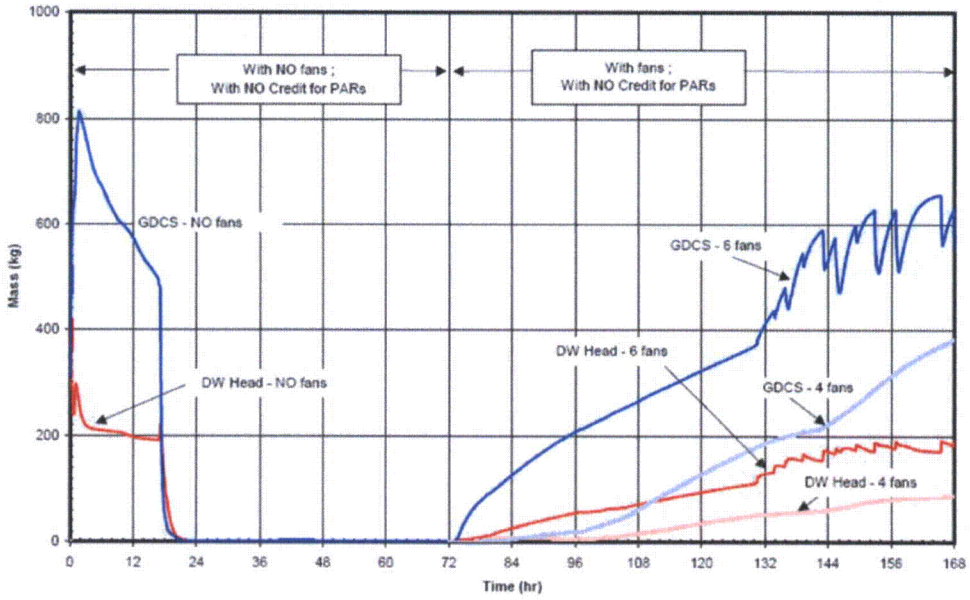

RAI 6.2-98S01R01 Figure 6.2-98S01R01-3. NC Gas Mass Responses in DW Head and GDCS Gas Spaces

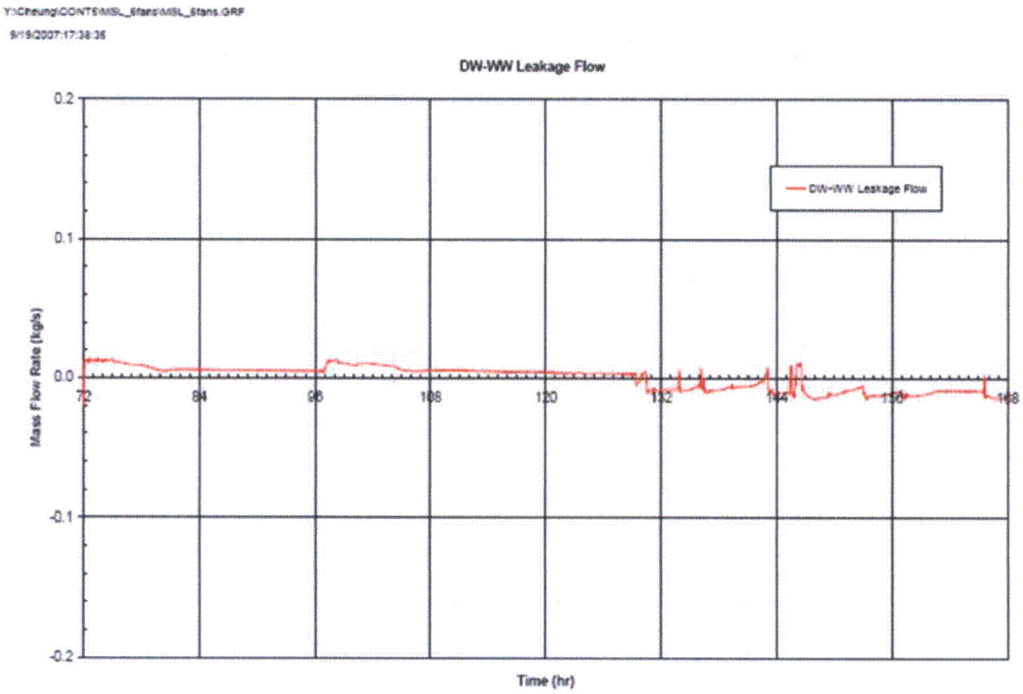

RAI 6.2-98S01R01 Figure 6.2-98S01R01-4. DW-WW Leakage Flow - Six PCC Vent Fans

(Negative value corresponding to leakage flow from DW to WW)

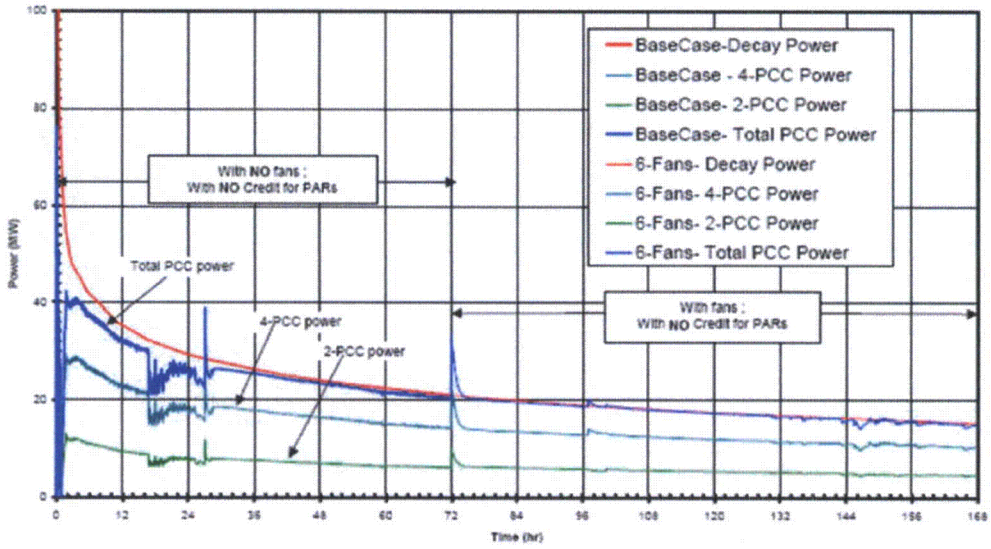

RAI 6.2-98S01R01 Figure 6.2-98S01R01-5. Decay Heat and PCC Condenser Heat Removal

- Six PCC Vent Fans

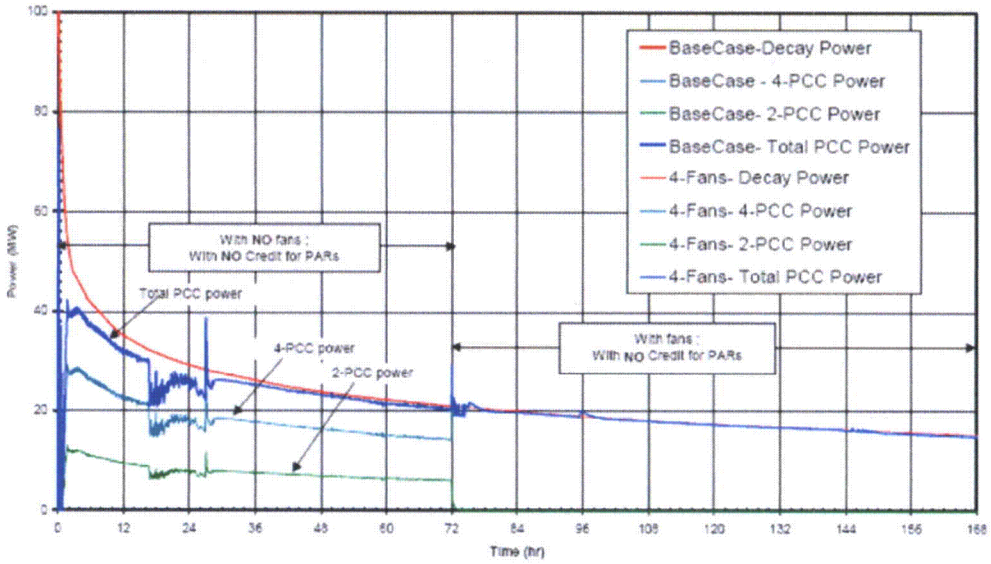

RAI 6.2-98S01R01 Figure 6.2-98S01R01-6. Decay Heat and PCC Condenser Heat Removal

– Four PCC Vent Fans

16.0 NRC RAI 3.6-11 S03

In its RAI response, GEH provided a Technical Report 0000-0102-6265-R0, which describes in detail the modeling procedure they plan to apply to ESBWR blast wave calculations. GEH demonstrates a calculation of a blast wave induced by a high energy line break inside containment of ESBWR feedwater piping. The blast wave propagates into the annular region between the Reactor Pressure Vessel (RPV) and the shield wall, and reflects between the boundaries of the annulus. GEH established that a two-dimensional (2D) approximation of the annulus is conservative by comparing 2D pressure amplitudes with those computed using a 3D model. GEH will use 2D models where applicable in ESBWR calculations. GEH also established that the mesh discretization used in their example is conservative by comparing pressures and velocities to those from a model generated with a coarser mesh. While the staff accepts the technical approach described in the report, GEH has not referenced the report in a revised version of the DCD. GEH is therefore, requested to reference GEH Technical Report 0000-0102-6265-R0 and briefly describe the modeling procedure discussed in the report in a revised version of Section 3.6.2.6 of the DCD.

16.1 GEH RESPONSE

GEH Technical Report 0000-0102-6265-R0 is included as Appendix A of this report. DCD Tier 2, Section 3.6.2.6 will be revised to briefly discuss the blast wave modeling procedure documented in Technical Report 0000-0102-6265-R0 and to reference Appendix A of this report.

17.0 NRC RAI 3.6-6 S04 PART B

B) Related to RAI 3.6-6 S03 Part (b): In its response to the RAI, GEH provided a Technical Report 0000-0105-2955-R3, which describes the modeling procedure they plan to apply to ESBWR high energy line breaks unsteady jet calculations. The report includes (1) GEH's general calculation procedure as applied to an unsteady jet configuration measured by Ho and Nosseir (J. Fluid Mech., Vol. 105, pp. 119-142, 1981) and (2) a demonstration of how GEH plan to use this procedure to model unsteady jets from high energy line breaks in ESBWR design calculations. The staff reviewed the information included in this technical report and found that while GEH's procedures are a significant improvement over the previous approach using ANS 58.2, they still have not been sufficiently proven to be conservative methods for computing unsteady resonant jet loads. GEH is requested to address the following staff's concerns.

(1) The current Ho and Nosseir simulations do not demonstrate the key behavior of unsteady jets with strong feedback phenomena. Specifically, the GEH simulations show that the unsteady loads decrease when feedback occurs (Mach number of 0.9) instead of increasing. GEH is requested to further analyze the Ho and Nosseir problem to establish CFD solutions which demonstrate realistic physical behavior, such as increasing unsteady pressures when jet instabilities occur (such as near a Mach Number of 0.9). GEH is also requested to demonstrate the sensitivity of the CFD solution with respect to critical parameters, such as distance between the jet and impingement surface, jet source boundary conditions (pressure and temperature), external conditions, and any other parameters which have a strong influence on the unsteady jet behavior. In summary, GEH is requested to demonstrate that their procedure is a conservative means of bounding the worst-case unsteady jet loads that may occur in an ESBWR high energy line break event.

(2) GEH is requested to establish that solution from the ESBWR MSL B jet flow demonstration is converged with respect to grid/mesh and time step resolution. A mesh convergence study showing that the strong degree of anisotropy in the existing grid does not influence the results would be useful.

(3) GEH is requested to modify the short formal description in the DCD (referencing GEH Technical Report 0000-0105-2955-R3 for further details) of the general procedure that GEH will use to assess dynamic blowdown forces caused by impinging jets emanating from high energy line breaks (the current description is on pages 3.6-21- 22 of Rev. 6 of the DCD). In particular, GEH is requested to include information such as the bullets on page 4 of GEH Technical Report 0000-0105-2955-R3, and some of the information in Tables 2-7 of that report. GEH is also requested to include guidelines and rules of thumb they will apply to generating meshes and grids, and for running FLUENT. Also, GEH is requested to include a description of the procedure they will apply for assessing convergence of their solutions (such as grid resolution studies), and for assessing the sensitivity of their solutions to uncertainties in problem parameters, such as physical distances between jets and impingement surfaces, jet boundary conditions, and external conditions. Finally, GEH is requested to formally list any bias errors and uncertainties they plan to apply to unsteady loads computed using their procedure.

17.1 GEH RESPONSE (REVISION 1)

Response to B(1):

Section 3.4.2 of Technical Report 0000-0105-2955, Revision 5 (forwarded by the original version of this response), presents the results of the simulation of the Mach number 0.9 case. Figures 3.13 and 3.14 show the pressure responses predicted by the computational fluid dynamics (CFD) simulation and measured in the Nossier-Ho experiment, respectively. As shown, the CFD predictions are conservative relative to the experimental data by an order of magnitude. Technical Report 0000-0105-2955 is currently being revised to include the attached analysis methodology for ESBWR pipe break analyses to ensure conservative predictions. When complete, the revised report will be formally provided by GEH in a separate MFN letter.

Response to B(2):

Section 3.4.4 of Technical Report 0000-0105-2955, Revision 5, discusses the results of the mesh independence study. The results indicate that the base mesh used in the analyses is sufficiently refined such that the predicted pressure response is not significantly impacted. Based on follow-up discussions, GEH has performed additional convergence studies. The results of these studies were provided to the NRC by MFN Letter 09-787 and will be included in the revised Technical Report 0000-0105-2955.

Response to B(3):

In lieu of including the requested information in the DCD, Technical Report 0000-0105-2955 will be included as Appendix B of NEDE-33440P, and DCD Tier 2, Section 3.6.2.3.1 will be revised to reference this NEDE report and to briefly summarize the contents.

DCD Impact (Revised)

DCD Tier 2, Section 3.6.2.3.1 and NEDE-33440P will be revised as noted in the attached markups. The attached analysis methodology will be added to Technical Report 0000-0105-2955.

Note: Technical Report 0000-0105-2955 is included as Appendix B of this report.

APPENDIX A: TECHNICAL REPORT 0000-0102-6265-R0: CFD MODELING OF BLAST WAVE PROPAGATION DURING AN ESBWR FEEDWATER LINE BREAK

HITACHI

GE Hitachi Nuclear Energy

CFD Modeling of Blast Wave Propagation During An ESBWR Feedwater Line Break

Technical Report 0000-0102-6265-R0

By

Dr. Jin Yan

Pijush K. Dey

NON-PROPRIETARY INFORMATION NOTICE

This is a non-proprietary version of NEDE-33440P, Revision 2, which has the proprietary information removed. Portions of the document that have been removed are indicated by an open and closed bracket as shown here [[ ]].

Table of Contents

List of Tables

List of Figures

1. INTRODUCTION

This report documents the blast wave magnitude as a result of a high energy line break inside containment of ESBWR feedwater piping as part of the Nuclear Regulatory Commission (NRC) request for additional information (RAI) RAI 3.6-11, Supplement 1 & 2. Specifically, the report includes an assessment of feedwater line break at the reactor pressure vessel (RPV) nozzle confined between the RPV and Reactor shield wall (RSW). The space between the RPV and RSW is identified as the Annulus region in the ESBWR plant layout.

The blast wave effects in the Annulus region behave somewhat differently compared to the break occurring in an open space. This report includes evaluation methodology and results of the blast wave pressure in the Annulus, which is carried out based on the computational fluid dynamics (CFD) calculations using the ANSYS computer code. The NRC RAI 3.6-11, Supplement 1 & 2 requested the following:

"In the event of a high pressure pipe rupture, the first significant fluid load on surrounding structures would be induced by a blast wave. A spherically expanding blast wave is reasonably approximated to be a short duration transient and analyzed independently of any subsequent jet formation. Since the blast wave is not considered in the ANS 58.2 or the ESBWR DCD for evaluating the dynamic effects associated with the postulated pipe rupture, omission of blast wave considerations is clearly non-conservative. Explain how the effects of blast loads on neighboring SSCs will be accounted for."

In the current CFD study, the Feed Water line break is modeled. During the Feed Water line break, the blast wave originating from the feedwater line rapidly propagates into the annular region between the RPV and the shield wall. In the meantime, the blast wave will also be reflected by the wall surfaces. The reflection waves will reinforce the waves at places and create higher pressure. In order to capture this phenomenon, the CFD geometry was required to include all significant solid surfaces such as RPV and Shield wall surface. The blast wave strength and the speed are primarily determined by the [[

]]

[[

]]

Figure 1. [[

]]

GEH has conducted [[ ]] in order to develop a CFD approach for the blast wave modeling. The overall objective of this evaluation is:

(1) To investigate the flow field at the break point and the surrounding environment.

(2) To investigate the interaction between the shock wave and any hard surface nearby during the even of Feed Water line break.

(3) To investigate the blow down pressure and the force on the nearby target components.

2. TECHNICAL APPROACH

In the CFD study, a commercial [[ ]] CFD code (CFX Version 11.0) was used. The code is a pressure based coupled solver. [[

]]

(1) Technical Approach Development and Validation

As shown in Yan [1], in order to develop a technical approach, the first task of this project was to [[

]]

[[

]]

Figure 2. [[ ]]

The [[ ]] is shown in Fig. 2. [[

]]

[[

]]

Figure 3. [[ ]]

[[

]]

Figure 4. [[ ]]

[[

]]

Figure 5. [[ ]]

From the [[ ]] in Fig. 3, it can be seen that the [[ ]] The [[ ]] in Fig. 4 shows [[

]] in Fig. 5 shows [[

]]

(2) Technical Assumptions for Feed Water line Break

The CFD simulation is able to capture the exact shape of the geometry of the RPV outer wall, the Feedwater nozzle, and the Shield wall.

Over and above the normal assumptions applicable to CFD analyses, this particular analysis assumes the following:

- [[
-
-

-

-]]

3. GEOMETRY AND MESH GENERATION

The geometry and mesh generation was carried out based on engineering drawings supplied in electronic (IGES) format. This pre-processing was carried out using ICEM V11.0 on a HP workstation. The ESBWR RPV and the nozzles, and pipes are shown in Fig. 6.

[[

]]

Figure 6. ESBWR RPV

(1) [[ ]] Geometry & Mesh

The [[ ]] surfaces including the ESBWR RPV (Fig. 6), Feedwater Nozzle and the broken end of the Feedwater line were created in ICEMCFD based on [[ ]] drawings of ESBWR. These surfaces were [[
]]

[[

]]

Figure 7. [[ ]]

The [[

]]

A meshing block was generated based on the geometry. [[

]]

[[

]]

Figure 8. [[ ]]

(2) [[ ]] Mesh for Mesh Sensitivity Study

Based on the same blocking structure as the mesh in the previous section, a [[

]] The results in Fig. 10 and Fig. 11 show that []]]

4. SOLVER SETTINGS & BOUNDARY CONDITIONS

The input parameters for the material properties, operating conditions, initial conditions, and boundary conditions that were used for all [[ ]] CFD calculations are kept the same. The solver and physical models selections are listed as following.

- [[
-
-
-
-
-
-]]

The initial conditions at time zero for the annulus region (the region between the RPV and the shield wall) are listed in Table 1. The initial conditions inside the Feed Water line pipe and the Feedwater line nozzle are listed in Table 2. The transient and numerical schemes used in the CFD models are listed in Table 3. The boundary conditions at the Nozzle inlet and the pipe inlet are shown in Table 4.

Table 1
Initial Conditions of The Annulus Region

[[	
	]]

Table 2
Initial Conditions of Feed Water Line

[[	
	]]

Table 3
Solver Controls

[[	
	]]

Table 4
Boundary Conditions

[[	
	]]

5. SIMULATION RESULTS

During the simulations, pressure at different points is monitored for each time step. The monitor point locations in all CFD models are kept the same as shown in Fig. 9 and Table 5.

[[

]]

Figure 9. Monitor Point Locations

Table 5
Monitor Point Locations

[[	
	]]

The transient results files are [[

]]

In order to ensure the grid independence has been achieved, [[

]] in Fig. 10 and

Fig. 11. [[

]]

[[

]]

Figure 10. [[ ]]

[[

]]

Figure 11. [[ ]]

[[

]]

The maximum pressure change at each monitor point caused by the blast wave is plotted against the distance from the Feedwater Line break in Fig. 17. It can be found that [[

]]

[[

]]

Figure 12. Absolute Pressure Time History at the Monitor Points

[[

Figure 13. Absolute Pressure Time History [[ ]]

[[

]]

Figure 14. Instantaneous Absolute Pressure Contours [[ ]]

[[

]]

Figure 15. Instantaneous Absolute Pressure Contours [[ ]]

[[

]]

Figure 16. Instantaneous Absolute Pressure Contours [[ ]]

[[

]]

Figure 17. Maximum Pressure Rise [[ ]]

[[

]]

Figure 18. Maximum Pressure Rise Comparison [[
]]

6. CONCLUSION

The maximum pressure rise values at the monitor points for [[ ]] are listed in Table 6. A 3D model would account for the attenuation as the wave moves radially away from the break location. The 2D model does not account for this radial attenuation. Therefore, a 2D model will be more conservative than a real 3D scenario. [[

]]

Note: GEH has conducted a serial of 3D calculations. The pressure rise values from the 3D CFD model were compared to those 2D values in Table 6. Through comparisons, it can be confirmed that [[

]]

Table 6
Pressure Rise at The Monitor Points

[[			
			]]

7. REFERENCES

[1] Yan, J., et, al. "Steam Dryer Acoustic Load Prediction in the Main Steam Line Break Event", The 16th International Conference on Nuclear Engineering, 2008, Orlando, USA.

[2] Nourgaliev, R.R., Dinh, T.N., Theofanous, T.G., "The Characteristics-Based Matching (CBM) Method for Compressible Flow With Moving Boundaries and Interfaces", Transactions of ASME: Journal of Fluids Engineering 126, pp.586-604, 2004.

APPENDIX B: TECHNICAL REPORT 0000-0105-2955-R6: ESBWR MAIN STEAM LINE BREAK - CFD MODELING: JET IMPINGEMENT DURING HIGH ENERGY LINE BREAK

GEH has not submitted a nonproprietary version of Appendix B in accordance with NRC information Notice 2009-07, Requirements for Submittals, (2): "In instances in which a nonproprietary version would be of no value to the public because of the extent of the proprietary information, the agency does not expect a nonproprietary version to be submitted."